Arabian Journal of Chemistry (2023) **16**, 104473

King Saud University

Arabian Journal of Chemistry

www.ksu.edu.sa
www.sciencedirect.com

REVIEW ARTICLE

Application of $BaTiO_3$-based catalysts for piezocatalytic, photocatalytic and piezo-photocatalytic degradation of organic pollutants and bacterial disinfection in wastewater: A comprehensive review

Daniel Masekela [a], Nomso C. Hintsho-Mbita [b], Simanye Sam [a], Tunde L. Yusuf [a], Nonhlangabezo Mabuba [a,*]

[a] *Department of Chemical Sciences (formerly known as Applied Chemistry), University of Johannesburg, P.O Box 17011, Doornfontein, Johannesburg 2028, South Africa*
[b] *Department of Chemistry, University of Limpopo, Sovenga, Polokwane 0727, South Africa*

Received 20 August 2022; accepted 26 November 2022
Available online 5 December 2022

KEYWORDS

Barium titanate;
Piezo-photocatalyst;
Organic pollutants;
Bacterial disinfection;
Wastewater treatment

Abstract The coupling of piezocatalysis and photocatalysis known as piezo-photocatalysis has attracted a lot of attention as one of the most effective advanced oxidation process (AOPs) for wastewater treatment, especially for the degradation of organic pollutants and disinfection of microbes. To advance this technology, there's a need to develop lead free piezoelectric materials to drive both piezocatalytic and photocatalytic process to prevent secondary pollution due to lead toxicity. Hence, barium titanate ($BaTiO_3$) has been widely used as lead free piezoelectric material for several applications including water splitting, bacterial disinfection, and wastewater treatment due to its exceptional optical and piezoelectric properties. This work presents a comprehensive review on the application of $BaTiO_3$ as a promising lead-free piezo-photocatalyst for the catalytic degradation of organic pollutants and bacterial disinfection from aqueous solution. This review article details the optical and piezoelectric properties, modification strategies, and synthetic meth-

* Corresponding author.
E-mail address: nmabuba@uj.ac.za (N. Mabuba).
Peer review under responsibility of King Saud University.

Production and hosting by Elsevier

https://doi.org/10.1016/j.arabjc.2022.104473

ods of $BaTiO_3$. Furthermore, the application of $BaTiO_3$ as a preferred piezo-photocatalyst for wastewater treatment and a future perspective is presented.

1. Introduction

Water still remains an essence of life, however with continuous discharge of waste into water bodies, access to clean and potable water has continued to dwindle. The detection of various waste organic contaminants such as pharmaceutical, dyes, pesticides, personal care products in surface, ground and drinking water is of major challenge globally due to their detrimental effects (Du and Zhou, 2021). For example, the consumption of water containing organic dyes like methylene blue (MB), rhodamine B (RhB) and methyl orange (MO) can cause eye irritation, bladder cancer and respiratory problems (Fernández et al., 2010; Rai et al., 2005; Tan et al., 2015). With the rapid growth of textile industries, one of the major industrial sources of organic dyes owing to > 100 000 tons of production of dyes per year, thus it is vital to monitor and treat these industrial waste dyes before reaching the environment (Abdi et al., 2017; Gupta et al., 2013; Gupta and Suhas, 2009; Holkar et al., 2016; Katheresan et al., 2018). Of major concern, are pharmaceutical products that have been widely used in various fields including households, agriculture and medicine. In medicine, products such as penicillin, ciprofloxacin, tetracycline and sulfamethoxazole are used as antibiotics to treat bacterial infections (Huang et al., 2021; Mo et al., 2017). The production of antibiotics increases daily due to their high demand for bacterial infection prevention or to cure diseases. The production of penicillin per year was reported to be approximately 28,000 tons, thus making it 68 % of the global consumption of antibiotics (An et al., 2015; Du and Liu, 2012). The presence of some of these antibiotics are of great concern due to their serious health effects such as vomiting, nausea, acute renal failure and diarrhea (Orimolade et al., 2020).

Other water contaminants which have been detected in different water bodies include pathogenic bacteria such as escherichia coli (*E.-coli*), *staphylococcus aureus* (*S. aureus*), *pseudomonas aeruginosa* (*P. aeruginosa*), enterococcus faecalis (*E.facelis*) and other microbes. Inappropriate disposal of sewage and animal waste are the most common sources of faecal matter in the environment. The discharge of these waste materials from the environment into different water bodies such as rivers, lakes, oceans and streams does not affect only chemical oxygen demand (COD), biological oxygen demand (BOD) and turbidity of the surface water but also increases the number of various pathogenic pollutants (viruses and bacteria) existing in them (Pandey et al., 2014). In 2020, approximately > 12 % of the global population was reported to be drinking water containing a substantial amount of unsafe pathogens. Drinking water containing these harmful pathogens can be lethal and cause some serious health issues and waterborne diseases such as diarrhoea, polio, typhoid and malaria *etc* (Pandey et al., 2014). According to the World Health Organisation (WHO) and standards, the allowed recommendable limitation concentration of organic dyes and bacteria should be below 1 ppm and 0 CFU/100 ml in drinking water, respectively (Katheresan et al., 2018; Masekela et al., 2020; Mahlaule-Glory et al., 2019). Thus, it is crucial to maintain the level of organic dyes, pharmaceutical and pathogenic bacterial within permissible limit so as to provide clean drinking water to humans and protect the environment.

Several water technologies and bacterial disinfection techniques including chlorination, chlorine dioxide, ozonation, ultraviolet light (UV), adsorption, membrane filtration and coagulation have been developed to maintain the level of waste water pollutants (organic dyes, bacteria and pharmaceuticals) within a safe level (Hassan et al., 2012; Masekela et al., 2022b; Saucier et al., 2017; Sirés et al., 2014; Sirés and Brillas, 2012a). However, these methods suffer from several limitations including generation of secondary toxic waste, high cost maintenance, incomplete removal of wastewater pollutants, poor recyclability and the use of toxic chemicals. Chlorination is one of the most popular and inexpensive bacterial disinfection techniques for the removal of all micro-organisms present in drinking water. Even though this technique is relatively less expensive, it produces harmful toxic by products such as trihalomethanes (THMs), haloacetonitriles (HANs), haloacetic acids (HAAs) *etc* (Xiang et al., 2018). These disinfection by products (DBPs) have negative impacts on human health as they can cause intestinal cancer. Additionally, chlorination with other methods like adsorption and filtration partially removes pharmaceuticals from wastewater, since 60 % of pharmaceutical residues remain even after treatment (Orimolade and Arotiba, 2020; Sirés and Brillas, 2012b; Xiao et al., 2015). Furthermore, adsorption and membrane filtration generate secondary toxic waste pollutants, thus require additional treatment which is very expensive (Gupta et al., 2012). Therefore, it is very important implement methods which are highly effective, economical and can completely degrade a majority of the wastewater pollutants into less harmful by products.

Advanced oxidation processes (AOPs) such photocatalysis and piezocatalysis have been used as effective methods for complete destruction of organic waste pollutants into less harmful by products. Photocatalysis and piezocatalysis uses generated strong oxidants such hydroxyl radicals (•OH) and superoxide anion ($\bullet O_2^-$) to completely decompose organic pollutants under the influence of visible light and ultrasonic vibration, respectively (Chen et al., 2020; Koe et al., 2020; Li et al., 2019; Liang et al., 2018; Wu et al., 2018a). Unlike other conventional methods, AOPs completely oxidise organic waste pollutants into less harmful by products such as carbon dioxide (CO_2) and water (H_2O). In the photocatalytic degradation process, one main disadvantage is the fast recombination of electrons and holes (X. Liu et al., 2020). Over the past years, several methods such as metallic or non-metallic doping, formation of heterojunction and composites have been employed to enhance their photocatalytic activity, however effective electron-holes separation still remains a problem (Alex et al., 2019; Kanhere et al., 2014; Qi et al., 2017; Wang et al., 2017; Yong Zhang et al., 2019). Consequently, a piezo-electric field that is built within semiconductors has been shown to effectively separate charge carriers (electron and holes) to prevent recombination reactions. Recently, piezoelectric perovskites (ABO_3) structure materials have been employed as an alternative way for better separation of charge carriers (e^- and h^+) (Y. Feng et al., 2018; Fu et al., 2021; X. Li et al., 2021, 2021; Liu et al., 2021; Y. Liu et al., 2020; J. Wu et al., 2020; J. Zhang et al., 2019).

Piezoelectric materials are known as smart materials which produce electric charges under the influence of applied mechanical vibration. These smart materials also tend to exhibit inverse piezoelectric effect, like the generation of mechanical stress under the influence of applied electric field (Xu et al., 2018). The generated electric charges on the opposite site of piezoelectric materials tends to form an electric field across the material. The built in electric field significantly separates the charge carrier (e^- and h^+) which further reacts with dissolved water and oxygen molecules to generate reactive oxygen species (hydroxyl and superoxide radicals), which are responsible for the breakdown of organic waste water pollutants (Y. Feng et al., 2018; Mushtaq et al., 2018; J. Wu et al., 2020).

Among the numerous piezoelectric materials which have been used as piezocatalysts for catalytic degradation of organic waste pollutants present in wastewater, ($BaTiO_3$) has grabbed more attention as a piezocatalyst due to its excellent piezoelectric properties and biocom-

patibility (Kumar et al., 2019a; Ray et al., 2021). Besides that, it is a lead-free piezoelectric material thus making it more appropriate to be applied in environmental applications. Previously, $BaTiO_3$ as a lead free piezocatalyst has been widely used in sensors. However, recently piezo-photocatalytic applications of $BaTiO_3$ as a piezo-photocatalyst has attracted more attention in environmental wastewater treatment (Aksel and Jones, 2010; Ray et al., 2021). Therefore, this review article gives an overview of the recent applications of $BaTiO_3$ as a piezo-photocatalyst for the catalytic breakdown of organic dyes, bacteria and pharmaceutical pollutants. Moreover, the concept of piezocatalysis, photocatalysis, different fabrication methods, relevant piezoelectric properties and modification methods of $BaTiO_3$ are discussed in detail.

2. Basic principle of piezocatalysis, photocatalysis and piezo-photocatalysis

Photocatalysis and piezocatalysis processes are regarded as advanced oxidation processes. These two processes have been widely used in many applications including water splitting, bacterial disinfection, degradation and wastewater treatment (Mengying et al., 2017). The concept of piezocatalysis is similar to that of photocatalysis, the only difference lies on the triggering source to generate reactive oxygen species (ROS) which participate in redox reactions to degrade organic pollutants. In photocatalysis, a light source is usually utilized in the presence of a semiconductor (photocatalyst) to generate electron-holes pairs. The semiconductor absorbs the irradiated UV light with high energy thus resulting in electron excitation from valence band (VB) to conduction band (CB) leaving holes behind as displayed in Fig. 1.

As shown in Fig. 1, the photo-generated electron-hole pairs move on separate active sites of the semi-conductor to initiate redox-reactions which generates reactive oxygen species (ROS) responsible for the decomposition of organic waste pollutants. Unfortunately, the rate of electron-holes recombination is very fast which limits the application of semiconductors for photocatalysis. However, in piezo-photocatalysis, an internal voltage is generated under ultrasonic vibration with a built-in-electric field within the semiconductor. The in-built electric field piezo-semiconductors assists in the separation of photo-generated charge carries thus improving the photoactivity of the semiconductor. As shown in Fig. 2(a) and (b), the separated charge carries due to piezoelectric effect at the opposite surfaces generates free radicals through redox reactions.

Piezo semiconductor materials under the influence of applied pressure have been shown to behave like electrocatalytic reactors. The free electric charges (electrons and holes) at opposite sides of these materials tend to act as anode and cathode (Liang et al., 2018). The reaction (1) and (3) shows the formation of reactive oxygen species from free electric charges on the opposite sites of piezoelectric semiconductor materials. As shown in equation (2) and (3), the free positive charges react with water to form hydroxyl radicals (•OH), whereas negative charges react with free oxygen molecules to form superoxide radicals ($\bullet O_2^-$). These reactive oxygen species ($\bullet O_2^-$ and •OH) are regarded as strong oxidants and are responsible for the degradation of organic dyes and bacterial disinfection.

$$BaTiO_3\ (\text{Piezoelectric material}) + \text{ultrasonic vibration} \rightarrow BaTiO_3\ (e^- + h^+) \quad (1)$$

Negatively charged surface of piezoelectric material

$$h^+ + H_2O \rightarrow \bullet OH + H^+ \quad (2)$$

$$h^+ + OH^- \rightarrow \bullet OH \quad (3)$$

Positively charged surface of piezoelectric material

$$e^- + O_2 \rightarrow \bullet O_2^- \quad (4)$$

Unlike photoelectrocatalysis which is another type of electrochemical advanced oxidation for wastewater treatment, this process requires an external high voltage to reduce the rate of electron-holes recombination. Instead of using an external voltage, piezoelectrics materials are used to produce an internal voltage under mechanical vibration. The most extensively used are lead based piezoelectric materials such as lead zirconate (PZT). However, PZT contains about 80 % of the lead (Pb) content thus limiting their use in various applications (Panda and Sahoo, 2015). Due to lead being toxic, it is very important to develop piezoelectric materials which are lead

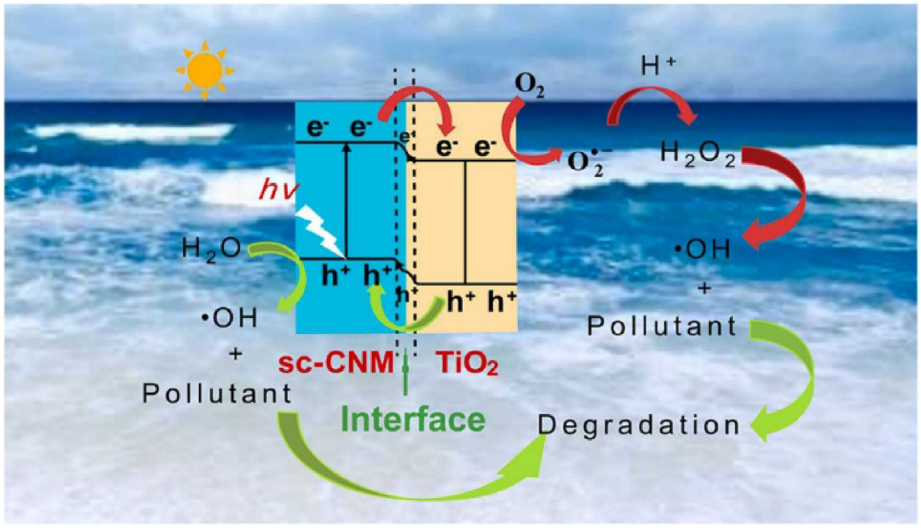

Fig. 1 Photocatalytic degradation mechanism (Zhang et al., 2022).

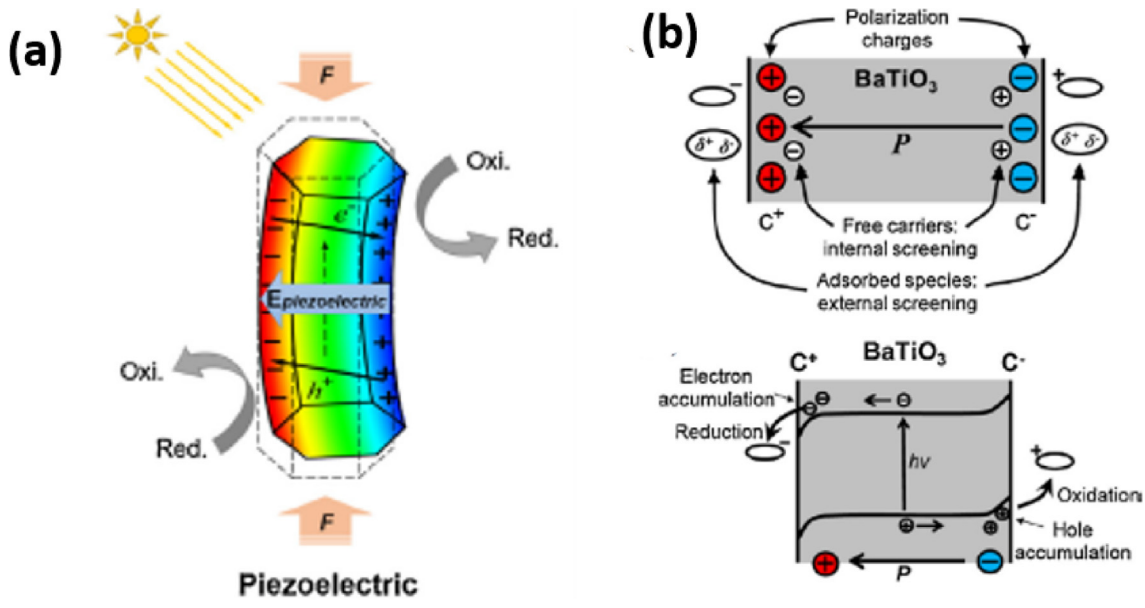

Fig. 2 Piezocatalytic degradation principle (Liang et al., 2019).

free. Over the past few years, barium titanate ($BaTiO_3$) has been given more attention as a lead free piezoelectric material for the production of piezoelectricity under mechanical vibration. Furthermore, recently $BaTiO_3$ has been widely used as one of the piezo semiconductors in piezo-photocatalytic wastewater treatment applications.

2.1. Piezo-photocatalytic experiment based on suspended powder catalyst

Piezo-photocatalytic experiments using powder catalyst involves dispersing a certain amount of the catalyst into a contaminated solution. Since powder catalyst offers high surface to volume ratio, the solution mixture consisting of the catalyst is stirred for a certain time, normally for 30 min to reach an adsorption–desorption equilibrium in the dark. Thereafter, the solution mixture gets exposed to a light source. Some of the important parameters which need to be considered during conducting piezo-photocatalytic experiments in suspension systems includes the type of the light source (solar or UV light), UV light power, Ultrasonic power, UV intensity, the amount of the material used (dosage), reaction time and pH of the solution. Recently, a majority of the piezoelectric semiconductors such as $BaTiO_3$ have been modified to convert their absorption from UV region to visible region (reduce their band gap) to utilize the visible light as a source of light, which constitutes of 43 % of the solar energy. For instance, the activity of piezoelectric semiconductors like ZnO and $BaTiO_3$ were tested under different light sources such as sunlight and artificial visible light (Xenon lamp 1000 W, which emits visible light in the wavelength between 400 and 800 nm). Under solar light irradiation, the total organic carbon (TOC) results showed complete mineralization of phenol at lower concentrations as compared to artificial visible light irradiation (Pardeshi and Patil, 2008).

The type of the vibration normally employed in piezo-photocatalysis process is ultrasonic vibration. Ultrasonic excitation, can be used to induce piezoelectric materials to produce piezoelectric potential, which can effectively encourage the deterioration of organic dyes. However, under stress the generated free carriers will move in a specific direction to their end two poles and shield the piezo-potential, reducing the driving force. As a result, to maintain the electric field during the piezocatalysis process, continual oscillation is necessary. The ultrasound has the capacity to deliver continuous stress as a physical expression of mechanical energy (Lu et al., 2022). It is important to note that prolonged ultrasonic vibration will have both sonochemical and piezoelectric effects on materials that are made of piezoelectric components (Torres et al., 2008). The sonochemical effect can also help in the degradation of organic or inorganic wastewater pollutants.

2.2. Piezo-photocatalytic experiment based on thin film electrode catalyst.

The issues associated with powder piezo-photocatalyst such as low separation efficiency, poor recovery and regeneration ability, could be resolved by fabricating piezo-photocatalysts supported on the substrate to produce thin film electrodes. Typically, powder catalysts are separated from aqueous solution via filtration and centrifugation process, thus time consuming and some of the catalyst residue might remain in the solution and lead to secondary pollution. Piezo-photocatalyst thin film electrodes offer a good recoverability and recyclability, unlike powder catalysts. However, thin film electrodes during degradation process do not offer the full contact with the solution as compared to powder catalyst. Due their limited contact with the solution or low surface area, thin films exhibit slow degradation rate and low degradation efficiency. Besides that, growing interest is being shown in thin films with nanostructures that are directly formed on the surface of the substrate and are particularly susceptible to exposure to the dye solution. The degradation of organic pollutants via piezo-photocatalytic processes can be illustrated in Fig. 3. As shown

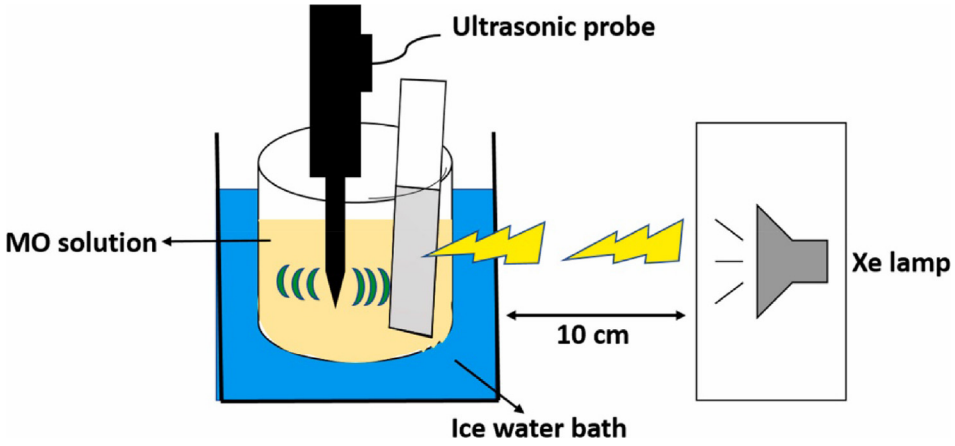

Fig. 3 Piezo-photocatalytic degradation experiment based on thin film (Masekela et al., 2022a).

in the Fig. 3 experiment, the prepared piezo-photocatalyst thin film is dispersed into a solution containing organic pollutants, thereafter exposed to light and ultrasonic irradiation. Just like piezo-photocatalytic experiment in suspension system, the parameters such as; the distance between the thin film electrode and light source, distance between thin film electrode and ultrasonic probe, ultrasonic power and light source need to be considered. Recently, floatable thin films are designed, which freely moves atop the water offering better utilization of sunlight. Unlike, steady thin film which requires photoreactor and external light source. Furthermore steady thin film requires a specific platform to control the distance between the light source and thin film electrode, which obviously raises the cost of scalable water purification (Yaozhong Zhang et al., 2019).

Another form of using thin film electrode is via sono (piezo)-photoelectrocatalytic degradation processes. Sono(piezo)-photoelectrocatalytic processes is a combination of sonocatalysis/piezocatalysis, photocatalysis and electrocatalysis. These processes have not yet been extensively investigated. In this experiment, light irradiation, ultrasonic vibration and bias voltage is applied on the surface of the thin film electrode. The degradation experiment is conducted using potentiostat/-galvanostat, the prepared piezo-photocatalyst thin film is employed as a working electrode in the presence of a reference (Ag/AgCl) and counter electrode (platinum wire). Generally, the fabricated thin film electrode is positioned vertically opposite to the ultrasonic probe and light source (Fig. 4).

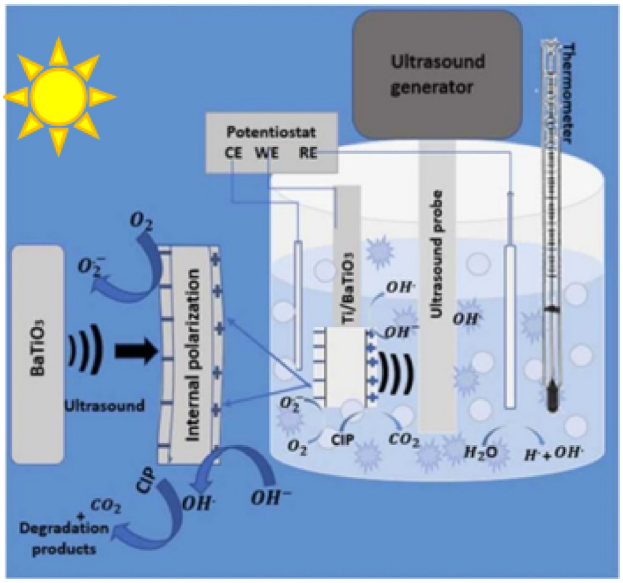

Fig. 4 Photo assisted sonoelectrochemical degradation experiment (Ojo et al., 2022).

3. Structural, piezoelectric, and optical properties of $BaTiO_3$

$BaTiO_3$ is one of the highly applied ferroelectric materials which exhibit piezoelectricity under any form of mechanical vibration. It belongs to the perovskites family (ABO_3), whereby A denotes a Barium (Ba) atom and B is a Titanium (Ti) atom. The crystal structure of $BaTiO_3$ consists of Ti^{4+} atoms co-ordinated to six oxygen atoms to produce octahedral cluster's (TiO_6) and Ba^{2+} co-ordinated to twelve oxygen atoms to form (BaO_{12}) clusters (Fig. 5). As shown in Fig. 5, Ba atoms are situated at every corner position, O atoms at face centred positions and Ti atoms at the centre.

Barium titanate can exist in different crystal structures such as cubic, tetragonal, orthorhombic and rhombohedral depending on the theta angles and phase transition temperature. The major distinction between cubic and tetragonal phases of $BaTiO_3$ lies on the slight shift of theta angles of octahedral (TiO_6) clusters from 90° to ≈ 93.3°, whereas the orthorhombic and rhombohedral phase occurs in the theta angles from approximately 89.9° to ~ 85.7°(Itoh et al., 1985). The $BaTiO_3$ crystal structures undergoes three different phase transitions under different temperatures. At temperature between 26.85 °C and 46.85 °C, cubic crystal structures transform into tetragonal structures, and to orthorhombic at approximately –23.15 °C to 6.85 °C, then ultimately to rhombohedral at temperatures around −73.15° C and –33.15 °C (Acosta et al., 2017; Oliveira et al., 2020). The band energy gap of each crystal structure of $BaTiO_3$ plays a significant role in the photocatalysis process. The cubic crystal structure of $BaTiO_3$ has a theoretical direct band energy gap of 4.68 eV, while orthorhombic, tetragonal and rhombohedral exhibit an indirect band energy gap of 5.06, 4.73 and 5.06 eV, respectively

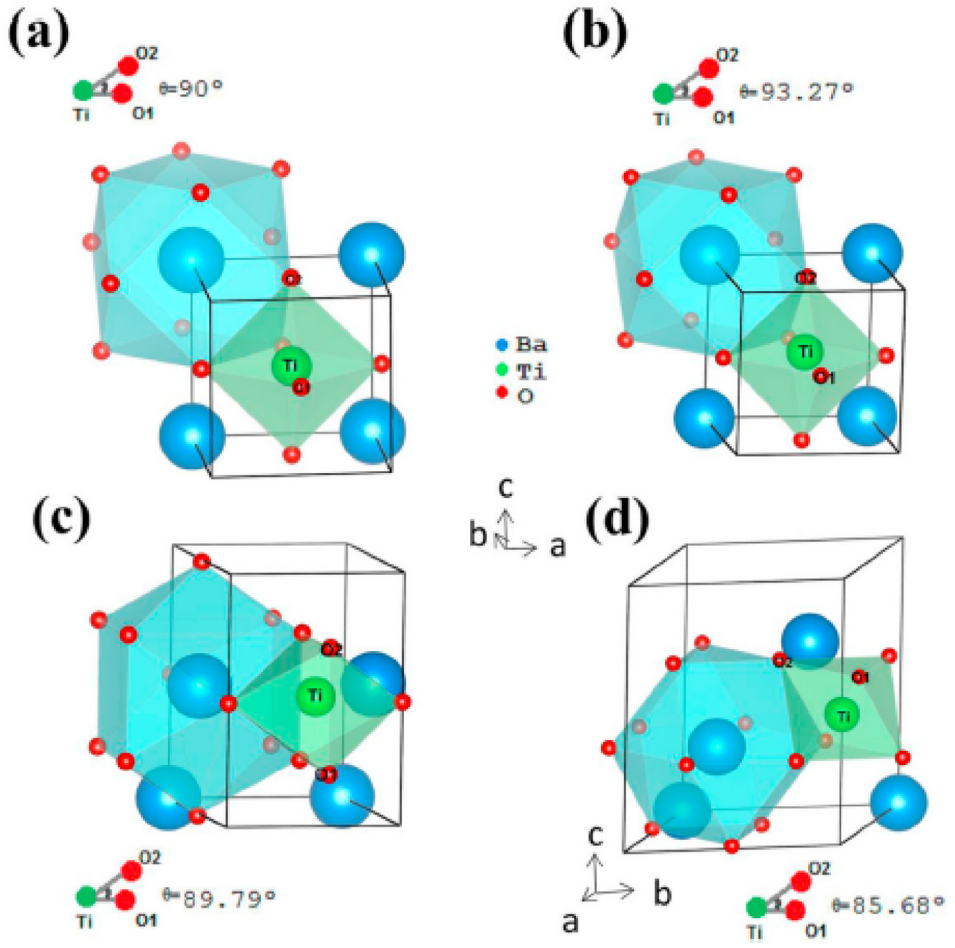

Fig. 5 Schematic illustrations of $BaTiO_3$ crystal structures for (a) cubic (b) tetragonal (c)orthorhombic and (e) rhombohedral (Oliveira et al., 2020).

(Oliveira et al., 2020; Piskunov et al., 2004). Amongst these crystal structures, tetragonal-$BaTiO_3$ (*t*-$BaTiO_3$) has the lowest band energy gap than other phases (orthorhombic and rhombohedral). Owing to its low energy band gap (t-$BaTiO_3$) when compared to other phases, this makes it a suitable piezo semiconductor for photocatalytic degradation of organic waste pollutants present in wastewater. Moreover, due to its well-positioned valence band, it also an important material in water splitting for hydrogen production.

Furthermore, $BaTiO_3$ has a wide band energy gap just like other metal oxides such as TiO_2, ZnO, SnO_2, WO_3 and $BiVO_4$ etc., and its photoactivity is limited by the recombination of photogenerated charge carriers (e^- and h^+), which occurs rapidly (Demircivi and Simsek, 2019). However, unlike normal semiconductors, $BaTiO_3$ is considered also as a piezo semiconductor which produces an internal piezo electric field under mechanical vibration. The induced built-in piezoelectric field separates the photogenerated charge carries, thus reducing their rate of recombination (X. Liu et al., 2020).

Several methods have been proposed to improve the photocatalytic performance of other metal oxide semiconductors such as metal/non-metal doping, formation of several metal oxide based composites, synthesis tailoring to attain certain morphology with improved photocatalytic activity and heterojunction formation with other semiconductors (Ray et al., 2021). These modification methods have been reported to help spatial charge separation and mitigate against fast recombination of photogenerated holes. However, to achieve effective degradation performance, it is proposed that the surface of the semiconductor must be loaded with a reduction cocatalyst and oxidation cocatalyst to achieve long live charge separation and speed up photogenerated hole transfer (G. C. Zhang et al., 2019). The next section, hence discusses the method of preparation and other modification strategies researchers have adopted to improve the performance of $BaTiO_3$.

4. Preparation methods for powdered $BaTiO_3$ and their thin films

Since the discovery of $BaTiO_3$ during World War II (1941–1944) (Bouzidi et al., 2019), there has been a progressive development of $BaTiO_3$ using different preparation approaches including sol–gel, hydrothermal/solvothermal, co-precipitation, mechanochemical and solid-state method. These synthesis methods have an impact on the physical and chemical characteristics of $BaTiO_3$. Thus, it is critical to select appropriate preparation methods, since piezo-photocatalytic activity greatly depends on the physical and chemical properties of $BaTiO_3$.

4.1. Methods to prepare powdered $BaTiO_3$

4.1.1. Hydrothermal method

Hydrothermal synthesis is one of the popular methods for the fabrication of powdered $BaTiO_3$ since it is not expensive and can form stable and pure materials. This method involves a reaction between Barium (Ba) and Titanium (Ti). During their synthesis the most widely used precursors include barium chloride ($BaCl_2$), barium hydroxide ($Ba(OH)_2$), $TiCl_4$ and TiO_2 materials. The hydrothermal reactions take place in an autoclave at temperatures above 100 °C. Several parameters including reaction time, temperature, solvents and solution pH can influence the morphology, particle size and crystal structure of $BaTiO_3$. Xia *et al.* prepared $BaTiO_3$ nano/microcrystals using commercial titanium dioxide (TiO_2) and $Ti(OH)_4$ as a titanium (Ti) precursor mixed with $Ba(OH)_4$ as barium (Ba) precursor (Xia et al., 1996). A very well crystalline and dispersed $BaTiO_3$ with a crystallite size < 100 nm was formed when $Ti(OH)_4$ gel and $Ba(OH)_2$ solution were used as precursors. The results showed that the starting precursors also had a strong impact on the morphology and crystallite size of the prepared $BaTiO_3$. Furthermore, the hydrothermal reaction temperature had a strong influence on the crystal structure. As shown in Table 1, the lattice constant "a" slightly decreased with an increase in reaction temperature. According of the study conducted by Wen *et al.*, it was found that lattice parameter *a* can affect photocatalytic activity of the semiconductor (Wen et al., n.d.). The photocatalyst (TiO_2) anatase material with same composition, morphology, phase, and surface states but different lattice parameter "*a*" were employed for photocatalytic degradation and photo-reduction of toluene and Cr (VI), respectively. However, greater catalytic activity was achieved by TiO_2 with the extended lattice parameter than standard TiO_2. Increasing in the length of the lattice parameter "*a*" caused the bottom of the TiO_2 conduction band to move higher, thus improving its photocatalytic activity.

Moreover, Habib *et al.* showed that the structural morphology of the powdered $BaTiO_3$ was temperature dependent (Habib et al., 2008). According to their result, the hydrothermal $BaTiO_3$ obtained at low temperature (90 °C) had less pores compared to those attained at 120 and 150 °C. The study involving the relationship between photocatalytic activity of $BaTiO_3$ thin film with porosity and surface area was conducted by Augurio *et al.*(Augurio et al., 2022). The porous $BaTiO_3$ thin films exhibited higher photocurrent response than non-porous $BaTiO_3$ thin film, indicating that porosity is beneficial in photocatalysis. This suggested that porous $BaTiO_3$ can enhance interfacial charge transfer whilst lowering the charge carrier recombination rates, thus improving the photocatalytic activity. In another study, Zhan *et al.* controlled the hydrothermal reaction time (from 15 min to 480 h) to obtain $BaTiO_3$ nanoparticles (Zhan et al., 2012). The XRD results showed no diffraction peaks after 15 min of hydrothermal reaction, demonstrating that the material lacked crystalline phases. However, longer hydrothermal reaction times (20 min to 48 h) led to the appearance of diffraction peaks in the XRD patterns that were attributed to the cubic $BaTiO_3$. A continuous increase in the intensity of the diffraction peaks was observed with an increase in reaction time, demonstrating a persistent rise in the crystallinity and size of the crystals. Surmenev *et al.* produced $BaTiO_3$ nano and micro rods via the hydrothermal method. The $BaTiO_3$ nano- and micro rods were obtained at a temperature of 160–210 °C, using 0.02 and 0.15 M (NaOH) concentration and within 45–90 min (Surmenev et al., 2021). The XRD results showed that $BaTiO_3$ purity drastically increased as NaOH concentration increased from 0.025 to 0.15 M. Furthermore, $BaTiO_3$ tetragonal phase was clearly visible after 6 hrs of hydrothermal synthesis at 210 °C and varied alkalinities (from 0.025 to 0.15 M), whereas 45 and 90 min produced a combination of cubic or tetragonal phases. The results showed that the hydrothermal reaction conditions such as temperature, alkalinity and time, have a great impact on the formation of $BaTiO_3$ structures with different morphologies. Wei *et al.* controlled the size of $BaTiO_3$ nanoparticles via hydrothermal approach with Fe doping and ethylenediamine (en) addition (Wei et al., 2008). The crystal size of the synthesized $BaTiO_3$ were investigated by X-ray powder diffraction (XRD), transmission electron microscopy (TEM), scanning electron microscope (SEM) and high-resolution transmission electron microscopy (HR-TEM). The results showed that $BaTiO_3$ crystal size decreased as it was doped with Fe, indicating that Fe-doping suppress the crystal growth. It was further noticed that as Fe doping concentration increases, the average particle size also decreases (Fig. 6). Additionally, the addition of en, which served as both a solvent and a capping agent, may inhibit particle growth and cause a contained effect that changed the shape of the particles from spherical to cubic. It has been reported that semiconductors with smaller particle sizes have excellent photocatalytic activity as compared to those with large particles.

$BaTiO_3$ heterostructures are easily fabricated using the hydrothermal method. Li *et al.* prepared $BaTiO_3/TiO_2$ - heterostructure nanotube arrays using a straight forward hydrothermal process, the hydrothermal reaction was carried out at different reaction times, temperature and concentration of $Ba(NO_3)_2$ (R. Li et al., 2013). Zhao *et al.* and Kappadan *et al.* demonstrated the preparation of $Ag_2O/BaTiO_3$ and $BaTiO_3/ZnO$ heterostructures, respectively, using hydrothermal method (Zhao et al., 2020)(Kappadan et al., 2020a). Based on their experimental results, $BaTiO_3$ nanoparticles were anchored on hexagonal rod-shaped ZnO (Kappadan et al., 2020a). The combination of hydrothermal and microwave method could be used to fabricate $BaTiO_3$ (Sun et al., 2006). For example, Amaechi *et al.* prepared Fe-doped $BaTiO_3$ via ultrafast microwave-assisted hydrothermal method (Amaechi et al., 2021). Furthermore, the hydrothermal approach could be used with the electrospinning method. By combining an electrospinning and a hydrothermal technique, Ren *et al.* developed $ZnO/BaTiO_3$ nanofiber heterostructures (Ren

Table 1 Influence of hydrothermal reaction temperature on lattice constant (Xia et al., 1996).

Temperature (°C)	Lattice constant "a" (Å)	Unit cell volume V_c ($Å^3$)
75	4.031	65.50
100	4.025	65.21
150	4.016	64.77
250	4.012	64.58
300	4.008	64.38
400	4.003	64.14

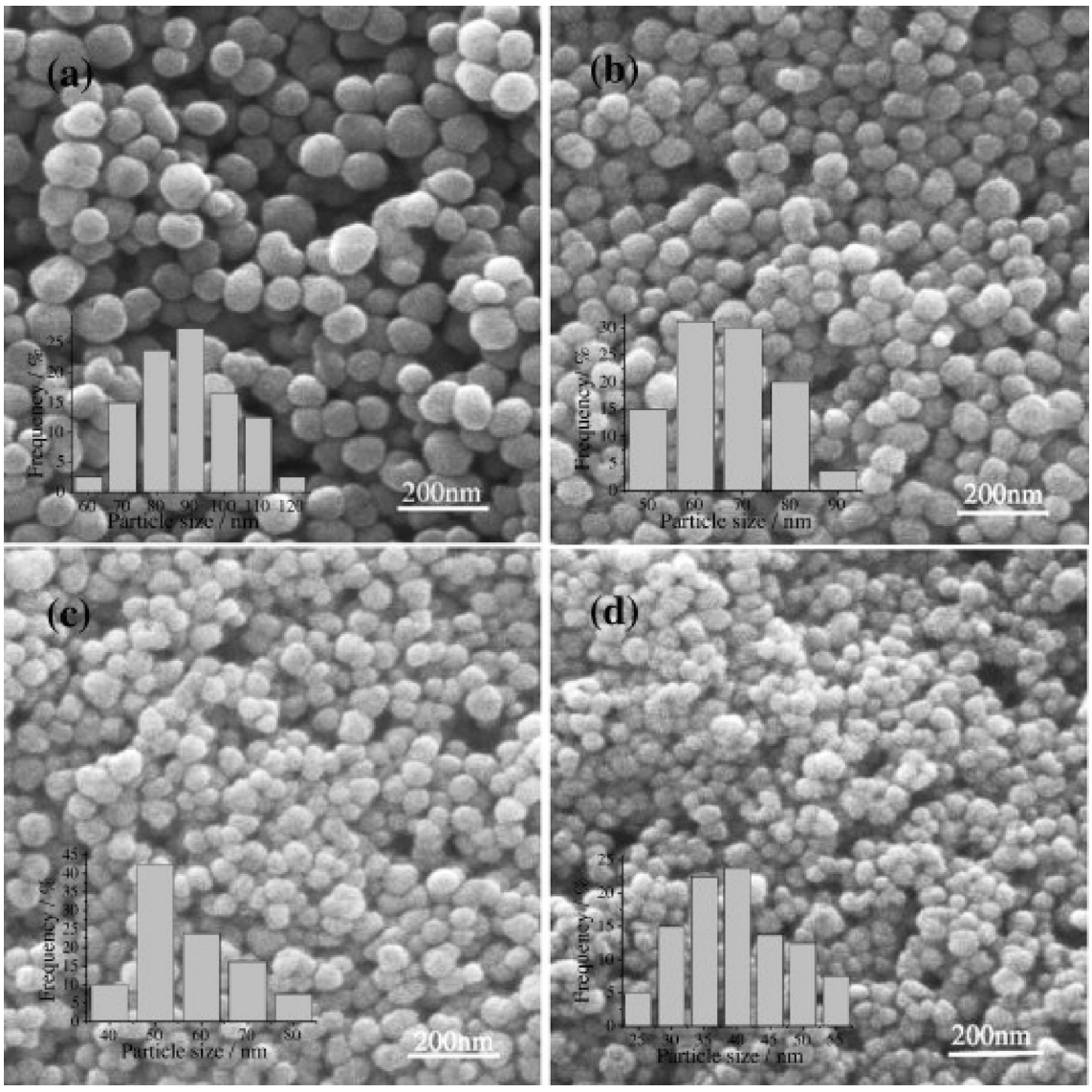

Fig. 6 SEM images of $BaTiO_3$ doped with different concentrations (a)Fe0%, (b) Fe2%, (c) Fe4%, and (d) Fe8% (Wei et al., 2008).

et al., 2012). As seen in Fig. 7(a), $BaTiO_3$ nanofibers had a rather smooth surface and formed a network topology. $BaTiO_3$ nanofibers ranged from 300 to 400 nm in diameter and up to several micrometers in length. The ZnO nanoparticles were uniformly dispersed on the rough surface of $BaTiO_3$ nanofibers (Fig. 7(b)). The elemental composition of the pure $BaTiO_3$ nanofibers and $ZnO/BaTiO_3$ nanofiber heterostructures showed the presence of Ba, Ti, O and Zn. The detected Al element was from aluminium foil.

4.1.2. Sol-gel method

The sol–gel method is another simple method that is used to prepare barium titanates such as $BaTiO_3$, $BaTi_4O_9$, Ba_2TiO_4 and $BaTi_2O_5$. Normally, barium acetate ($Ba(OAc)_2$ and titanium (VI) isopropoxide ($C_{12}H_{28}O_4Ti$) are used as barium and titanium precursors, respectively. The mixture of titanium (VI) isopropoxide and barium acetate solution tends to form $BaTiO_3$-gel which is further dried and calcined at high temperatures (400–1200 °C) (Kavian and Saidi, 2009). The synergic sol gel and template method was used to fabricate $BaTiO_3$ nanotubes (Cao et al., 2006). The formation of $BaTiO_3$-gel was attained via mixing $(Ba(OAc)_2$ and titanium isopropoxide, thereafter the nanostructured $BaTiO_3$-gel grew on the porous alumina membrane (pore size 200 nm). The resultant alumina template covered with $BaTiO_3$-gel was calcined at 700 °C to form $BaTiO_3$ nanotubes with 50 μm length. The calcination temperature had a significant impact on the BET surface area of the $BaTiO_3$. Pffaf (Pfaff, 1992) indicated that the BET surface area of $BaTiO_3$ prepared via sol–gel method decreased as the calcination temperature increased (Table 2). The high specific surface was obtained when $BaTiO_3$-gel was calcined at low temperature (200 °C). It has been reported that at elevated temperatures, nanoparticles tend to agglomerate extensively thus resulting in a significant reduction in BET surface area and pore diameter (Zhang et al., 2015).

However, XRD diffraction showed highly pure crystalline $BaTiO_3$ obtained at higher temperature. At high calcination temperatures above 800 °C, the crystal structure of $BaTiO_3$

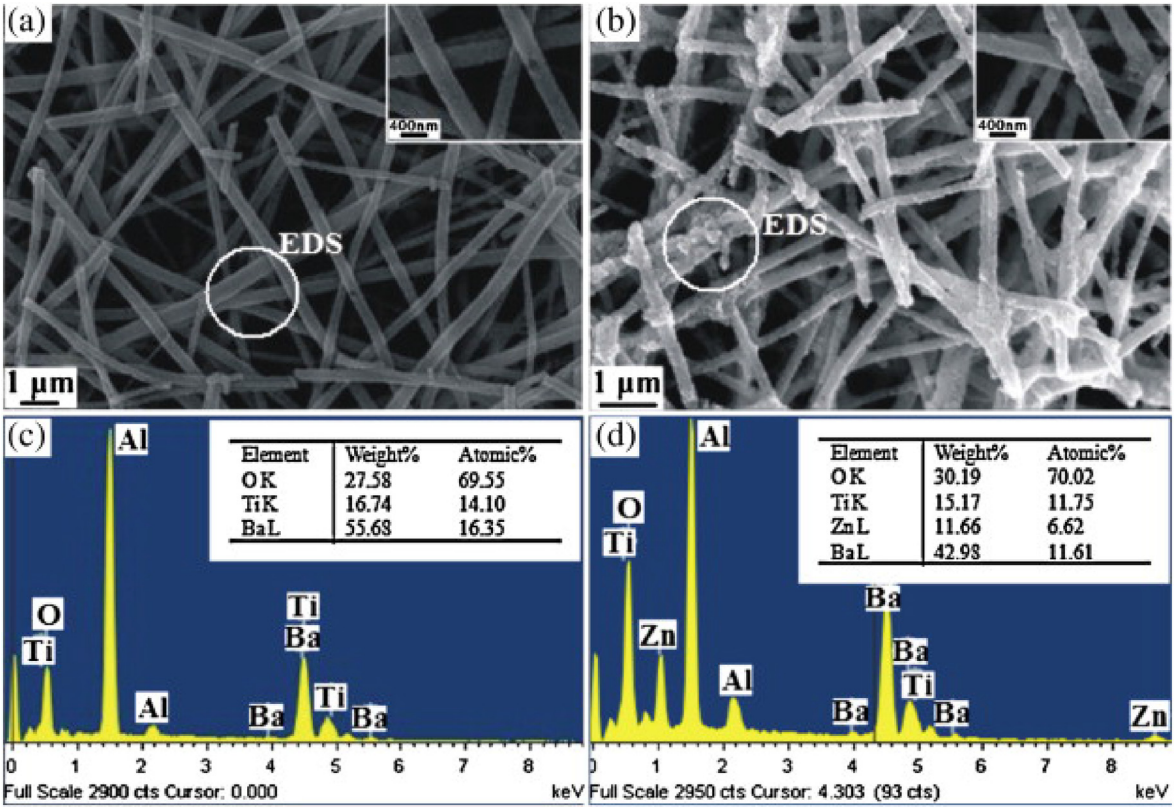

Fig. 7 SEM images of (a) pure $BaTiO_3$ nanofibers, (b) ZnO/$BaTiO_3$ heterostructures, (c) EDS of $BaTiO_3$ nanofibers and (d) EDS of ZnO/$BaTiO_3$ heterostructures (Ren et al., 2012).

Table 2 Effect of calcination temperature on the BET surface area of $BaTiO_3$ (Pfaff, 1992).

Calcination temperature (°C)	Specific surface area (m^2/g)	Average particle diameter (μm)
200	125	0.01
400	105	0.01
500	80	0.01
600	55	0.02
700	37	0.03
800	23	0.04
900	14	0.07

transformed from cubic to tetragonal structure. This crystal structure transformation (cubic to tetragonal) was depicted by XRD peak splitting at 2θ value approximately 45° (Fig. 8) [70]. From this study, it can be noted that crystallinity did have an influence on the optical properties of the semiconductors. According to literature, the optical band energy gap of the semiconductors decreases with an increase in crystallinity. Nishioka and Maeda (Nishioka and Maeda, 2015) studied the influence of the post heating of the hydrothermally synthesized Rhodium-doped barium titanate ($BaTiO_3$:Rh) which could increase crystallinity and further improve photocatalytic activity. The XRD patterns were stronger and narrower after post heating 900 °C, thus confirming crystallization. However, the specific surface area was reduced from 8 to 4 m^2 g^{-1}. UV–vis diffuse reflectance spectroscopy (DRS) was employed to investigate the optical properties of $BaTiO_3$:Rh. Upon post heating, DRS exhibited a series of changes as the temperature increased (with exception of the sample at 1150 °C). At higher temperatures, Rh^{4+} species induced greater absorption at longer wavelengths. This would make sense because at a high-temperature heat treatment increased the oxidation of Rh^{3+} to Rh^{4+} in $BaTiO_3$:Rh. In terms of photocatalytic activity, unheated samples tend to show low activity, while on the other hand the activity increased with an increase in post heating temperature until 1000 °C. At elevated temperature above 1000 °C, the photocatalytic activity of $BaTiO_3$:Rh decreased drastically.

Sol gel was combined with low temperature hydrothermal reaction procedure to prepare $BaTiO_3$ nanopowder (Wang et al., 2013). In the study reported by Wang *et al.*, it was found that experimental conditions such as potassium hydroxide concentration (KOH), reaction temperature and time had a significant role on the crystallinity and morphology of $BaTiO_3$ powder (Wang et al., 2013). A highly crystalline pure $BaTiO_3$ with a cubic structure was obtained at 120 °C (after 2 h of reaction time) with KOH concentration over 1.0 M. The hydrothermal and reaction time showed less effect on the crystallinity and morphology, whereas KOH concentration showed a significant impact on the crystallinity and morphology. It was observed that, when the KOH concentration rised from 1.0 M to 8.0 M, the average size of the $BaTiO_3$ particles decreased from 370 nm to 100 nm.

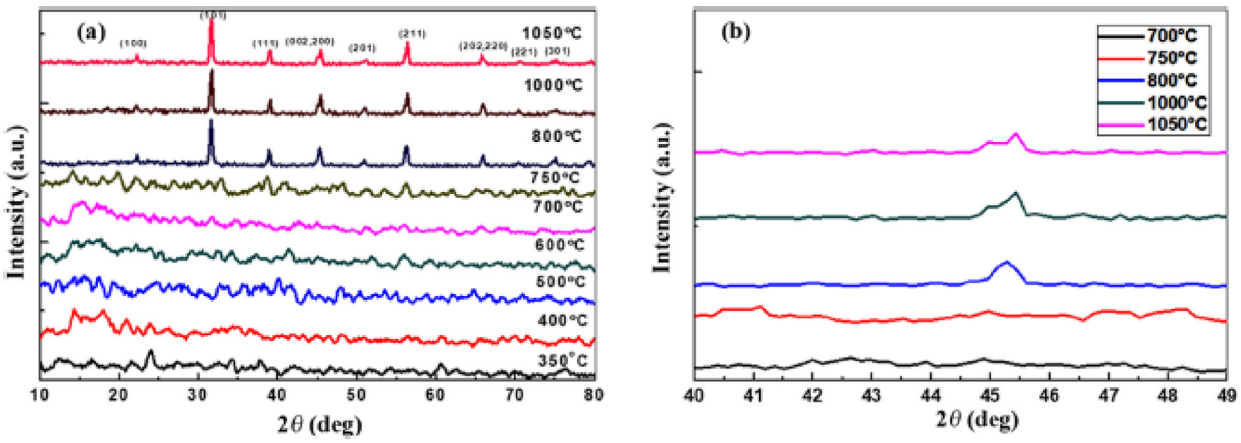

Fig. 8 (a) and (b) XRD patterns for $BaTiO_3$ (El-Sayed et al., 2020).

4.1.3. Solid state-method

Solid state synthesis is a common method which is usually employed to produce polycrystalline materials such as barium titanate ($BaTiO_3$). This method requires a very high temperature, however its benefits include simplicity and high yield production. The main factors which affect solid state reaction include reaction temperature, pressure, chemical and morphological properties of the starting reagents/materials. The solid state synthesis of $BaTiO_3$ nanoparticles was reported by Qi *et al.* (Qi et al., 2020). In their studies, different molar ratios of Barium nitrate ($Ba(NO_3)_2$) and Ti powder (Ba/Ti) as starting materials were varied and calcined at different temperatures (500, 550 and 600 °C). The calcination temperature played a crucial role in the formation of $BaTiO_3$. This was confirmed by the XRD pattern which showed that there was no formation of $BaTiO_3$ at temperatures below 500 °C, since only XRD peaks for starting materials ($Ba(NO_3)_2$ and Ti) were revealed (Fig. 9). At high temperature (600 °C), the peaks were almost indexed to $BaTiO_3$ material, thus now confirming the effect of calcination temperature on these materials. Other studies reported the thermal decomposition reaction of barium carbonate ($BaCO_3$) and titanium dioxide (TiO_2) for the formation of $BaTiO_3$ (Pithan et al., 2005). Since the rate of reaction is controlled by the diffusion rate of Ba ions into Titanium dioxide (TiO_2) lattice, the shape and size of the $BaTiO_3$ produced was more influenced by the TiO_2 morphology. The formation of titanates were explained in detail in the literature (Beauger et al., 1983). Trzebiatowski *et al.* reported that the formation of barium titanate ($BaTiO_3$) and barium orthotitanate (Ba_2TiO_4) occurs simultaneously via the below chemical reaction (Brdi et al., 1950);

$$BaCO_3 + TiO_2 \rightarrow BaTiO_3 + CO_2 \quad (1)$$

$$2BaCO_3 + TiO_2 \rightarrow Ba_2TiO_4 + 2CO_2 \quad (2)$$

In other studies they have reported that Ba_2TiO_4 forms when $BaTiO_3$ reacts with TiO_2 as shown in equation (4), thereafter the formed Ba_2TiO_4 reacts with the remaining TiO_2 to produce meta titanate as shown in equation (5) (Beauger et al., 1983).

$$BaTiO_3 + BaCO_3 \rightarrow Ba_2TiO_4 \quad (4)$$

$$Ba_2TiO_4 + TiO_2 \rightarrow 2BaTi\ O3$$

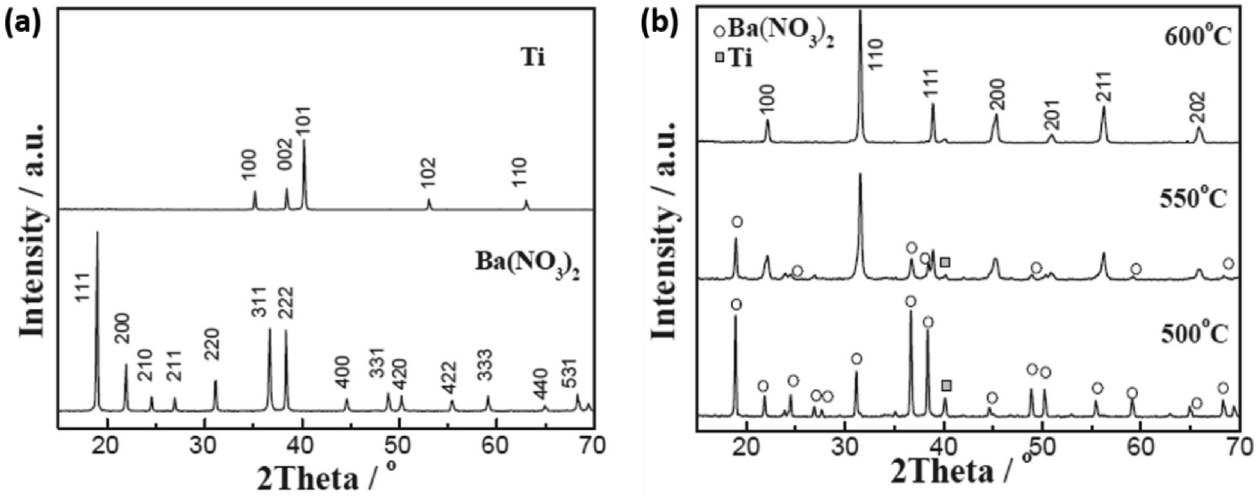

Fig. 9 (a) and (b) XRD patterns for $BaTiO_3$ (Qi et al., 2020).

Solid state reaction method could be combined with sol–gel method. Mi *et al.* prepared nano $BaTiO_3$ ceramics using TiO_2 - precursor gel and $BaCO_3$ as starting raw materials (Mi et al., 2020). The XRD results showed the initial formation of $BaTiO_3$ at calcination temperatures of 600 °C. A cubic $BaTiO_3$ structure was formed when the calcination temperature reached 800 °C. At 900 °C calcination temperature, the diffraction peak of (200) separated into peaks of (002) and (003), thus suggesting phase transition from cubic to tetragonal phase. In another experiment, Ren *et al.* used a solid state method to fabricate $Bi_2O_3/BaTiO_3$ heterostructure (Ren et al., 2013). Firstly, $BaTiO_3$ was prepared from $Ba(CH_3COO)_2$ and $TiCl_4$ via the hydrothermal treatment process. Thereafter, $Bi_2O_3/BaTiO_3$ heterostructure were prepared through ball milling and calcination process using the prepared $BaTiO_3$ and commercial Bi_2O_3 (mass ratio $BaTiO_3$: Bi_2O_3 = 4:1). After the calcination procedure, it was discovered that Bi^{3+} had dissolved in the $BaTiO_3$ lattice and that a chemical connection had been created at the interface between Bi_2O_3 and $BaTiO_3$.

4.1.4. Ultrasound assisted

Recently sound energy has been utilized to prepare different metal oxide semiconductors such as $BaTiO_3$ for different applications. In contrast to basic reactions, ultrasound-assisted reactions actually have a lot of advantages. High pressure, low pressure, and localized boiling zones are all produced by ultrasound in the reaction mixture. This shortens the reaction period and makes room-temperature synthesis possible. It has been noted that ultrasonography facilitates the uniform dispersion of reactants in a reaction mixture. Dang *et al.* reported sonochemically synthesized $BaTiO_3$ nanoparticles (Dang et al., 2011). In their study, mixtures of ethanol and distilled water were prepared with different volume ratios. Thereafter, $BaCl_2$ and $TiCl_4$ (molar ratio Ba:Ti = 1:1 were added to the above solution mixture, followed by addition of NaOH. The solution suspension was exposed to ultrasonic irradiation for 40 min at low temperature (50 °C). The applied ultrasonic energy was 150 W/cm^2. Following synthesis, the precipitate was centrifugally separated, twice washed with deionized water, and then dried for two hours in a vacuum at 100 °C. In another study, $BaTiO_3$ submicronic particles were prepared following multiple procedures such ultrasonication, microwave drying and thermal treatment (Rotaru et al., 2017). Mixture of $BaCO_3$ and TiO_2 as raw materials were ultrasonicated (ultrasonic frequency: 20 kHz, 750 W nominal electric power) in milli-Q ultrapure water. After 30 and 60 min of ultrasonication, the prepared samples were dried in the microwave furnace for 10 min. The last procedure was thermal treatment of the samples at different temperatures (780–1300 °C) for 3 hrs. Ashiri *et al.* reported similar approach to obtain $BaTiO_3$ nanocrystals via rapid ultrasound-assisted wet chemical method (Ashiri et al., 2015). Utara and Hunpratub synthesized cubic structure of $BaTiO_3$ nanoparticles using ultrasonic method at room temperature without thermal treatment step (Utara and Hunpratub, 2018a). The starting precursors were barium hydroxide $(BaOH)_2$ and diisopropoxytitanium bis (acetylacetonate) ($C_{12}H_{28}O_6Ti$). The effect of ultrasonic reaction time on the morphology of $BaTiO_3$ nanoparticles (NPs) was investigated using TEM micrographs. It was found that the particle sizes of the $BaTiO_3$ NPs decreased with increase in ultrasonic reaction time. The average particle size reduced from 56.69 ± 30.14 nm (30 min of ultrasonic irradiation) to 32.72 ± 11.83 nm (4 hr of ultrasonic irradiation). Similar observations were reported by Moghtada and Ashiri (Moghtada and Ashiri, 2016). It was concluded that smaller particles were produced as a result of ultrasonic irradiation at 50 °C.

4.1.5. Co-precipitation

Co-precipitation method is the most frequently utilized synthesis approach for metal oxides (Rao et al., 2017). This method involves dissolving of metals salts in an appropriate solvent, followed by the addition of a precipitating agent. The most widely used precipitating agents include sodium hydroxide (NaOH), ammonium hydroxide (NH_4OH) and potassium hydroxide (KOH). In case of preparing $BaTiO_3$ using oxalate co-precipitation, it is challenging to obtain optimal conditions where both Barium (Ba) and Titanium (Ti) precipitates at the same time. Since Titanium (Ti) precipitates as titanly oxalate in the presence of alcohol at pH $\leq$ 2 whereas Barium (Ba) precipitates as BaC_2O_4 at pH $\geq$ 4. Titanium generates soluble anionic species such as $TiO(C_2O_4)_2^{2-}$ in the pH between 2 and 4, thus influencing the stoichiometry ratio of Ba/Ti simultaneously (Geetha et al., 2016). It has been reported that through manipulation of several chemical conditions such as pH, reactants, and reaction medium, it is possible to make Ba and Ti to precipitate at the same time. Prasadarao *et al.* investigated the influence of pH (range 2–10) on the synthesis of $BaTiO_3$ from barium chloride ($BaCl_2$) and potassium titanyl oxalate (KTO) (Prasadarao et al., 2001). The formation of barium titanyl oxalate was obtained at pH 2.5 and an increase in pH to 5 led to the formation of barium titanyl hydroxy oxalate. At higher pH values (7–9), precipitation reactions yielded a mixture of titanium dioxide (TiO_2) and barium oxalate (BaC_2O_4). He *et al.* also prepared $BaTiO_3$ powder via the co-precipiation of $BaCl_2$ and $TiOCl_2$ in an highly-alkaline environment (He et al., 2014). The pH solution and concentration of the starting precursors ($BaCl_2$ and $TiOCl_2$) had an effect on the particle grain size and homogeneity of the $BaTiO_3$ powder. An average particle size of approximately 80 nm was obtained at pH 14 and reaction temperature of 80 °C. In another study, Zhang *et al.* used $BaCl_2$, $TiCl_4$ as starting raw materials and tartaric acid as a precipitant agent for the preparation of tetragonal $BaTiO_3$ nano-powder (X. Zhang et al., 2021). The white precipitated were formed by adding slowly a solution of ammonium hydroxide solution. Followed by thermal treatment at different calcination temperatures (750–1050 °C) for 4 hrs. The microwave assisted co-precipitation was reported to produce $BaTiO_3$@rGO nanocomposite (Khan et al., 2021a). $BaTiO_3$ and GO as starting materials were prepared separately via the sol–gel method and modified Hummers method, respectively. Thereafter, a certain amount of $BaTiO_3$ and rGO were added to 50 ml of deionised water and stirred for 1 hr at room temperature. Then, NaOH solution was slowly added to the above mixture solution, and heated for 1 hr in a microwave oven. The reduction of GO into rGO was confirmed by color change of the solution from brown to black. The co-precipitated nanocomposite was washed with mixture of ethanol/water and dried at 60 °C in an oven for 12 hr. The TEM images of pure $BaTiO_3$ and $BaTiO_3$@rGO are shown in Fig. 10 **(a-b)**. As shown in Fig. 10(a), pure $BaTiO_3$ exhibits

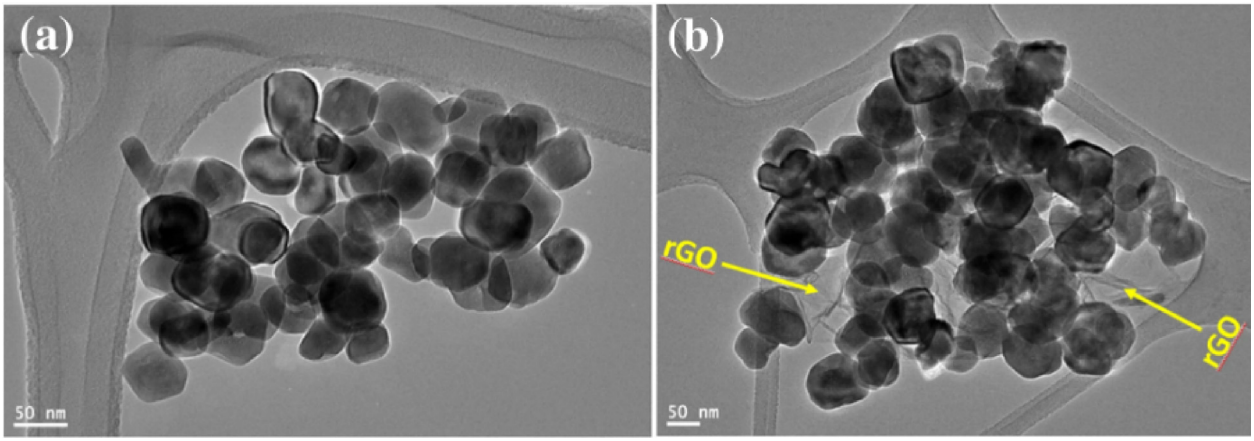

Fig. 10 TEM images for (a) pure $BaTiO_3$ and (b) $BaTiO_3$@rGO (Khan et al., 2021a).

Table 3 Various synthetic procedures and morphologies.

Materials	Synthesis method	Starting materials	Morphology	Ref
$BaTiO_3$	Hydrothermal	$Ba(OH)_2{\cdot}8H_2O$, TiO_2	Cubic phase	(Zhan et al., 2012)
$BaTiO_3$	Hydrothermal	$Ba(OH)_2{\cdot}8H_2O$, $Ti(OBu)_4$	Cubic, Tetragonal	(Ji et al., 2022)
$BaTiO_3$	Sol-gel	$C_4H_6BaO_4$, $C_{12}H_{28}O_4Ti$	Tetragonal phase	(Kavian and Saidi, 2009)
$BaTiO_3$	Sol-gel template	$Ba(OAc)_2$, $Ti(OPri)_4$	Nanotubes	(Cao et al., 2006)
$BaTiO_3$	Hydrothermal	$(Ba(NO_3)_2$, TiO_2	Spherical like, Tetragonal	(Li et al., 2020)
$BaTiO_3$	Sol-gel and solid state	$BaCO_3$, TiO_2	Whisker like, Cubic, Tetragonal	(Mi et al., 2020)
$BaTiO_3/TiO_2$	Hydrothermal	$(Ba(NO_3)_2$, TiO_2	Nanotube arrays	(R. Li et al., 2013)
$BaTiO_3$	Hydrothermal	$Ba(OH)_2{\cdot}8H_2O$, $Na_2Ti_3O_7$, TiO_2	Nanoparticles, Nanowires, Nanosheets	(Yu et al., 2021)
$BaTiO_3$@rGO	Microwave assisted- co-precipitation	$C_4H_6BaO_4$, $C_{12}H_{28}O_4Ti$	Spherical	(Khan et al., 2021a)
$BaTiO_3$	Sonochemical	$Ba(OH)_2$, $C_{12}H_{28}O_6Ti$	Irregular Bowl-like structure	(Utara and Hunpratub, 2018b)
$BaTiO_3$	Microwave-hydrothermal	$Ba(OH)_2{\cdot}8H_2O$, $(Ba(NO_3)_2$ $BaCl_2$, $Ti(OBu)_4$	Nanocuboid	(Chen et al., 2016)

spherical nanoparticles with a size distribution of 10–30 nm, whereas Fig. 10(b) shows spherical $BaTiO_3$ nanoparticles with an average particle size range of 15–34 nm, which are uniformly distributed on the surface of rGO sheet. Table 3 highlights the summary of some of the synthetic methods for $BaTiO_3$ powder.

These techniques are mostly applied to prepare powdered $BaTiO_3$, however powdered piezo-photocatalyst are difficult to be recycled in practical applications. For instance, after the degradation process, some parts of the powdered catalyst may persist in the aqueous solution, thus leading to secondary pollution. Therefore, recently piezo-photocatalyst based thin films are being developed for better recoverability, thus in the next section some common techniques that are used to produce $BaTiO_3$ based thin films will be highlighted.

4.2. Preparation $BaTiO_3$ based thin films

There are various methods implemented for the preparation of $BaTiO_3$ thin films, these include physical and chemical techniques. The physical methods include sputtering deposition, pulsed laser deposition (PLD), spin coating, dip coating and the Dr Blade method (Asadzadeh et al., 2021; Cernea, 2004). Chemical methods include chemical vapour deposition (CVD), sol–gel method and hydrothermal method. All of these have their own advantages and disadvantages. Cernea *et al.* explained most of these methods basic principle and their own benefits (Cernea, 2004). In this review, a few common physical and chemical methods are discussed below.

4.2.1. Dip coating

Dip coating is one of the most popular liquid-phase deposition methods for the fabrication of thin-films. This method involves dipping a substrate in the solution containing a starting material/ceramic powder, binder, solvent and dispersant. Once the material of interest has been deposited, the substrate is removed slowly from the solution and dried at ambient temperature. Several parameters such as immersion period, withdrawal rate, number of immersion cycles, solution composition, concentration and temperature tends to affect the film characteristics, smoothness and thickness (Schneller et al., 2013). This method has been used for the production

of numerous piezoelectric thin-films including Pb (Zr, Ti)O_3, $CaBi_4Ti_4O_{15}$, ZnO, PVDF and $BaTiO_3$. Ashiri *et al.* reported a crack-free nanostructured $BaTiO_3$ produced from a modified sol–gel dip coating method (Ashiri et al., 2014). The silica substrate was immersed into a sol prepared from barium acetate, glacial acetic acid, titanium tetraisopropyl alkoxide and 2-propanol. After deposition, the substrate with coated $BaTiO_3$ was taken out from the sol–gel solution with a withdrawal rate of 1 cm/min and dried at 100 °C. The resultant substrate coated with $BaTiO_3$ was further calcined at 800 °C for 1 hr (heating rate 5 °C/min) to produce a thin film with a thickness of approximately 2 nm.

4.2.2. Spin coating

In the spin coating process, the coating material is firstly dissolved in an appropriate solvent and the solution is dropped at the centre of the solid substrate surface. The solid substrate is then spun at controlled high speed. During this process, the solid substrate is rotated around an axis which is perpendicular to the coated region. The thickness and other properties of the final thin film depends greatly on the spinning rate of the substrate, viscosity of the solution, solvent evaporation rate, spinning time and surface wettability. This method is suitable and can be used for fabrication of several ceramics, including barium titanates such as $BaTiO_3$ (Aminirastabi et al., 2020).

4.2.3. Chemical vapour deposition (CVD)

Chemical vapour deposition is a widely used method to produce 2D nanomaterials and thin films. In this process, a solid material is deposited from the vapour by a chemical reaction occurring on or in the vicinity of a typically heated substrate (Mittal et al., 2021). The thin film nanostructures and thickness can be tuned by controlling the deposition conditions and the CVD system key factors. These include the substrate material and precursors, composition of reaction gas mixture, total pressure gas flows and temperature. Suzuki and Kijima (Suzuki and Kijima, 2006) prepared nanostructured $BaTiO_3$ thin film from bis-dipivaloylmethanate barium ($Ba(DPM)_2$) and titanium (IV) isopropoxide ($Ti(OiPr)_4$ deposited on platinum/alumina/silica/silicon ($Pt/Al_2O_3/SiO_2/Si$) substrate using the CVD technique assisted with Inductively Coupled Plasma (ICP). The size of the resultant nanostructured $BaTiO_3$ thin film was greatly influenced by substrate temperature. The single phase $BaTiO_3$ structure and particles sizes of approximately 30 nm were successfully obtained at temperature of 500 °C (Fig. 11(a)). The deposited spherical $BaTiO_3$ nanoparticles on the surface of the substrate were more agglomerated with less pores. Fig. 11(b) shows a cross section image of the deposited dense nanoparticles on the substrate surface, however the thickness of the thin film was not determined. At substrate temperatures above 600 °C, the deposited $BaTiO_3$ nanoparticles fused into a columnar form as shown in Fig. 11(-c)-(d). The bottom of the thin films formed, exhibited a columnar structure, whereas the structure surrounding the surface was made of nanoparticles.

4.2.4. Dr Blade /Tape casting method

Tape casting known as the Dr.Blade method has been widely used for the production of ceramic thin films. This technique is usually used to obtain thin films with a thickness ranging from 10 to 1000 μm. In this method, the powdered starting materials are mixed with appropriate solvents and binders to form a homogeneous mixture which is tape casted on the solid substrate (Asadzadeh et al., 2021). Thereafter, the tape casted substrate is dried at certain temperatures. The drying rate and temperature tend to be the most important factors which control the crack free of the thin film. Other factors which can affect the thin film properties and thickness include relative content of ceramic powder (starting materials), solvent and binder. Lilge *et al.* hydrothermally synthesized $BaTiO_3$ powder from $BaCl_2.8H_2O$ and Ti $[OCH(CH_3)_2]_4$ (Lilge et al., 2020). The hydrothermal reaction place was performed in a microwave for 120 min at 140 °C. The resultant $BaTiO_3$ powder was further used to prepare a photoanode electrode using the Dr Blade method. For the preparation of the photoanode electrode, the powdered $BaTiO_3$ was mixed with ethylene glycol Triton X-100 and ethanol. The slurry mixture was then taped casted on the FTO substrate (area of 1 cm^2) to form a thin film. The $BaTiO_3$ pasted on the surface of FTO appeared to be spherical in shape and agglomerated (Fig. 12).

5. Modification of $BaTiO_3$ for enhanced piezo-photocatalytic efficiency

Despite the fact that $BaTiO_3$ as a semiconductor has received a lot of attention for piezo-photocatalytic applications due to its incredible ferroelectric/piezoelectric properties and accessibility in a wide assortment of sizes and morphologies, it has significant limitations, most which are linked to its photocatalytic activity (X. Liu et al., 2020; Ray et al., 2021). Owing to its wide energy band gap of approximately 3.2 and 3.4 eV, it is associated with rapid recombination of photogenerated electron-holes which reduces its photocatalytic activity. Recently, various strategies have been explored including tailoring the morphology and particle sizes, doping and fabrication of heterojunction/composite photocatalyst to prevent some of these limitations (Scheme 1).

5.1. Tailoring $BaTiO_3$ morphology and particle size

The surface morphology and particles size of the semiconductor photocatalyst/piezocatalyst plays an important role in the catalytic degradation of organic waste pollutants. It has been reported that $BaTiO_3$ with different morphological structures including nanowires, nanofibers, nanorods, nanotubes, nanocubes and nanoparticles exhibits different piezoelectricity. For example, 1-D fiber/wire piezoelectric materials show a superior piezocatalytic response as compared to spherical particles. Whereas, thin sheet-like 2-D structures also generate more piezoelectricity under mechanical vibration (Mondal et al., 2022). As piezocatalyst, Liu *et al.* explored different nanostructures (nanocubes (NCs), nanoparticles (NPs) and nanofibers (NFs)) of $BaTiO_3$ for piezocatalytic degradation of Rhodamine B (Rh B) (D. Liu et al., 2020). $BaTiO_3$ nanofibres showed greater piezocatalytic performance as compared to nanocubes (NCs) and nanoparticles (NPs) due to a higher surface area, easy deformation structure and fine crystal size. Moreover, Jiao *et al.* prepared different $BaTiO_3$ nanostructures via the hydrothermal route at different reaction times (starting from 4 to 16 hr) (Jiao et al., 2017). Spherical $BaTiO_3$ nanoparticles formed at 4–8 hrs were more effective for photocatalytic degradation of Rh B dye than other morphological

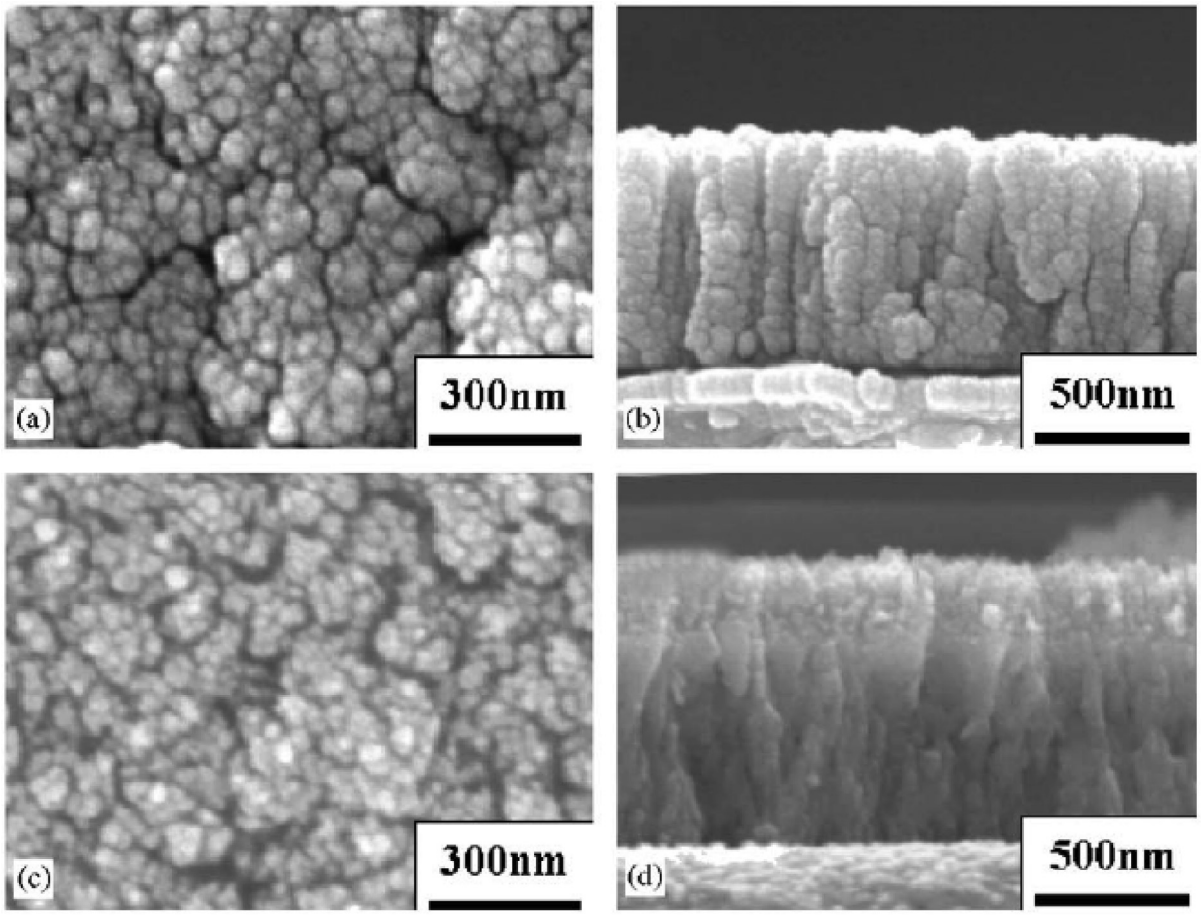

Fig. 11 Surface SEM images and cross section images of the films deposited at different substrate temperatures; (a) surface image at 500 °C, (b) cross section at 500 °C, (c) surface at 600 °C and (d) cross section at 600 °C (Suzuki and Kijima, 2006).

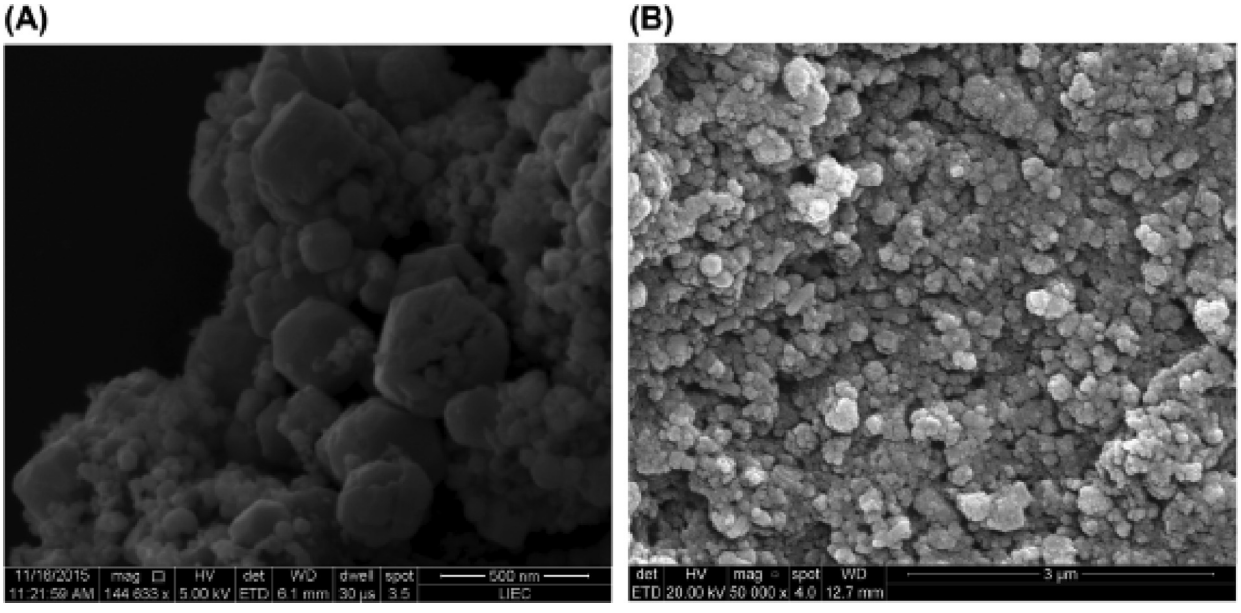

Fig. 12 (a) and (b) Surface SEM images of FTO/$BaTiO_3$ (Lilge et al., 2020).

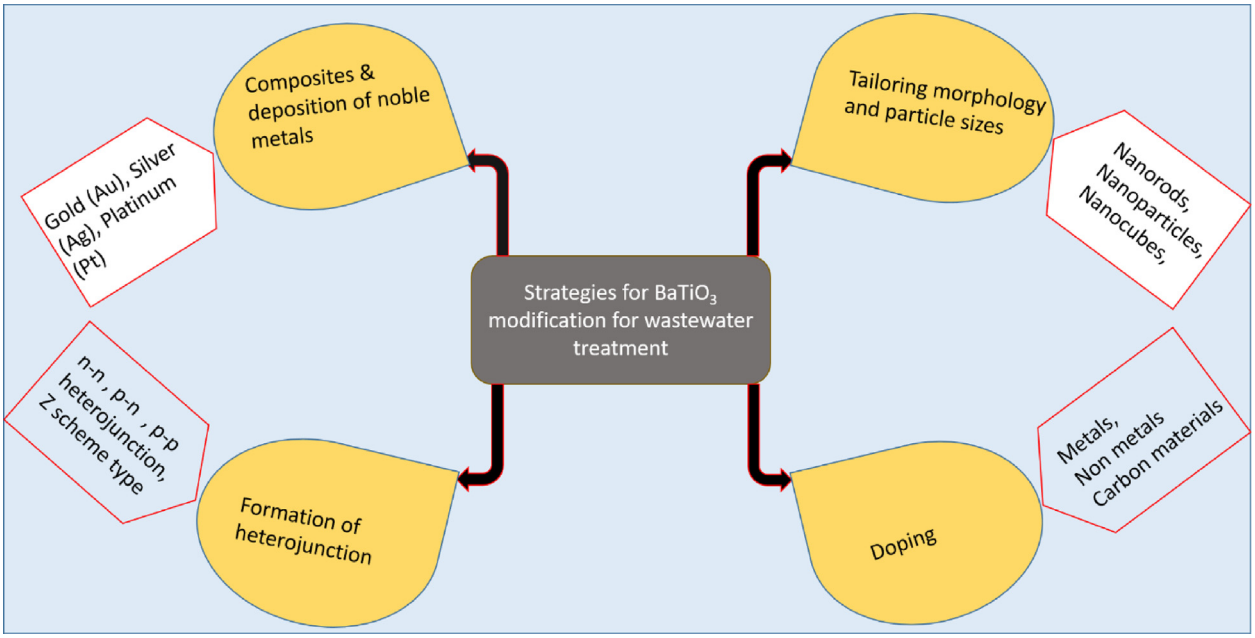

Scheme 1 Illustrations of $BaTiO_3$ modifications for water and wastewater treatment.

nanostructures such as bowl like and agglomerated spherical particles. To further understand the enhancement in photocatalytic activity due to morphological-tuning of the semiconductor photocatalyst, different analyses including BET surface area, photon energy, electrochemical Impedance Spectroscopy (EIS), photoluminescence (PL) and photocurrent also need to be conducted. Since the method of preparation has an impact on the final morphological product, various authors have also synthesized these piezomaterials using varying methods Xiong *et al.* fabricated $BaTiO_3$ nanocubes, since cubic structures are known to have the best ability to reduce crystal defects and increase the surface-to-volume ratio (Xiong et al., 2015). The effect of reaction time (24, 48, 74 hr) using the hydrothermal method was employed to produce the cubic like $BaTiO_3$ structure (Fig. 13(a)-(f)). The particle size increased with an increase in hydrothermal synthesis duration. Furthermore, the edges of the cube got sharper as the reaction time increased, showing an increase in the cubic phase's crystallinity. The $BaTiO_3$ nanocubes formed over period of 48 hrs exhibited impressive photocatalytic performance under light irradiation. This better performance was due to more uniform morphological distribution, higher crystallinity, small particle size and higher surface area which lead to more active sites, reduction in migration path of charge carriers, narrowing the energy band gap and reducing the rate of charge carrier's recombination.

The optical properties of the $BaTiO_3$ nanocubes calcined at different temperature were investigated by photoluminescence (PL) and UV vis spectrophotometer. The calcination temperature had an effect on the optical properties of the hydrothermally synthesized $BaTiO_3$ reported by Hasbullah *et al.* (Hasbullah et al., 2019). The energy band gap calculated from tauc's plot (Fig. 14) for $BaTiO_3$ calcined at 500, 600, 700 and 1000 °C were 3.18, 2.87, 2.83 and 2.74 eV, respectively. Upon increasing the calcination temperature, the energy band gaps of $BaTiO_3$ were expected to increase due to their high crystallinity. However, $BaTiO_3$ resulted in lower energy band gap than expected. This could be due to inadequate oxygen delivery during the calcination process in ambient air resulted in oxygen deficiency in $BaTiO_3$ structures (Orhan et al., 2005). As a result, the calcined $BaTiO_3$ had a greater density of oxygen vacancy or non-bridging oxygen. The oxygen vacancy has the potential to change the $BaTiO_3$ structure and cause localized electronic states. Therefore, resulting in reduction of energy band gaps for extremely crystalline $BaTiO_3$ structures.

Moreover, photoluminescence (PL) was employed to study the rate of photogenerated electrons and holes recombination. As seen in Fig. 15(a)-(f), the PL intensity was expected to decrease with increase in crystallinity. However, in this study the PL intensity reached its highest peak as the calcination temperature was elevated to 1000 °C. It was hypothesized that the increase in photoluminescence intensities is due to the presence of a localized state within $BaTiO_3$ structures. With sufficient stimulation, the localized state effectively lowers the band gap of $BaTiO_3$ structures, hence resulting in strong photoluminescence intensity.

5.2. Doping

Metal or non-metal doping is one of the most popular methods used to modify semiconductor photocatalysts to improve their optical properties such as a reduction of band gap and photogenerated charge carriers (electron-holes), increase in photocurrent response and interfacial charge carries. The improvement of these properties tends to enhance the photocatalytic and piezo-photocatalytic degradation of organic wastewater pollutants. It has been reported that the modification of photocatalyst semiconductors such as TiO_2 (Khairy and Zakaria, 2014), ZnO (Kaur and Singhal, 2014), WO_3 (Peleyeju and Viljoen, 2021), $BiVO_4$ (Orimolade and Arotiba, 2020)and $BaTiO_3$ (Ray et al., 2021) by metal ion doping can successfully shift their optical absorption to the visible light region, thus narrowing their band gaps. Recently, a lot of

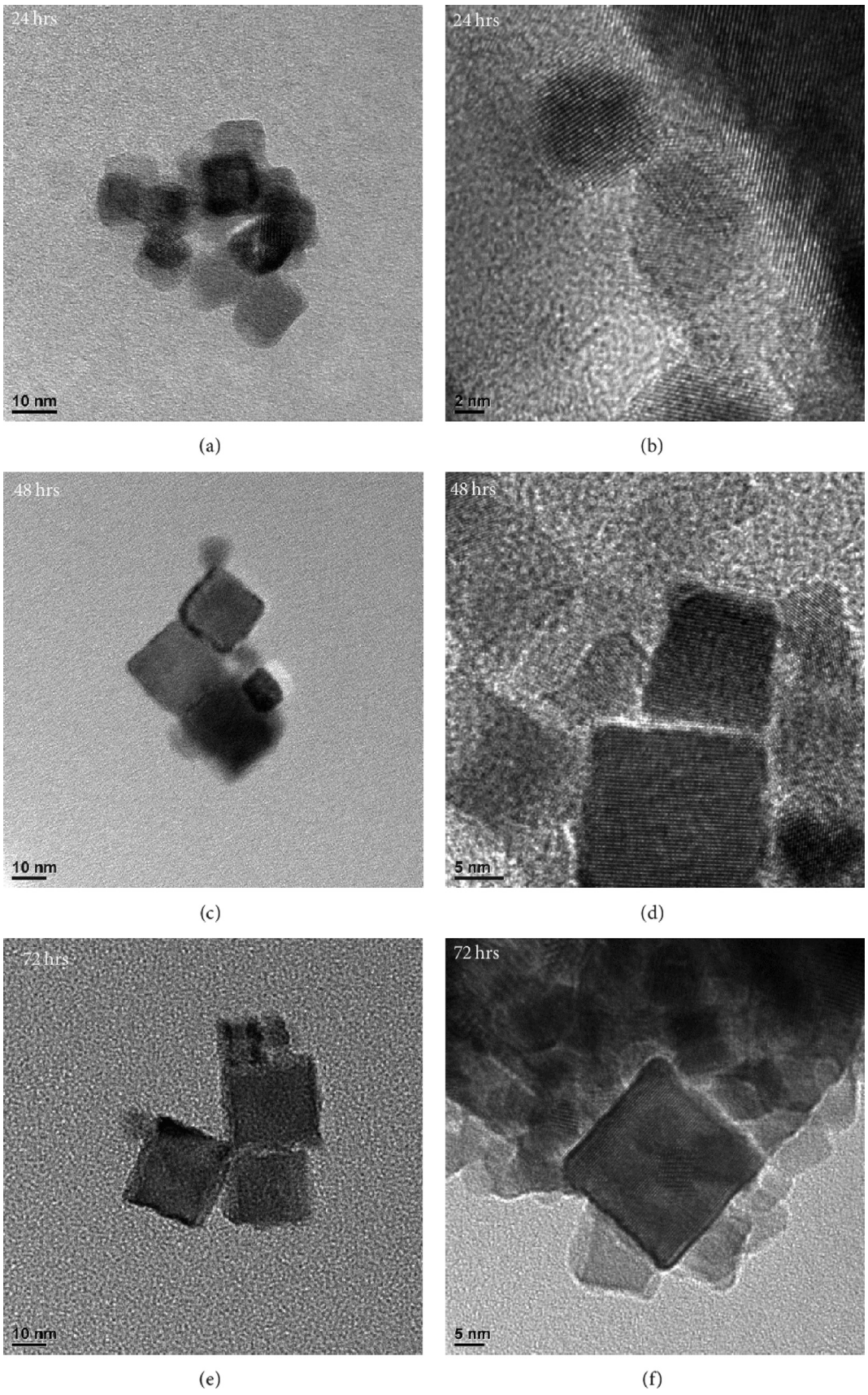

Fig. 13 (a)-(f) TEM images of cubic like structure of $BaTiO_3$ synthesized at various temperatures [90].

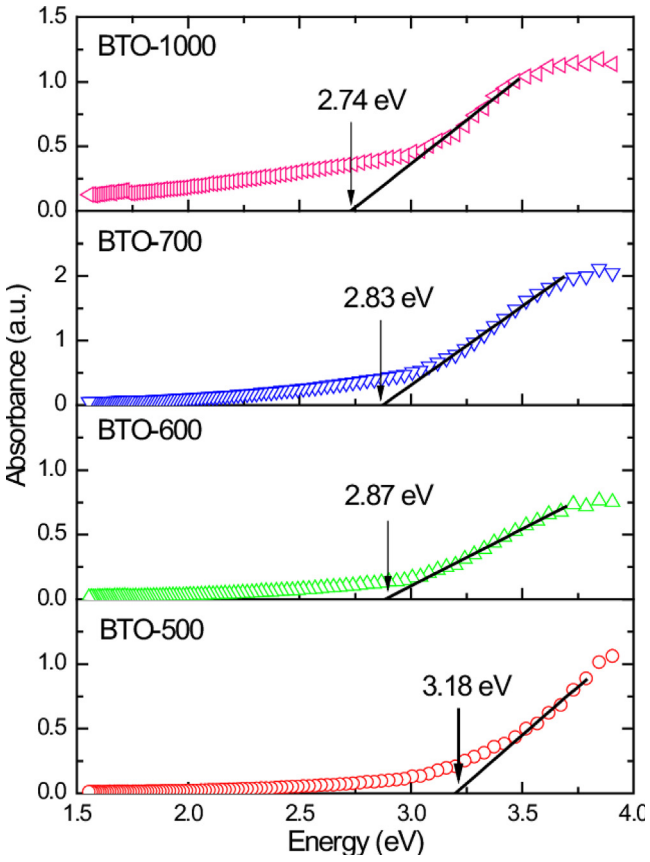

Fig. 14 Tauc's plot for $BaTiO_3$ calcined at different temperatures (Hasbullah et al., 2019).

research has shifted towards metal doping rather than non-metal doping since metal doping synthesis is easily achievable. To date, many transition metals including copper (Cu), Iron (Fe), Manganese (Mn), Tungsten (W) and Cerium (Ce) to mention a few have been explored as $BaTiO_3$ photocatalyst dopants for their improved break down of several organic contaminates like methylene blue (MB), tetraclycline (TC), methyl orange (MO), and atrazine. Among these transition metal dopants, Cu has been shown to be the most efficient $BaTiO_3$ dopants due to the fact it has shown greater improvement in degradation of organic pollutants as compared to Mn-, Fe-, Ce-, W- and Cr doped $BaTiO_3$ (I. C. Amaechi et al., 2019; Ifeanyichukwu C. Amaechi et al., 2019; Basaleh and Mohamed, 2020; Nageri and Kumar, 2018; Senthilkumar et al., 2019). Basaleh and Mohamed (Basaleh and Mohamed, 2020) investigated the degradation activity of undoped and cu-doped $BaTiO_3$ for the removal atrazine from wastewater. According to their outcomes, 5 wt% $Cu/BaTiO_3$ showed the highest degradation efficiency of 100 % after 60 min, which was 33 times better compared to the undoped $BaTiO_3$. The addition of Cu to the $BaTiO_3$ surface reduced the band gap of undopoed $BaTiO_3$ sample from 3.28 to 2.77 eV, thus improving the photocatalytic activity of the Cu-doped $BaTiO_3$ sample.

Noble metals including gold (Au), silver (Ag), platinum (Pt) and palladium (Pd) have been shown to improve the $BaTiO_3$ piezo-photocatalyst sensitivity either under visible light or ultrasonic vibration. These noble metals are receiving more attention from researchers because of their superb utilisation of the solar spectrum, from visible to infrared, through the SPR effect (Chao et al., 2020; Cui et al., 2013). The $BaTiO_3$ plasmonic photocatalyst have been fabricated from doping these noble metals with pure $BaTiO_3$ sample. Under solar irradiation, the plasmonic photocatalyst generates an internal electric field which causes the photogenerated charge carriers to move in opposite directions. According to the charge transfer process in plasmonic photocatalysts, electrons from noble metal NPs can travel to the photocatalyst's CB and vice versa. Therefore, resulting in improved separation of charge carriers of plasmonic photocatalyst for better photocatalytic performance. In a study conducted by Xu *et al.,* plasmonic piezo-photocatalyst ($Ag/BaTiO_3$) compared to pure $BaTiO_3$ showed an improved absorption under simulated solar irradiation (Xu et al., 2019). Due to this improvement, they discovered that $Ag/BaTiO_3$ had a greater photocatalytic effectiveness than pure $BaTiO_3$. The SPR of silver (Ag) nanoparticles resulting from internal band transitions from the 5d band to and within the 6sp band of the noble metal resulted in an increase in the piezo-photocatalytic activity of the modified $BaTiO_3$.

Another way of adjusting the band gap and improving the photocatalytic performance of the semiconductor is via non-metal doping. Unlike noble metals which are very expensive, non-metal materials are less expensive and can be applied as dopants for several photocatalyst to be used in wastewater treatment. Carbon based materials have been widely used as non-metal dopants to improve piezo-photocatalytic performance of $BaTiO_3$ since they can improve the rate of electron transfer and also reduce the electron-hole recombination rate. Some of the widely used carbon-based materials include carbon nanotubes (CNTs), activated carbon nanofibres (ACFs), graphene oxide (GO), Biochar, and Carbon nanodots (CNDs) to mention a few (Orimolade et al., 2021a). These distinct carbonaceous materials have different morphologies (surface area and pore size) and surface chemical characteristics (functional groups, hydrophobicity, and hydrophilicity) which all have a significant role in photocatalytic degradation of waste pollutants. Over past years, several few types of these carbonaceous materials have been employed to modify $BaTiO_3$ structure. However, the utilization of graphene oxide (GO) has been shown to be the most effective strategy. Unlike other carbons, GO offers a variety of benefits including high UV–visible light transmittance, quick electrical and thermal conductivity, superior mechanical and tribological characteristics, and corrosion resistance. In addition, the delocalization of pi (π) network of the layers effectively suppresses electron-hole recombination thus resulting in improved photocatalytic performance (Zou et al., 2019). For instance, Zhao *et al.* showed an improved photocatalytic performance of $BaTiO_3$ after loading it with different mass ratios of graphene oxide (Zhao et al., 2018). Firstly, the graphene oxide was prepared from the oxidation of graphite powder using the Hummer's method and, later the freeze drying method was employed for the preparation of graphene oxide-$BaTiO_3$ hybrid photocatalyst (Fig. 16(a)). Under light exposure, the hybrid material had superior photocatalytic performance than the unmodified $BaTiO_3$, as shown in Fig. 16**(b-c)**. Similar observations were reported by Rastogi *et al.* and Wang *et al.*, whereby the introduction of graphene oxide (GO) into $BaTiO_3$ lattice structure resulted in a higher photoresponse under the ultraviolet region or in the visible

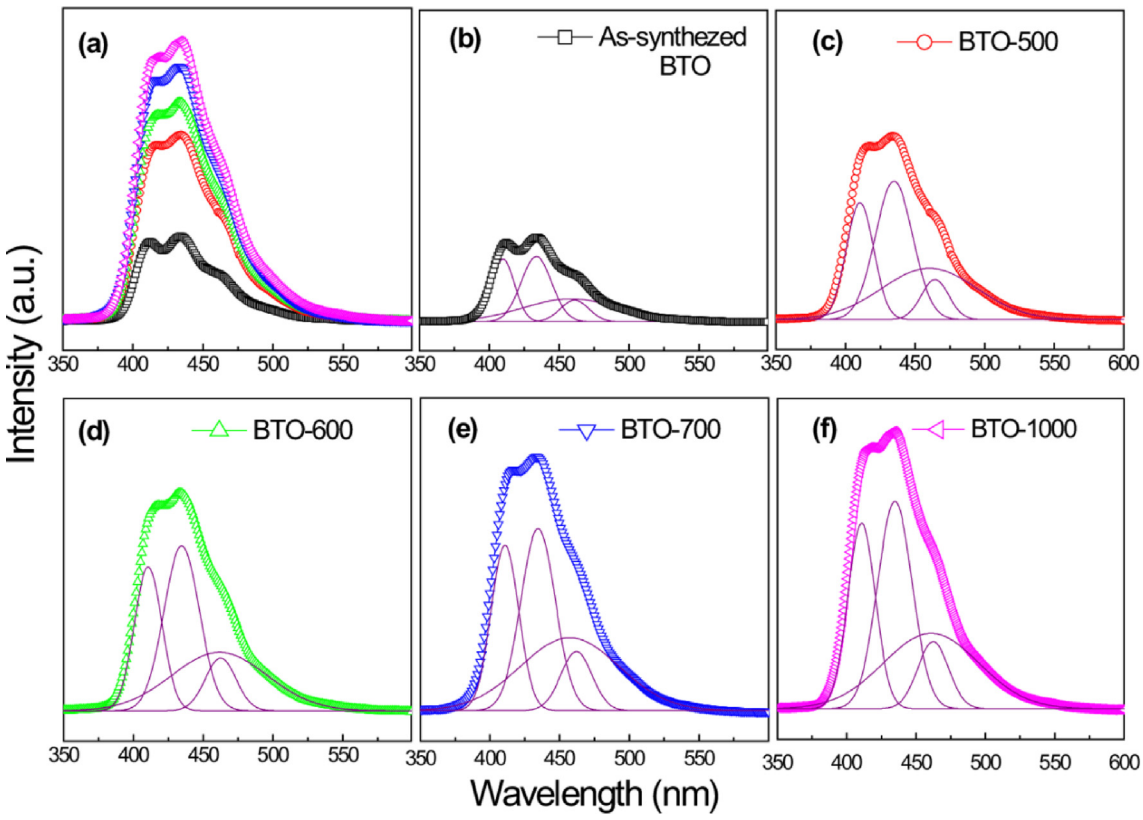

Fig. 15 (a)-(f) Photoluminescence emission and Gaussian deconvolution plots for $BaTiO_3$ calcined at different temperatures (Hasbullah et al., 2019).

region than $BaTiO_3$ pristine (Rastogi et al., 2016b) (Wang et al., 2015).

5.3. Formation of semiconductor heterojunction photocatalyst

The combination of $BaTiO_3$ with other several semiconductors to form $BaTiO_3$ based heterojunction photocatalyst is another approach of improving piezo-photocatalytic efficiency of the $BaTiO_3$ pristine. Mostly metal oxide semiconductors such as TiO_2, ZnO, SnO_2, Bi_2O_3, Bi_2WO_6 and Cu_2O which have an unequal band gap as $BaTiO_3$ are used to form heterojunctions (Mengying et al., 2017; Ray et al., 2021; Sharma et al., 2016; Wang et al., 2021). The formation of a heterojunction results in a band alignment which promotes the extension lifetime of the photoexcited holes and electrons within the heterostructured catalyst, thus reducing the rate of electron and holes recombination. Heterojunctions such as p-n (between a p-type semiconductor and an *n*-type semiconductor), *n-n* (between two *n*-type semiconductors), and p-p (between two p-type semiconductors) can be created depending on the kind of semiconductors that are combined. Furthermore, the band alignment of the heterostructured catalyst can be classified as Type I (straddling), Type II (staggered), and Type III (broken). In semiconductors, type II (including Z scheme) have been reported to efficiently improve electrons and holes separation (Orimolade and Arotiba, 2020). The charge transfer mechanism of type II was explained more in detail by Orimolade *et al.*, Zhang *et al.* and Peleyeju *et al.* (Orimolade and Arotiba, 2020)(Zhang and Jaroniec, 2018)(Peleyeju and Arotiba, 2018). As shown in Fig. 17, electron transfer within a heterojunction interface commonly follows a two-step pathway depending on the Femi energy level of the coupled semiconductors. On the first pathway mechanisms (Fig. 17(a)), when the Fermi energy level of SC-1 (p-type semiconductor) is smaller than that of SC-2 (*n*-type semiconductor), electrons (e^-) migrate from SC-1 conduction band (CB) to SC-2 conduction band (CB), while holes (h^+) migrate from SC-2′s valence band (VB) to SC-1′s valence band (VB). However, when the Fermi energy level of SC-1 is greater than that of SC-2, electrons (e^-) from SC-2 merge with the holes (h^+) from SC-1 following band alignment in the heterojunction, thus resulting in electrons and holes separation from SC-1 and SC-2 in Fig. 17 (b). The accessible separated holes (h^+) in SC-2 and electrons (e^-) in SC-1 are responsible for piezo-photocatalytic breakdown of organic waste pollutants. This type mechanism pathway of electrons and holes separation is known also as Z-scheme (Fig. 17(b)).

Several $BaTiO_3$ based heterojunctions have been fabricated using different synthetic methods such as hydrothermal, sol–gel, solid state method and co-precipitation method for various applications, including wastewater treatment. In water and wastewater treatment, $BaTiO_3$ have been coupled with several metal oxide semiconductors including ZnO, SnO_2, TiO_2, Bi_2O_3, Fe_2O_3 and MnO_2 for better piezocatalytic/photocatalytic removal performance. Other non-metal oxides including g-C_3N_4, Ag_3PO_4 and AgBr have also been coupled with $BaTiO_3$ for improved photocatalytic/piezocatalytic activity (Mengying et al., 2017; Ray et al., 2021). Feng *et al.* synthe-

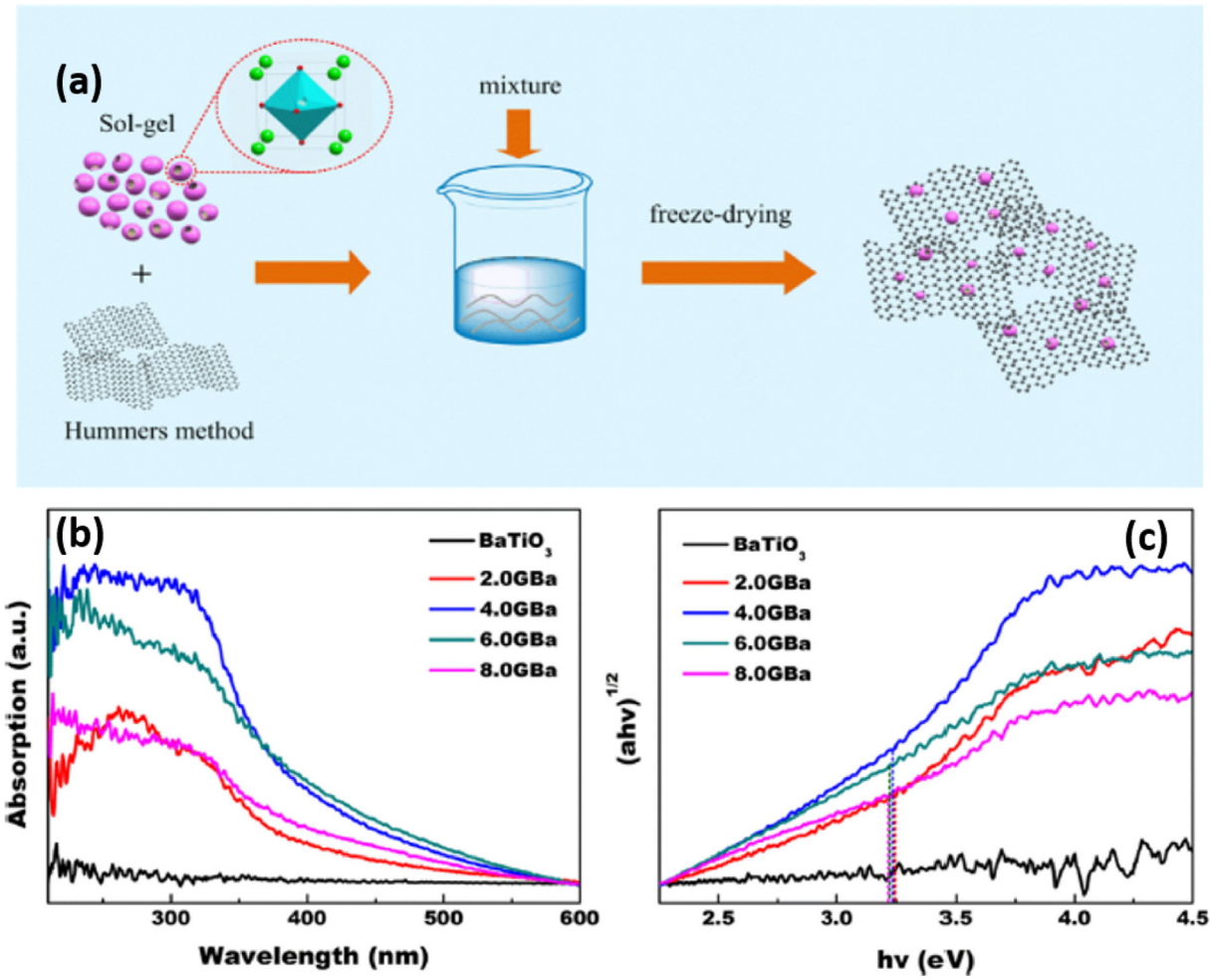

Fig. 16 (a) schematic illustrations of $BaTiO_3$/GO synthesis, (b) UV–vis absorption spectra and (c) Tauc's plot (Photon energy curves) for composites (Zhao et al., 2018).

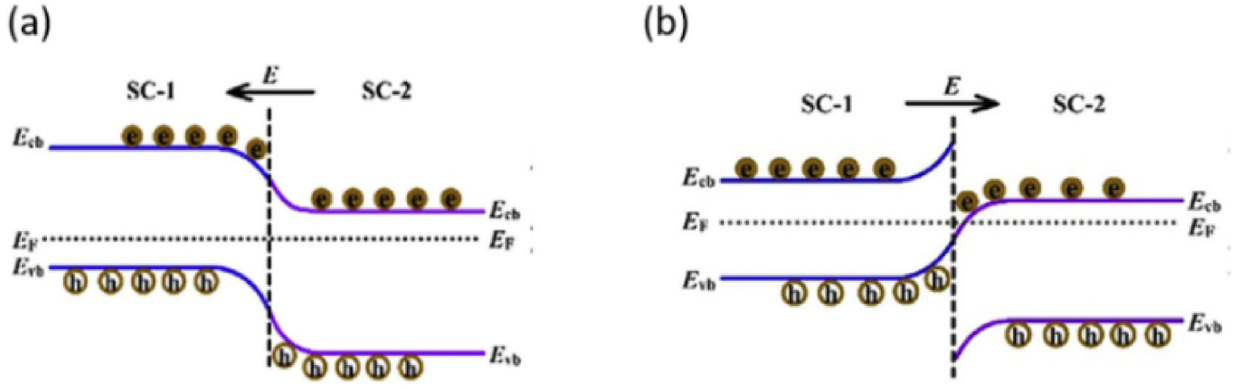

Fig. 17 (a) Electrons and holes separation pathway in type II heterojunction and (b) Z-scheme heterojunction charge separation pathway (Zhang and Jaroniec, 2018).

sized $BaTiO_3/SnO_2$ hybrid heterostructured catalyst using the hydrothermal method for piezocatalytic degradation of organic contaminates (Feng et al., 2020). The effect of SnO_2 loading on $BaTiO_3$ had a huge impact of piezo-current response, as shown in Fig. 18(a), $BaTiO_3$ loaded with SnO_2 and SnO_2-Sb generated greater piezoelectrochemical current response than pure $BaTiO_3$. Furthermore, electrochemical impedance measurements showed the evidence of improved

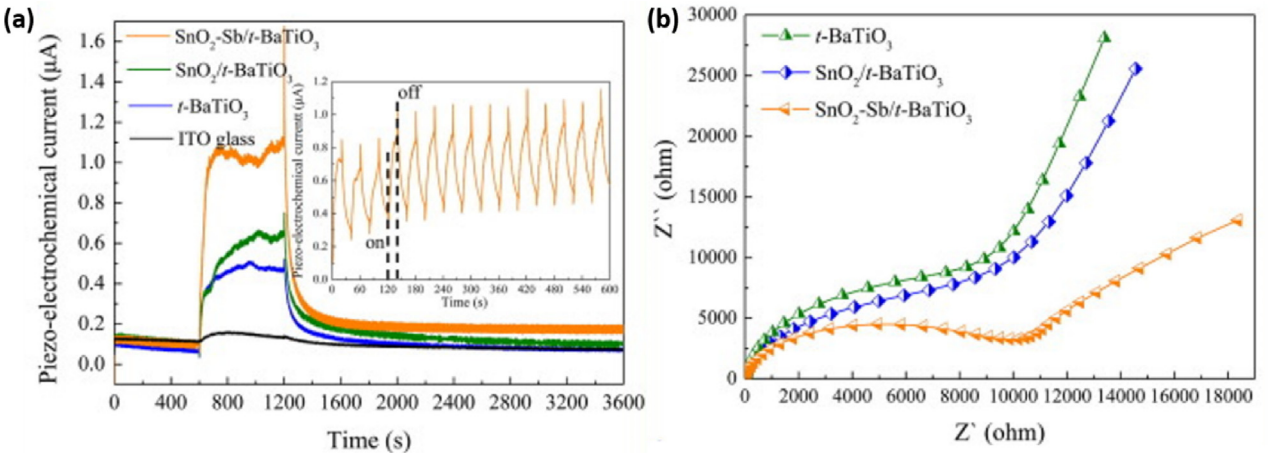

Fig. 18 (a) Piezoelectrochemical current response and (b) electrochemical impedance (EIS) for $BaTiO_3$, $BaTiO_3/SnO_2$ and $BaTiO_3$/SnO-Sb (Feng et al., 2020).

electron mobility via reduction in charge transfer resistance (Rct) of the composites ($BaTiO_3/SnO_2$ and $BaTiO_3$/SnO-Sb) (Fig. 18(b)).

6. Piezocatalytic, photocatalytic and piezo-photocatalytic removal of organic waste pollutants and bacteria

Over the past decades, several wastewater technologies including non-destructive and destructive methods as shown in Fig. 19, have been employed to remove toxic organic contaminates and pathogenic bacteria. Among them, advanced oxidation methods have been extensively applied as the most effective methods that accelerates the oxidation and degradation of a wide range of organic and inorganic chemicals that are resistant to traditional treatment methods. Piezocatalaysis is one of the emerging AOPs which uses energy harvesting materials called piezoelectric materials to convert mechanical energy into electrical energy. Recently, pieozocatalysis has gained much attention in several electrochemical applications including bacterial disinfection (Kumar et al., 2019a), hydrogen production (Hong et al., 2010), wastewater treatment and degradation of water pollutants (Mengying et al., 2017).

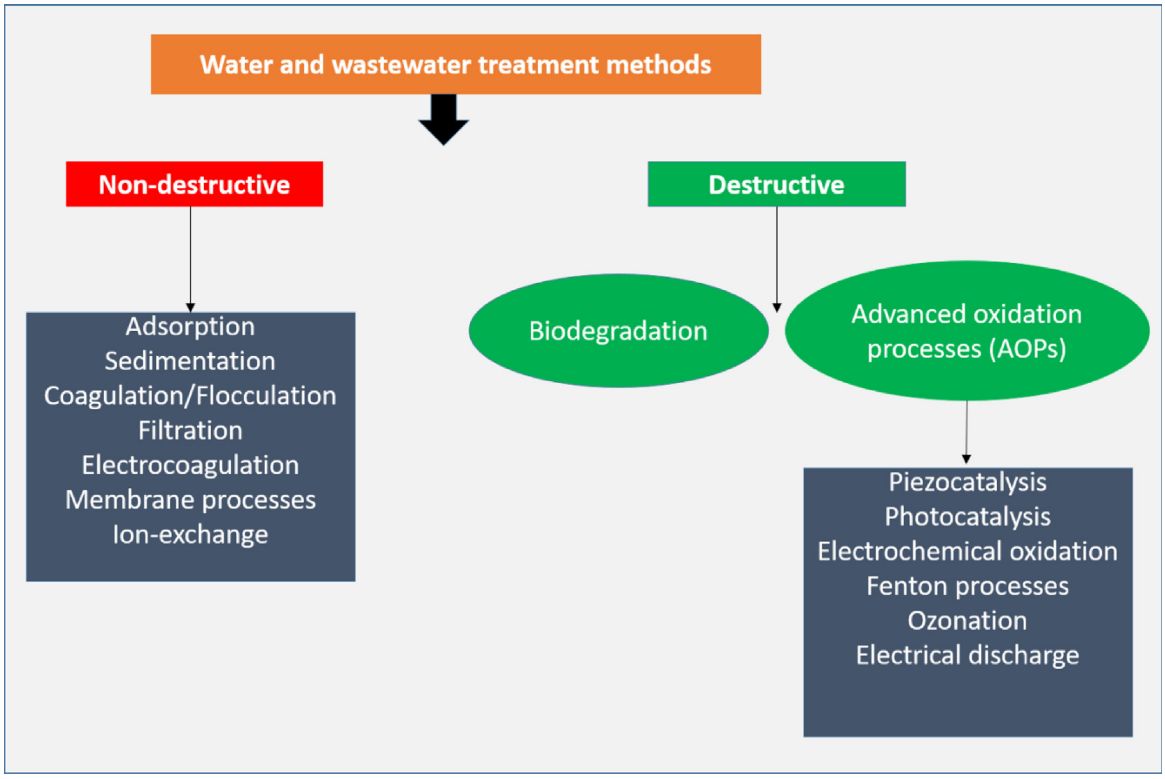

Fig. 19 Schematic diagram of non-destructive and destructive water and wastewater treatment methods.

In bacterial disinfection and degradation of pollutants, the piezoelectric materials (piezocatalyst) generate negative and positive electric charges under the influence of mechanical vibration at opposite surfaces. These free electric charges are responsible for redox reactions resulting in highly reactive species (ROS) such as $\bullet O^{2-}$ and •OH. These strong reactive oxygen species (ROS) are capable of breaking down toxic organic compounds into less toxic compounds, hydroxyl radicals (•OH) have been recognized as secondary oxidants (after the strongest fluorine) due to their high standard reduction potential (E^{o} $\bullet OH/H_2O$) of roughly 2.8 V versus SHE. Coupling piezocatalysis with photocatalysis can enhance the degradation performance of piezo-photocatalyst and supress the rate of electron and holes recombination in photocatalytic degradation processes. Therefore, this article intends to review enhanced piezo-photocatalytic degradation of organic dyes (section 6.1), pharmaceuticals (section 6.2) and bacteria (section 6.3) using $BaTiO_3$ based catalysts.

6.1. Decomposition organic dyes

In the past, $BaTiO_3$ based catalysts have been extensively investigated for their piezocatalytic and piezo-photocatalytic removal ability of several wastewater pollutants including organic dyes. For example, Wu *et al.* synthesized $BaTiO_3$ nanoparticles and nanowires using a two-step hydrothermal method for piezocatalytic removal of methyl orange (MO) from wastewater (Wu et al., 2018b). Under ultrasonic vibration, $BaTiO_3$ nanowires (NWs) were easily deformed therefore showed better piezocatalytic performance as compared to $BaTiO_3$ nanoparticles (NPs) with poor deformability. The highest piezocatalytic efficiency obtained by $BaTiO_3$ NWs under ultrasonic vibration (power 80 W) was about 92 % within 160 min, with reaction processes following pseudo-first order kinetics model (Fig. 20(a)). Scavenger studies were conducted to investigate the reactive oxygen species that were more effective in breaking down of MO into CO_2 and H_2O. Various trapping agents such as *tert*-butyl alcohol (TBA), benzoquinone (BQ) and disodium ethylene diamine tetra-acetate dehydrates (EDTA-2Na) were used to supress hydroxyl radicals (•OH), superoxide ($\bullet O^{2-}$) and holes (h^{+}), respectively. As shown in Fig. 20(b), upon the addition of TBA, the degradation efficiency reduced dramatically thus confirming that hydroxyl radicals (•OH) were the most effective ROS species for MO break down, followed by superoxide radicals (($\bullet O^{2-}$). Another study was conducted by Hong *et al.,* were $BaTiO_3$ as a piezocatalyst generated more hydroxyl radicals (•OH) and superoxide radicals (($\bullet O_2^-$) to break down Acid orange 7 (AO7) dye into CO_2 and H_2O (Hong et al., 2012). Under piezoelectric effect, the strained $BaTiO_3$ dendrites decomposed about 80 % of the AO7 dye after 90 min. Several factors including influence of pH, catalyst dose and initial concentration which can affect the piezocatalytic process were investigated. In case of catalyst loading, the piezocatalytic efficiency increased with an increase in catalyst dosage until reaching a plateau region with 0.025 g of $BaTiO_3$ catalyst. This was due to more available strained induced charges on the surface of $BaTiO_3$ as its total surface-active sites increased with an increase in the amount of catalyst dosage. Therefore, resulting in enhancement of piezocatalytic degradation efficiency. The pH solution and initial AO7 concentration significantly influenced piezocatalytic processes, the piezocatalytic efficiency decreased with an increase in intial AO7 concentration. It was speculated that as initial concentration increases, more AO7 molecules increases which cover less active surface sites of the catalyst thus leading to a decrease in piezocatalytic efficiency. The highest piezocatalytic efficiency was slightly reduced in alkaline media and enhanced in acidic media. In acidic conditions, the surface of the $BaTiO_3$ dendrites is protonated (positively charged) thus enlarges electrostatic interaction between anionic AO7 dye (negatively charged) and positively charged $BaTiO_3$ surface, and resulting in higher piezocatalytic removal of AO7.

To improve the photocatalytic activity of $BaTiO_3$, Li *et al.* fabricated new hybrid composites (Ag_2O-$BaTiO_3$) by combining $BaTiO_3$ ferroelectric with Ag_2O semiconductor. Under ultrasonic vibration, an internal electric field was generated by ferroelectric $BaTiO_3$ nanocrystal to reduce the rate of electrons and holes recombination thus enhancing the photocatalytic performance of the hybrid composite (Ag_2O-$BaTiO_3$)

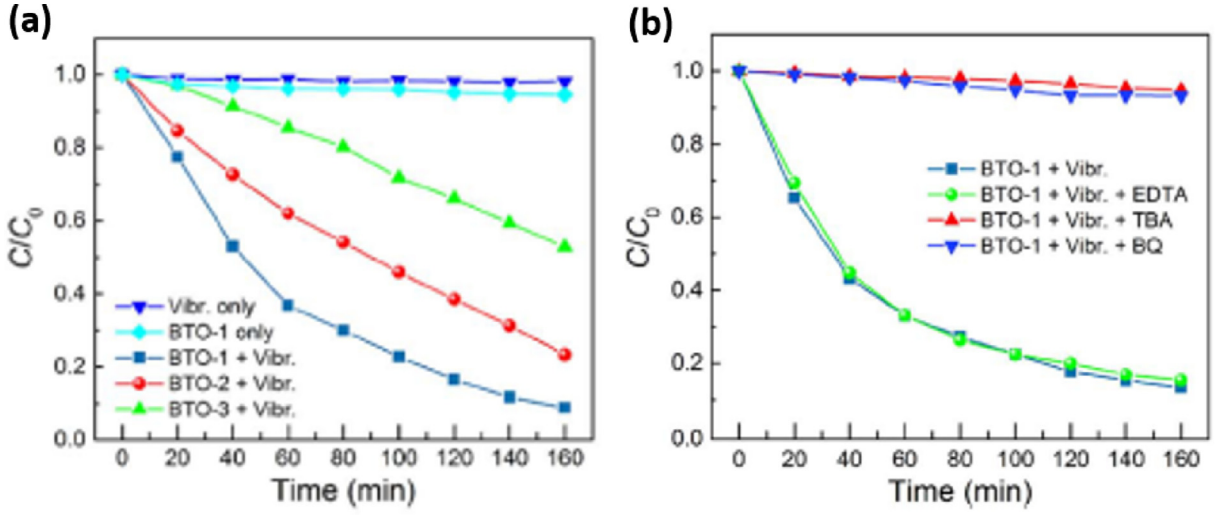

Fig. 20 (a) Piezocatalytic degradation of MO by $BaTiO_3$ NWs and (b) Scavenger studies (Wu et al., 2018b).

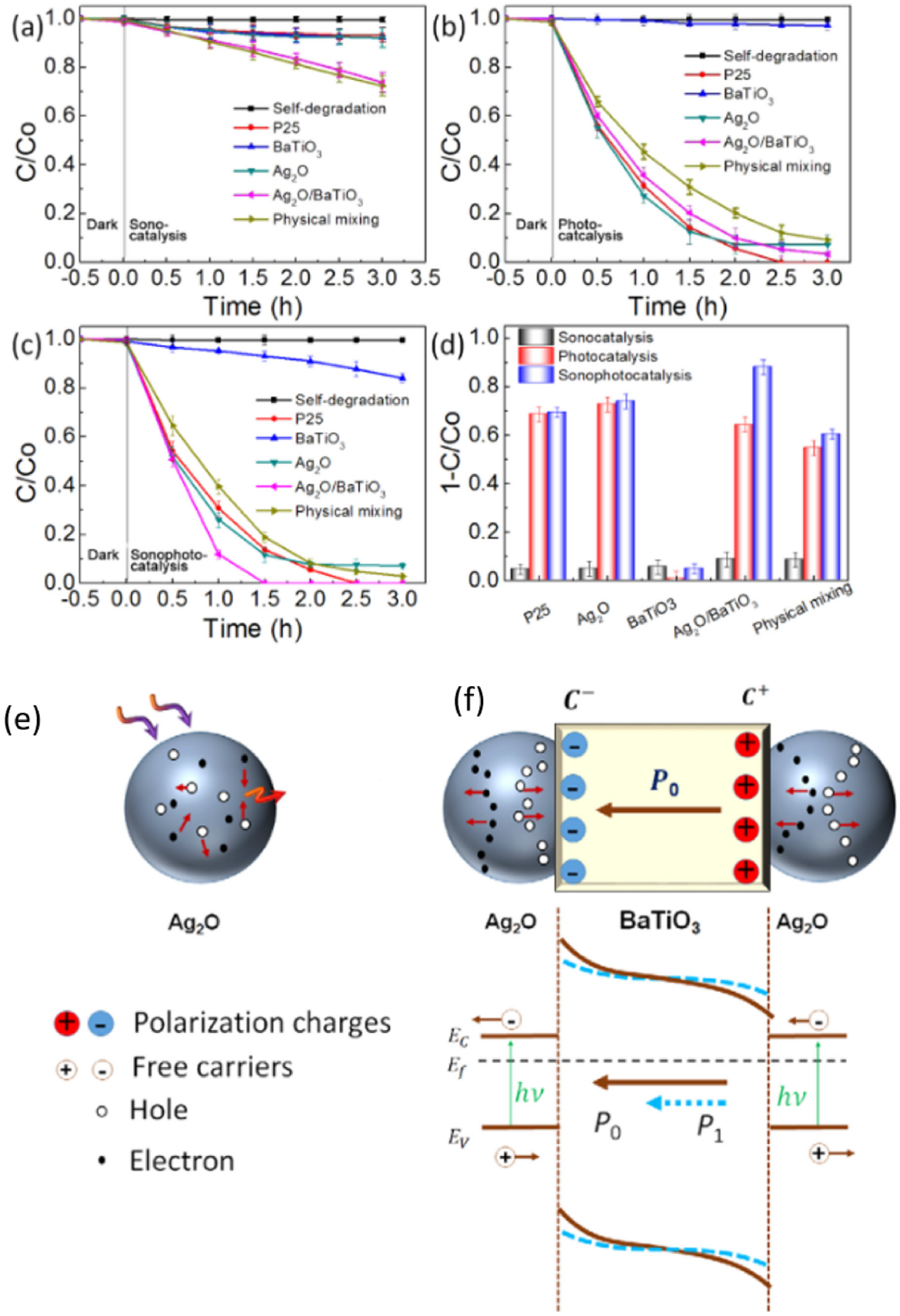

Fig. 21 (a) sonocatalytic, (b) photocatalytic, (c) sono-photocatalytic degradation of Rh B (d) sono-photocatalytic kinetics and (e-f) sono-photocatalytic mechanism (Li et al., 2015).

(Li et al., 2015). Fig. 21 shows the effect of ultrasonic vibration on the photocatalytic degradation of Rh B dye using hybrid Ag_2O-$BaTiO_3$ photocatalyst. Four photocatalyst materials such as commercial P25 nanoparticles, Ag_2O, $BaTiO_3$, mixture of $BaTiO_3$ and Ag_2O were used for photocatalytic degradation comparison study. As depicted in Fig. 21(a), P25, $BaTiO_3$ nanocubes, or Ag_2O nanoparticles were not effective in the degradation of Rh B under ultrasonic irradiation only. However, the physical mixture of Ag_2O and $BaTiO_3$ as well as the Ag_2O-$BaTiO_3$ hybrid composite showed a slight deterioration of Rh B. These results shows that the combination of ferrolectric $BaTiO_3$ nanoctrystal and Ag_2O semiconductor can improve piezocatalysis/sonocatalysis performance of the Ag_2O-$BaTiO_3$ hybrid piezocatalyst. Fig. 21(b) illustrates the photocatalytic degradation of Rh B with all four samples in the absence of an ultrasonic irradiation. The synthesized $BaTiO_3$ showed no photocatalytic degradation towards Rh B, whereas Ag_2O, Ag_2O-$BaTiO_3$ and their physical mixtures showed higher photocatalytic degradation performance towards the removal of Rh B. Under both UV light and ultrasonic irradiation, Ag_2O-$BaTiO_3$ hybrid photocatalyst completely degraded all Rh B within a short space of time (1.5 h) (Fig. 21**(c-d)**). Their piezo-photocatalytic or sono-photocatalytic mechanisms were explained as follows: under UV light irradiation, the Ag_2O surface generates electrons (e^-) and holes (h^+), these charge carriers (e^-, h^+) are required to be separated in order to produce reactive oxygen species (ROS) such as hydroxyl and superoxide radicals for deterioration of Rh B. Under ultrasonic vibration, the ferroelectric $BaTiO_3$ nanocrystal in the Ag_2O-$BaTiO_3$ hybrid composite generated an internal piezo-electric field which acted as a driving force for the separation of charge carrier's (electrons and holes) (Fig. 21**(e-f)**). The suppression of rapid electrons and holes recombination separation led to an improved photocatalytic activity of the hybrid composite (Ag_2O-$BaTiO_3$).

In addition, $BaTiO_3$ photocatalytic performance was further improved by modifying it with several co-catalysts such as ZnO, SnO_2, Fe_2O_3, TiO_2 and Bi_2O_3. Heterostructured $BaTiO_3$/ZnO composites were prepared using the sol–gel and hydrothermal methods for the degradation of MB, MO, and RhB (Kappadan et al., 2020b; Karunakaran et al., 2014; L. Wang et al., 2019). In the study conducted by Kappadan *et al.,* hydrothermal method was employed to prepare *n-n* heterojunction photocatalyst of $BaTiO_3$/ZnO using Barium acetate, titanium tetra isopropoxide and Zinc nitrate hexahydrate as precursors (Kappadan et al., 2020b). The scanning electron microscopic images of the composite ($BaTiO_3$/ZnO) clearly showed spherical $BaTiO_3$ nanoparticles anchored on hexagonal rod-shaped ZnO. The formation of *n-n* heterojunction resulted in improved photocatalytic performance, as evidenced by the reduction of band gap energy from 3.1 to 2.97 eV and charge transfer resistance from 871 to 745 Ω. The mechanisms, as shown in Fig. 22(a), revealed that an improved charge carriers separation was achieved by forming a typical type II band alignment within the $BaTiO_3$/ZnO heterojunction interface, which allowed $BaTiO_3$ photogenerated electrons to migrate into the conduction band (CB) of ZnO, whereas ZnO photogenerated holes were transported into the valence band (VB) of $BaTiO_3$. The prepared heterostructured $BaTiO_3$/ZnO (BTZ) photocatalyst showed good stability since even after the 3rd cycle the degradation efficiency was above 91 % for methylene blue (MB) (Fig. 22 (b)). However, after the 4th cycle the photocatalytic degradation efficiency slightly reduced from 91 to 86 %. The total mineralisation of MB dye was calculated using TOC, under UV light irradiation, the BTZ heterostructure recorded a TOC removal of 87.1 % after 60 min. A recent report by Liu *et al.* modified $BaTiO_3$ with TiO_2 via hydrothermal process to form $BaTiO_3$-TiO_2 core–shell heterostructures (Liu et al., 2019). The heterostructured photocatalyst was applied for photocatalytic deterioration of Rh B dye from wastewater. The ratio of $BaTiO_3$:TiO_2 played a significant role in the photocatalytic degradation of Rh B. All $BaTiO_3$-TiO_2 core–shell heterostructures with different molar ratios exhibited better photocatalytic removal towards Rh B as compared to pure $BaTiO_3$. The $BaTiO_3$-TiO_2 core–shell heterostructures (1.2:1) showed the greatest photocatalytic performance compared to other samples, its performance was 1.8 times greater than pure TiO_2. The improved photodegradation activity was due to the fact that $BaTiO_3$-TiO_2 core–shell heterostructures (1.2:1) exhibited the lowest photoluminiscent (PL) intensity thus lowering the rate of electrons and holes recombination. Wu *et al.* boosted the photocatalytic activity of heterostructured $BaTiO_3$/TiO_2 nanocomposites with piezotronic effect under ultrasonic vibration (J. Wu et al., 2020). Under ultrasonic activation, the built-in electric field exhibited by ferroelectric $BaTiO_3$ facilitated the charge transfer and separation within $BaTiO_3$/TiO_2, thus improving its photocatalytic activity. Comparing with other $BaTiO_3$ based metal oxides (Alex et al., 2019; Cui et al., 2017; Fan et al., 2012; Karunakaran et al., 2014; Lin et al., 2007; Liu et al., 2019; Selvarajan et al., 2017; Zhou et al., 2019), $BaTiO_3$/TiO_2 composite outperformed them in terms of photocatalytic performance due to excellent suppression of electrons and holes recombination.

Plasmonic photocatalysts have also attracted a lot of attention in the photocatalytic removal of organic pollutants in wastewater. Several noble metals including platinum (Pt), gold (Au), rhodium (Rh) and silver (Ag) have been doped with $BaTiO_3$ to promote chemical redox reaction under UV light and ultrasonic irradiation. For example, chao *et al.* fabricated a heterostructured Au@$BaTiO_3$ photocatalyst using the hydrothermal method for the breakdown of Rh B under UV light exposure (Chao et al., 2020). The plasmonic heterostructured photocatalyst showed an enhanced photocatalytic activity towards the removal of Rh B. The heterostructured composite (Au@$BaTiO_3$) nearly degraded about 100 % of Rh B after 36 min and the reaction process followed Langmuir-Hinshelwood model. The degradation rate constant (k) obtained from Langmuir-Hinshelwood model were 0.05446 and 0.01118 min^{-1} for Au@$BaTiO_3$ and pure $BaTiO_3$, respectively. The apparent rate constant (k) for Au@$BaTiO_3$ was 4.9 times than that of pristine $BaTiO_3$. These results confirmed an enhancement in the photocatalytic properties of heterostructured Au@$BaTiO_3$ photocatalyst. Several studies investigated the photocatalytic performance of silver (Ag) doped $BaTiO_3$ photocatalyst for the catalytic degradation of hazardous organic dyes (Rh B and MO) (Cui et al., 2013; Lin et al., 2021; Nithya and Devi, 2019; Xu et al., 2019). For instance, Khan *et al.* reported Ag-doped $BaTiO_3$ prepared via sol–gel method for photodegradation of Rh B (Khan et al., 2021b). The XRD and HR-TEM results confirmed their tetragonal phase and crystallite size range of 46–54 nm, respectively. The incorporation of silver (Ag) dopants into $BaTiO_3$ reduced its band gap from 3.87 to 3.47 eV. Furthermore, they observed

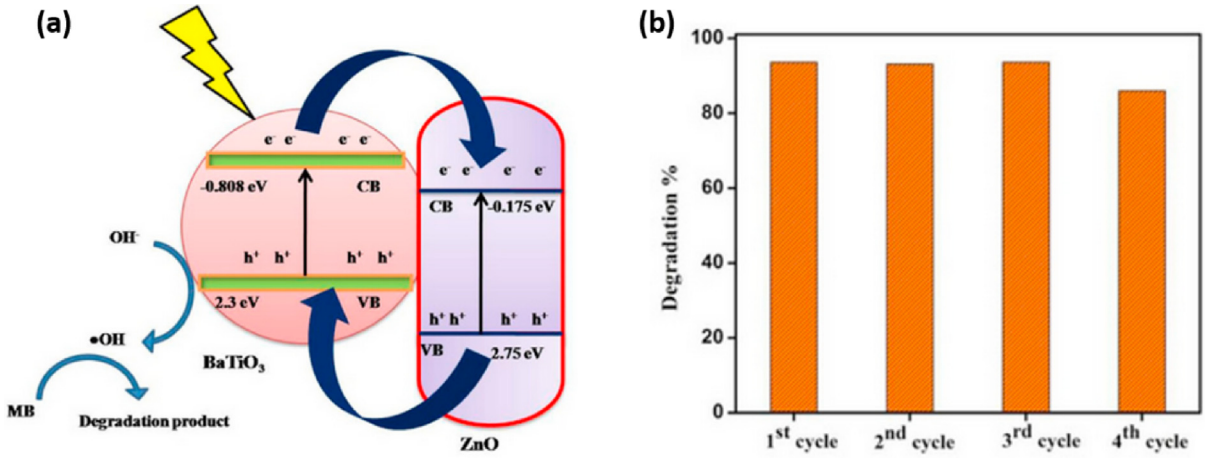

Fig. 22 (a) Photocatalytic degradation mechanism of MB using $BaTiO_3$/ZnO and (b) re-usability of $BaTiO_3$/ZnO (Kappadan et al., 2020b).

a reduction in photoluminescent peak intensity upon addition of silver ions into tetragonal $BaTiO_3$, confirming restrain in electrons and holes recombination. The BET surface of Ag (5 %)-doped $BaTiO_3$ had a higher surface area of 20.1 $m^2.g^{-1}$ as compared to pure $BaTiO_3$ (15.4 $m^2.g^{-1}$). Therefore, due to Ag-doped $BaTiO_3$ having a higher surface area and lower band gap, their photocatalytic performance was improved. Under light irradiation (400 W sodium lamp), 1 %Ag@ $BaTiO_3$, 3 %Ag@$BaTiO_3$ and 5 %Ag@$BaTiO_3$ showed better photocatalytic performance than pure $BaTiO_3$. The improved photocatalytic activity of Ag-doped $BaTiO_3$ could be due to the reduced rate of electrons and holes recombination, surface area increase and reduction in band gap energy after Ag-deposition. The highest photocatalytic removal for Rh B was 79, 58, 46 and 51 % when 5 % Ag@$BaTiO_3$, 3 %Ag@ $BaTiO_3$, 1 %Ag@ $BaTiO_3$ and $BaTiO_3$ were applied as photocatalysts, respectively. Niu and Xu observed the same photocatalytic enhancement when Ag-$BaTiO_3$ was further co-doped with other metal dopants such as Ni, Pd and Pd–Sn–Ni through a one-step ball milling process (Niu and Xu, 2019). The co-doped Ag@$BaTiO_3$ rate constant was 4.5 times greater than undoped $BaTiO_3$. Table 4 summarizes an overview application of $BaTiO_3$-based piezo/photocatalyst for catalytic degradation of organic dyes in water and wastewater.

6.2. Pharmaceuticals

In recent decades, antibiotics have been identified as emerging contaminants owing to their endurance in aquatic ecosystems. They are widely used for treating numerous bacterial infections. However, they find their way into several waterbodies through incorrect disposal of unused or expired medications and human excretion. In ground and surface water, antibiotics are found in lower concentrations ranging from μg/L to mg/L (Cabeza et al., 2012; Orimolade et al., 2021b; Wang and Wang, 2016). Unfortunately, the detection of these pharmaceuticals in aquatic environment can lead to several harmful biological and economic impacts. For example, continuous ingestion of drinking water contaminated with pharmaceuticals can result in the formation of drug-resistant bacterium strains to humans and animals. The elimination of several emerging pharmaceuticals by $BaTiO_3$ based ferroelectric/piezo-photocatalyst system have attracted so much attention recently. Kurniawan *et al.* investigated the photocatalytic performance of $BaTiO_3$ and $BaTiO_3/TiO_2$ composites for the removal of acetaminophen (Ace) from distilled water under UV–vis irradiation (Kurniawan et al., 2018). The XRD patterns confirmed the cubic phase structure of $BaTiO_3$ nanoparticles. The $BaTiO_3/TiO_2$ composites as compared to individual pristine ($BaTiO_3$ and TiO_2) performed better, thus confirming that the synergetic effect of the two semiconductors can improve visible light absorption and efficient charge separation. Furthermore, it was found that the photocatalytic performance of the composites ($BaTiO_3/TiO_2$) can be enhanced by varying the molar weight ratios (w/w) of $BaTiO_3$ and TiO_2. Under optimal conditions, dosage of 1 g/L, pH 7, 4 hrs reaction time and initial Ace concentration of 5 mg/L, $BaTiO_3$, TiO_2 and $BaTiO_3/TiO_2$ photocatalytically degraded about 18, 33 and 95 % of Ace respectively. As shown in Fig. 23, initial degradation pathways for Ace were through hydroxylation and photolysis. The intermediates formed during this route included hydroquinone and 1,4-benzoquinone, which were consistent with the results obtained by Zhang *et al.* and Aguilar *et al.* (Zhang et al., 2008) (Aguilar et al., 2011). The hydroxyl radicals (•OH) further attacked these intermediates to form hydroxylation products. The first detected intermediate was quinoneimine which was effortlessly hydrolized to 1,4-benzoquinone. The intermediates were then oxidized further into carboxylate acid and carbon dioxide by destroying their aromatic structures. The total mineralization via photocatalysis process generally does not occur quickly, however after some few hours these organics can be totally mineralized. Demircivi and Simsek reported tungsten-doped $BaTiO_3$ (W-$BaTiO_3$) for enchanted photocatalytic removal of tetracycline under and visible light-driven and UV-A light irradiation (Demircivi and Simsek, 2019). The composite was prepared through a simple hydrothermal method using a Teflon-lined stainless-steel autoclave at 200 °C, followed by washing, drying and calcination for 2 hrs at 700 °C. The effect of tungsten (W) loading on $BaTiO_3$ was investigated for tetracycline degradation. It was found that $BaTiO_3$ doped with low amounts of tungsten (W) exhibited higher photocatalytic activity than pure $BaTiO_3$ and

Table 4 Removal of organic dyes using $BaTiO_3$-based catalyst in wastewater.

Catalyst	Organic dyes	Reaction conditions	% Removal & reaction time	Refs
$BaTiO_3$	MO	80 W Ultrasonic	92 %, 160 min	(Wu et al., 2018b)
	AO7	40 kHz Ultrasonic	80 %, 90 min	(Hong et al., 2012)
Ag_2O-$BaTiO_3$	Rh B	50 W ultrasonic + UV light	100 %, 90 min	(Li et al., 2015)
$BaTiO_3$/ZnO	MB	250 W UV lamp	93.6 %, 60 min	(Kappadan et al., 2020b)
	Rh B	Mercury vapor lamp (8 W)	100 %, 60 min	(Karunakaran et al., 2014)
	Rh B	120 W Ultrasonic + Xe lamp (500 W)	97 %, 30 min	(Zhou et al., 2019b)
	MO	50 W high-presure mercury lamp	NA	(Ren et al., 2012)
$BaTiO_3$-TiO_2	Rh B	mercury-xenon lamp (200 W)	>70 %, 120 min	(Liu et al., 2019)
	Rh B	300 W Ultrasonic + mercury lamp(250 W)	~100 %, 60 min	(J. Wu et al., 2020)
	Rh B, MB & IC	Ultrasonic (45 kHz, 200 W) + Xe lamp (300 W)	99.5, 99.8 & 99. 7 %	(Liu et al., 2022)
$BaTiO_3$/BiOI	MO	Ultrasonic (40 kHz, 300 W) + 300 W Xe lamp	95.4 %, 90 min	(Liu et al., 2022)
$BiFeO_3$ − $BaTiO_3$	Rh B, MB & MO	Ultrasonic (100 W, 40 kHz)	99.5, 90.1 & 84.5 %	(Sun et al., 2021)
$CoFe_2O_4$/$BaTiO_3$	MB	Osram UV lamp (250 W)	99.3 %, 5 hr	(Dang et al., 2018)
Ag– $BaTiO_3$/TiO_2	MB	Xenon lamp (300 W)	95 %, 180 min	(Q. Li et al., 2013)
Bi_2O_3/$BaTiO_3$	MO	500 W high-pressure mercury lamp	98.9 %, 50 min	(Lin et al., 2007)
	Rh B	500 W mercury lamp	100 %	(Fan et al., 2012)
	MO	50 W high-pressure mercury lamp	NA, 140 min	(Ren et al., 2013)
$BaTiO_3$/SnO_2	MB	300 W Xenon lamp	83.67 %, 180 min	(Selvarajan et al., 2017)
	MB	300 W Tungsten lamp	>85 %, 300 min	(Nageri et al., 2017)
Ag-$BaTiO_3$	MO	350 W high-pressure mercury lamP	98.53 %, 60 min	(Liu et al., 2012)
	Rh B	solar simulator (100 mW cm − 2)	~100 %, 60 min	(Cui et al., 2013)
	Rh B	solar light, visible light and UV	99 %, 60 min	(Cui et al., 2015)
	MO	ultrasonic cleaner (120 W)	81 %, 120 min	(Lin et al., 2018)
	Rh B	ultrasonic (70 W)	~94 %, 150 min	(Z. He et al., 2021)
Au-$BaTiO_3$	Rh B	UV light	100 %, 36 min	(Chao et al., 2020)
Au_x/$BaTiO_3$ film	Rh B	500 W Xe lamp film	45 %, 300 min	(Zhang et al., 2016)
Mn-$BaTiO_3$	MB	300 W Tungsten lamp	97.04 %, 360 min	(Nageri and Kumar, 2018)
Ce-$BaTiO_3$	MB, CR & MV	300 W Tungsten lamp	90, 78.5 & 82.4 %	(Senthilkumar et al., 2019)
I-$BaTiO_3$	CR	125 W mercury vapor lamp	89.33 %, 150 min	(P.M and Devi, 2020)
$BaTiO_3$/AgI	Rh B	Visible light	92.2 %, 15 min	(C. He et al., 2021)
OA-BaTiO3	Rh B	Ultrasonic bath (40 kHz, 100 W)	>87 %, 30 min	(Gao et al., 2021)
n-$BaTiO_3$/Ag/p-AgBr	Rh B	200-W xenon lamp	99.3 %, 12 min	(Y. Wang et al., 2020)
Ag/$BaTiO_3$/MnOx	Rh B	300 W xenon lamp	98.10 %, 120 min	(Cui et al., 2020)
Ag-Ag_2S)/$BaTiO_3$	MO	UV light + Ultrasonic vibration	90 %, 30 min	(Y. Wang et al., 2020)
$BaTiO_3$/GO	MB	Xe lamp (GX-500)	69.5 %, 8 hr	(Wang et al., 2015)
	MB	irradiation of Xe light	80 %, 150 min	(Zhao et al., 2018)
	Rh B	500 W halogen lamp	>80 %, 90 min	(Rastogi et al., 2016b)
	Rh B & MO	Ultrasonic (35 kHz, 200 W) + 150 W halogen lamp	97.3 & 81.9 %	(Rastogi et al., 2016a)
	MB	Ultrasonic cleaner (100 W, 40 kHz)	98 %, 120 min	(J. Wang et al., 2020)
$BaTiO_3$/MoO_3	Rh B	150 W halogen lamp	86 %, 60 min	(Alex et al., 2019)
$BaTiO_3$/g-C_3N_4	Rh B	vibration source (40 kHz)	82 %, 200 min	(Zheng et al., 2020)
	MO	200 W xenon lamp	76 %, 6 hr	(Xian et al., 2015)
	MB	Sun light	91 %, 60 min	(Kappadan et al., 2021)
	MB	Visible light (75 W–220 V lamp)	98.72 %, 7 hr	(Nguyen et al., 2021)
$BaTiO_3$/CuO	MO	Ultrasonic cleaner + 200 W xenon lamp	~100 %, 90 min	(Yu et al., 2022)
$BaTiO_3$/$KNbO_3$	DLB 5B	300 W xenon lamp + ultrasonic cleaner (45 KHz)	93.3 %, 180 min	(Y. Zhang et al., 2021)
$BaTiO_3$/Au/g-C_3N_4	Rh B	300 W xenon lamp	100 %, 20 min	(M. Wu et al., 2020)
$BaTiO_3$/In_2S_3	MO	350 W-xenon lamp	93 %, 90 min	(Wei et al., 2019)
SnS_2/$BaTiO_3$	MO	350 W-xenon	98 %, 20 min	(Zhang et al., 2016)

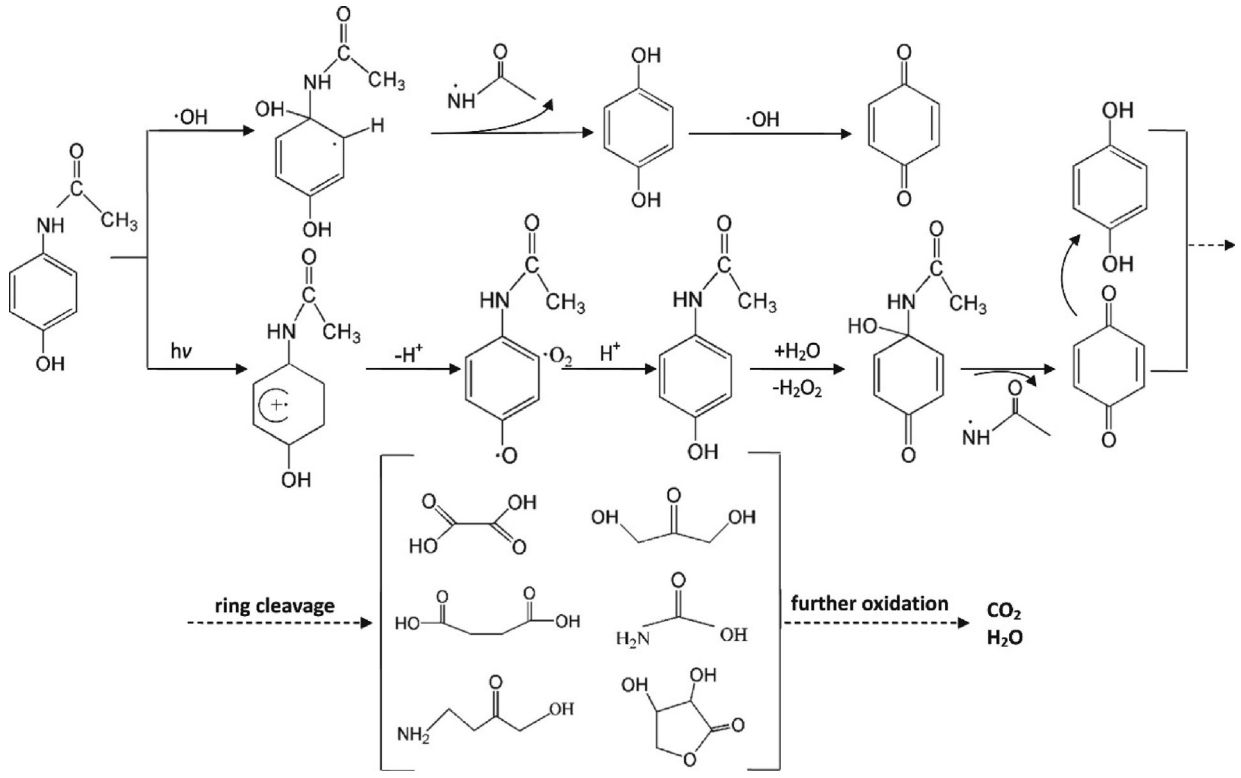

Fig. 23 Photocatalytic degradation pathway for acetaminophen (Ace) (Kurniawan et al., 2018).

$BaTiO_3$ doped with higher amount of tungsten (W). According to this study, pH played a significant role in the photocatalytic degradation of tetracycline. The photocatalytic degradation removal percentage increased with an increase in pH solution. The degradation efficiency was recorded to be 3, 80 and 90 % at pH 3, 5.60 and 10, respectively. In addition, tungsten-doped $BaTiO_3$ (W-$BaTiO_3$) was used to treat spiked real water samples.

(tap and drinking water). Under light irradiation (after 3 hrs), the composite achieved a degradation efficiency of 74 and 76 % in drinking and tap water, respectively. The decrease in the degradation efficiency from tap and drinking water was due to other various pollutants or ions detected in the water matrices, which has some negative effect on the photocatalytic process (Bilgin Simsek, 2017). In a study conducted by Demircivi *et al.,* decorated $BaTiO_3$ with carbon fibers (CFs) were synthesized for enhanced photocatalytic degradation of tetracycline (Demircivi et al., 2020). The incorporation of CFs to $BaTiO_3$ reduced the band gap of the composite and showed enhancement in photocatalytic activity of $BaTiO_3$/CF. Under UV and visible light irradiation, $BaTiO_3$/CF showed the highest degradation efficiency of 96 % as compared to $BaTiO_3$ (W-$BaTiO_3$). According to re-usability studies, the composite showed the highest stability within 5 cycles. However, after 6 cycles, a sharp decline in degradation efficiency was observed from 96 to 77 %. This could be due to the loss of tiny photocatalyst powder with an increase in recyclability. Almost a 100 % degradation efficiency was reported when Ti_{32}-oxo-cluster/$BaTiO_3$/CuS p-n heterojunction was employed for wastewater treatment under both visible light irradiation and mechanical vibration (Piezo-photocatalysis) (Zhou et al., 2021).

The piezoelectric/ferroelectric materials including $ZnSnO_3$, MoS_2, $NaNbO_3$, $BiFeO_3$, $KNbO_3$, BiOCl, Bi_4 Ti_3O_{12} and $BaTiO_3$ nanoparticles in powder forms have been utilized as promising piezocatalysts for several applications. However their applications are limited in cleaning water due to the inability of being recovered from aqueous solution (Lin et al., 2020). Sharma *et al.* investigated the piezocatalytic activity of cement-based $BaTiO_3$ composites for the removal of several pollutants in water such as pharmaceutical (paracetamol) and dyes ((Rh B), (MO) and (MB)) (Sharma et al., 2020). Sharma and co-workers, combined powdered $BaTiO_3$ nanoparticles with cement to form cement-ferroelectric composites which can be easily recovered from aqueous solution after wastewater treatment. Under ultrasonic vibration, the poled $BaTiO_3$ cement composites showed significant piezocatalytic removal of all organic pollutants. The poled composite exhibited the highest piezocatalytic degradation of approximately > 90, 86, 85, and 79 % for Rh B, MB, MO and paracetamol, respectively. The composites could be reused up to the 5th cycle of piezocatalysis under ultrasonic vibration. Another antibiotic drug which is in the class of fluoroquinolone antibiotics is Norfloxacin (NFX). This antibiotic drug is not easily degradable and can further contribute to antibiotic resistance when used. Therefore, the double Z-scheme of $BiFeO_3$/$CuBi_2O_4$/$BaTiO_3$ was fabricated by Zhang *et al.*, and employed for photocatalytic degradation of Norfloxacin (NFX) under solar-light irradiation (Zhang et al., 2020). The combination of $BiFeO_3$, $CuBi_2O_4$ and $BaTiO_3$ to form the composites, extended the light absorption to UV–visible and near-infrared (NIR) light to allow efficient use of the whole solar light spectrum. As shown in Fig. 24(a), the nanocomposites Z-scheme of $BiFeO_3$/$CuBi_2O_4$/$BaTiO_3$

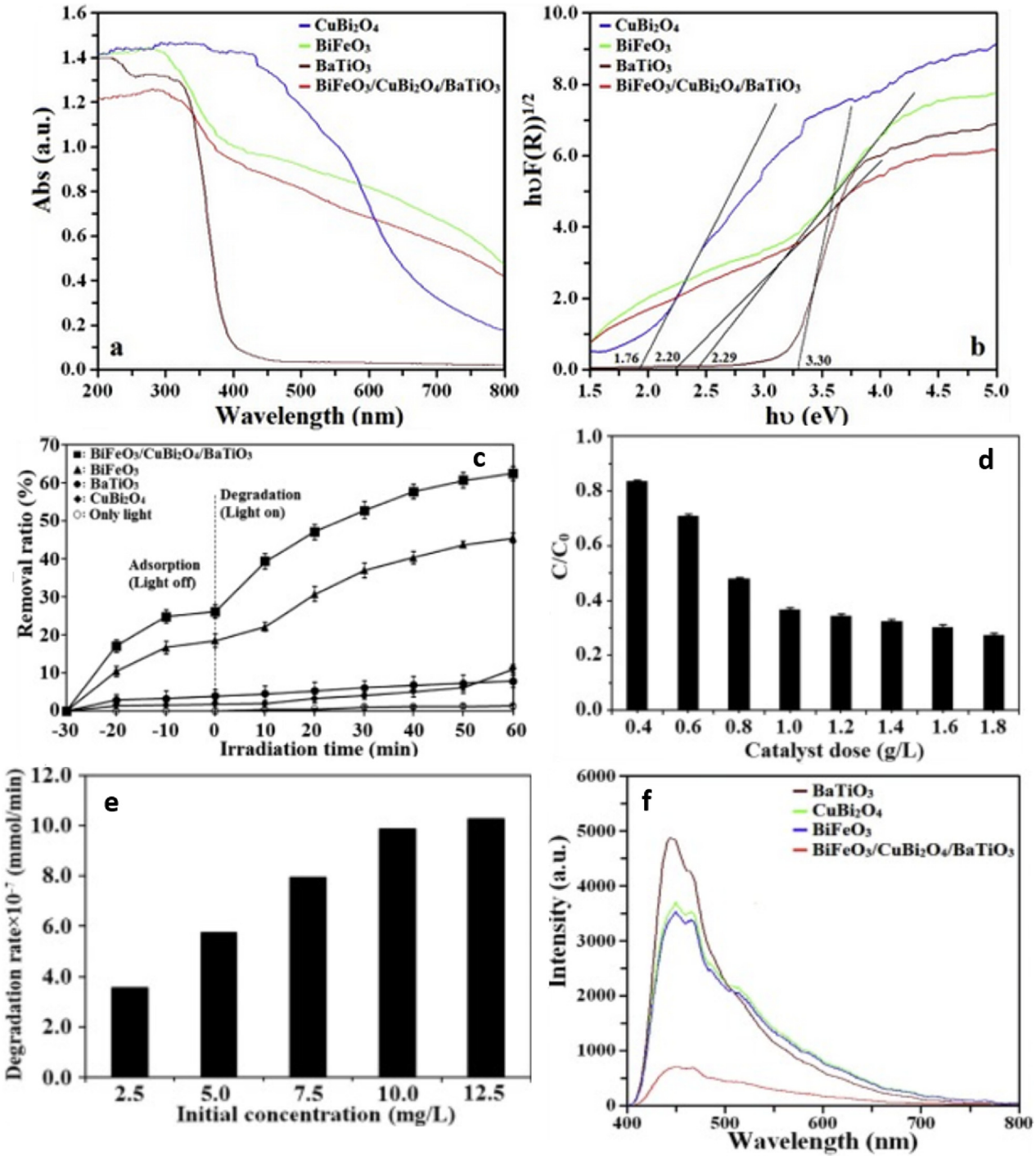

Fig. 24 (a) UV–vis DRS spectra and (b) Tauc's plot curves for $BiFeO_3$, CuBi2O_4, $BaTiO_3$ and $BiFeO_3/CuBi_2O_4/BaTiO_3$, (c) effect of irradiation time (d) effect of catalyst dosage (e) effect of initial concentration o photocatalytic degradation and (f) (PL) spectra's of materials (Zhang et al., 2020).

strongly absorbed in the 200–800 nm range. The calculated optical band energy gap from the tauc's plot were approximately 3.30, 1.76, 2.29 and 2.20 eV for $BaTiO_3$, $CuBi_2O_4$, $BiFeO_3$ and $BiFeO_3/CuBi_2O_4/BaTiO_3$, respectively (Fig. 24 (b)). The effect of irradiation time, catalyst amount and initial NFX concentration were investigated on the photocatalytic performance of the Z-scheme composites. It was noticed that as irradiation time and catalyst dosage increased, the degradation efficiency also increased (Fig. 24**(c-d)**). The degradation rate increased with an increase in initial NFX concentration within a particular concentration range (Fig. 24(e)), this was due to the fact that more NFX molecules remained in aqueous solution at higher concentrations. Under the same optimal parameters (dosage of 1.0 g/L, within 60 min, and NFX concentration of 2.5 mg/L), $BiFeO_3/CuBi_2O_4/BaTiO_3$ nanocomposites had a better photocatalytic activity than individual

samples of $BaTiO_3$, $CuBi_2O_4$, $BiFeO_3$. The composite reached its highest degradation of 93.5 % which could be attributed to a better separation of electrons (e^-) and holes (h^+) to improve the redox ability thus enhancing the photocatalytic activity of the catalyst. The electrons and holes separation were confirmed by photoluminescence (PL) spectrum (Fig. 24(f)). Generally, a low PL intensity reveals greater electrons (e^-) and holes (h^+) separation efficiency. As shown in Fig. 24(f), $BiFeO_3/CuBi_2O_4/BaTiO_3$ had the lowest PL intensity than $BaTiO_3$, $CuBi_2O_4$ and $BiFeO_3$, thus indicating better enhancement in photocatalytic activity of the composite. The extent of mineralization of NFX (10.0 mg/L) obtained from TOC was 3.9, 6.8, 40.9 and 60.3 % for $BaTiO_3$, $CuBi_2O_4$, $BiFeO_3$ and $BiFeO_3/CuBi_2O_4/BaTiO_3$, respectively. However, the extent of mineralization for NFX (2.5 mg/L) reached up to 93.5 % within 1 hr. According to scavenger experiments conducted, it was found that hydroxyl radicals (•OH) and holes (h^+) played an important role in the deterioration of NFX than superoxide radicals ($\bullet O_2^-$).

Pharmaceuticals used in aquaculture are also a source of pollution that is delivered directly into surface water. For example, atrazine is a well-known herbicide that is used to control broadleaf and grassy weeds in water. It was banned in most countries because of its negative impact on aquaculture and humans (Cavas, 2011). Due to that, Basaleh and Mohamed (Basaleh and Mohamed, n.d.) developed Copper (Cu)-doped $BaTiO_3$ photocatalyst for the removal of this toxic herbicide (atrazine) from wastewater so as to provide clean water to the environment. The photocatalyst (Cu-$BaTiO_3$) was prepared through the hydrothermal and photo-assisted deposition method. The prepared photocatalyst was added into 300 ml atrazine solution (50 ppm) and irradiated with Xenon lamp. The photocatalytic removal for atrazine using 0.5 Cu/$BaTiO_3$, 1.0 Cu/$BaTiO_3$, 3.0 Cu/$BaTiO_3$ and 5.0 Cu/$BaTiO_3$ were recorded to be 45, 65, 100 and 100 %, respectively. As for pure $BaTiO_3$, the removal efficiency was low as 3 % due to the high electron and holes recombination. These results confirmed that doping $BaTiO_3$ with Cu can suppress the rate of electrons and holes recombination, thus increasing photocatalytic performance of Cu-$BaTiO_3$. The suppression of electrons and holes recombination was confirmed by photocurrent response and photoluminescence (PL) spectrum. The Cu/$BaTiO_3$ had a greater photocurrent response of 12.8 mA cm^{-2} than pure $BaTiO_3$ (2.8 mA cm^{-2}). In another study, $BaTiO_3$ was co-loaded with two electrocatalyst (Pt and RuO_2) to promote sufficient redox ability for piezocatalytic degradation of tricyclazole under mechanical vibration (Feng et al., 2019). The platinum (Pt) was selected since it has been considered as the best catalyst for oxygen reduction, whereas RuO_2 can produce large amounts of hydroxyl radicals and facilitate protons transport during electrocatalytic reaction. The loading of co-catalysts to $BaTiO_3$ resulted in surface area increment from 25.5 to 28.8 m^2g^{-1}. Specific surface area of the materials is another factor which can influence the photocatalytic performance of the photocatalyst. Under ultrasonic vibration (40 kHz, 110 W), the composite achieved the highest removal percentage of 86 % which was higher than the values obtained using RuO_2/t-$BaTiO_3$ (51.0 %) and Pt/t-$BaTiO_3$ (75.9 %). According to apparent rate constant values (k) obtained from pseudo-first order kinetics, the piezocatalytic reaction rate for the composites ($k = 0.0320\ min^{-1}$) was 3.11 times greater than pure $BaTiO_3$ ($k = 0.0103\ min^{-1}$) and the sum of k values of Pt/t-$BaTiO_3$ (0.0125 min^{-1}) and RuO_2/t-$BaTiO_3$ (0.0124 min^{-1}). The outstanding performance of the composite confirmed that coupling ferroelectric materials with a good catalyst can yield a synergistic enhancement effect on the piezocatalytic degradation. Another $BaTiO_3$ based heterostructured catalyst which has been employed for piezocatalytic/photocatalytic and piezo-photocatalytic removal of pharmaceutical pollutants is $BaTiO_3/La_2Ti_2O_7$ heterojunction. Li *et al*. prepared $BaTiO_3/La_2Ti_2O_7$ composites via a two-step hydrothermal and microwave hydrothermal synthesis for piezo-photocatalytic degradation of ciprofloxacin (Y. Li et al., 2021). After 90 min of photocatalytic degradation, $BaTiO_3/La_2Ti_2O_7$ recorded a degradation efficiency of 16.5 and 22.7 % greater than that of $BaTiO_3$ and $La_2Ti_2O_7$, respectively, thus indicating that the formation of a heterojunction improved the photocatalytic degradation process. Under ultrasonic vibration (piezocatalysis), the degrading efficiency of CIP over $BaTiO_3/La_2Ti_2O_7$ (37.7 %) was roughly 19 % greater than that of $BaTiO_3$ and $La_2Ti_2O_7$. The degradation rate constant (k value) obtained from pseudo first-order kinetics model was 0.00593 min^{-1} for $BaTiO_3/La_2Ti_2O_7$, which is roughly 2.8 and 2.3 times greater than $BaTiO_3$ and $La_2Ti_2O_7$, respectively. The higher degradation efficiency of 50.2 % was achieved when piezocatalysis and photocatalysis were merged. For all samples, the performance of piezo-photocatalysis was superior to that of photocatalysis or piezocatalysis. This might be due to photocatalysis's low visible-light absorption and low carrier separation efficiency. The catalytic performance was likewise low during the piezocatalytic procedure due to the restricted amount of free charge carriers created. Photogenerated charge carriers were efficiently separated under the combined action of visible light and ultrasound, and CIP degradation efficiency was greatly increased when compared to sole-ultrasound and sole-visible-light irradiation. The composites showed higher catalytic activity than individual samples, thus indicating that the $BaTiO_3/La_2Ti_2O_7$ heterojunctions boost the catalytic process. The photocatalytic degradation of tetracycline and Rh B was reported by Zheng *et al.,* using a Z-type $BaTiO_3/\gamma$-Bi_2O_3 heterojunction which was prepared via hydrothermal, co-precipitation, and calcination (Zheng et al., 2022). The morphological structure of the prepared samples appeared to be of a tetrahedron shape, irregular nano-particles and a mixture of both shapes (tetrahedron and nanoparticles) for γ-Bi_2O_3, $BaTiO_3$ and $BaTiO_3/\gamma$-Bi_2O_3 heterojunction, respectively (Fig. 25**(a-c)**). It was found that the calcination temperature had no effect on the morphology, the obtained average particles for γ-Bi_2O_3, $BaTiO_3$ and $BaTiO_3/\gamma$-Bi_2O_3 (HS3) were roughly around 5.9 μm, 425.9 nm, and 1.9 μm, respectively. The effect of catalyst dose, pH of the solution and different water bodies on photodegradation of tetracycline was explored, however these parameters had a little impact on the photocatalytic degradation process (Fig. 25**(d-g)**). The degradation efficiency for both pristine (γ-Bi_2O_3 and $BaTiO_3$) were below 67 %, for γ-Bi_2O_3 and $BaTiO_3$ were found to be 59.65 and 66.28 %, respectively. However, for all Z-type $BaTiO_3/\gamma$-Bi_2O_3 (HS) heterojunctions with different molar ratio, reaction time and calcination temperature, the degradation removal percentages were above 93 %, with HS3 exhibiting the highest degradation efficiency of 97.95 % for tetracycline. Even for Rh B dye, the degradation efficiency for single γ-Bi_2O_3 and $BaTiO_3$ were below 67 %. It was found that γ-Bi_2O_3 and $BaTiO_3$ degraded about 63.34 and 45.35 %,

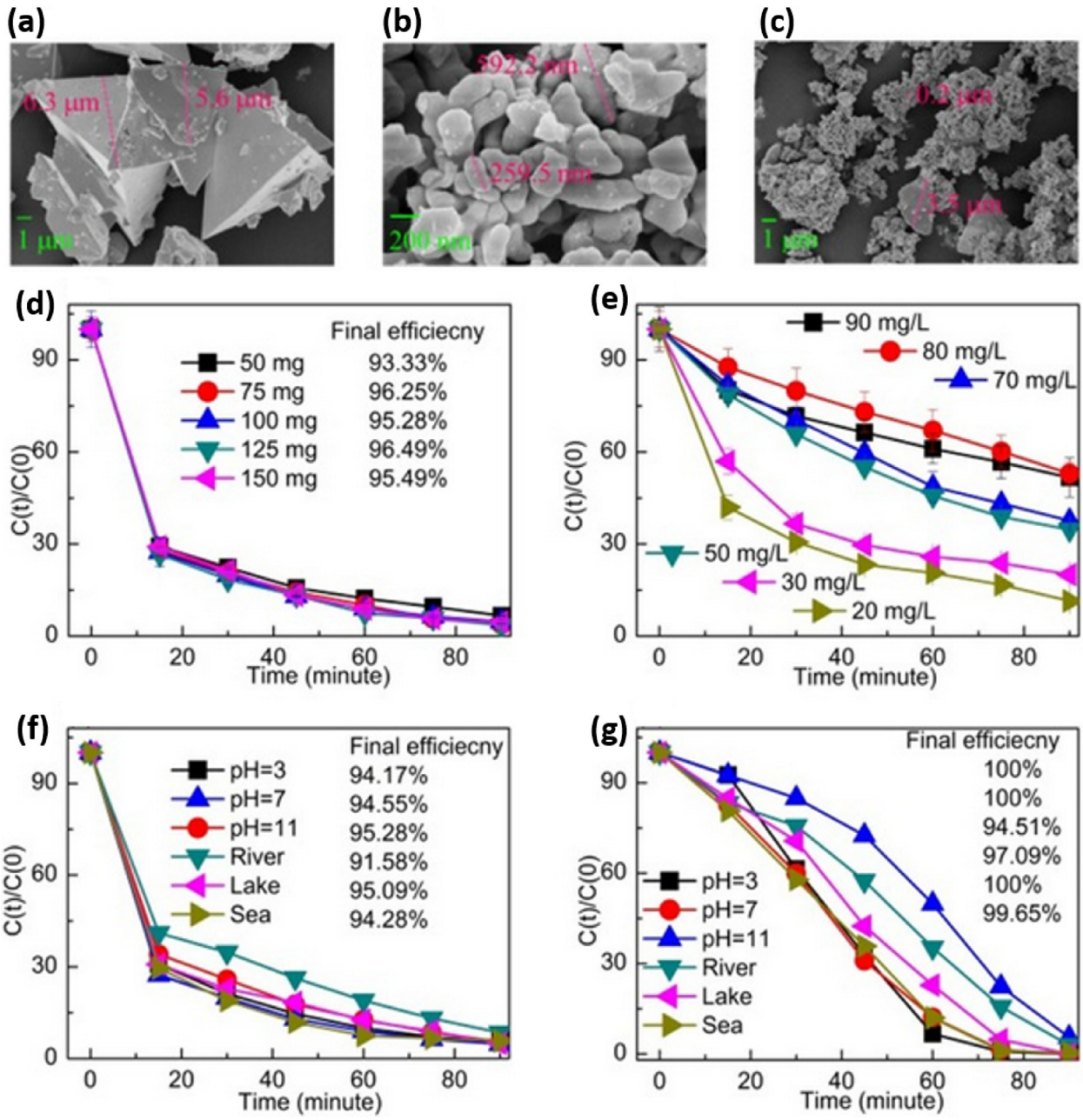

Fig. 25 (a) Effect of catalyst dosage, (b) initial concentration on degradation of tetracycline, as well as effect of pH and water bodies on the degradation of (f) tetracycline and (g) Rh B (Zheng et al., 2022).

respectively. The photocatalytic degradation efficiencies for all HS heterojunction samples were above 73 %, with HS3, HS4, and HS5 breaking down the Rh B molecule entirely. The enhanced photocatalytic activity was due to electrons transferred via Z-type from Bi_2O_3 conductor band (CB) to $BaTiO_3$ valence band (VB) by work function and charge density difference which resulted in charge separation.

Another type of hydrothermally synthesized Z scheme heterojunction of $La(OH)_3$@$BaTiO_3$ (LB) composite was investigated for deterioration of an A-ring of tetracycline (Zheng et al., 2022). The reactive oxygen species (ROS) such as hydroxyl radicals (OH), superoxide (O_2^-), holes and electrons completely degraded 100 % of tetracycline. The scavenger studies confirmed that four active species played a role in their photocatalytic degradation, as follows: $h^+ = \bullet O_2^- > \bullet OH > e^-$ (before 20 min reaction) and $h^+ > \bullet OH > \bullet O_2^- > e^-$ (after 20 min reaction). According to these results, it means that holes (h^+) played a major role in the photocatalytic degradation whereas electrons (e^-) showed the least contribution during the photocatalytic degradation of tetracycline. The application of $BaTiO_3$-based catalyst for removal of pharmaceuticals is summarized in Table 5.

Despite using $BaTiO_3$-based catalyst for piezo-photocatalytic degradation of organic dyes and pharmaceuticals, there are some factors which affects the piezo-photocatalytic degradation process negatively. Some of these

Table 5 Effect of various $BaTiO_3$-based catalyst for catalytic degradation of pharmaceuticals.

Catalyst	Pharmaceuticals	Reaction conditions	% Removal & reaction time	Refs
$BaTiO_3/TiO_2$	Ace	500 W xenon lamp	95 %, 4 hr	(Kurniawan et al., 2018)
W-$BaTiO_3$	TC	18 UV lamps	80 %, 180 min	(Demircivi and Simsek, 2019)
$BaTiO_3$/CF	TC	UV-A light & visible light	96 %, 180 min	(Demircivi et al., 2020)
$BaTiO_3$ –cement	PCT	Ultrasonic (40 kHz, 70 W)	> 79 %, 240 min	(Sharma et al., 2020)
Cu-$BaTiO_3$	ATZ	Xenon lamp (cut-off filter, 420 nm)	100 %, 60 min	(Basaleh and Mohamed, n.d.)
RuO_2/t-$BaTiO_3$/Pt	TCZ	Ultrasonic Cleaner (40 kHz, 110 W)	86 %, 60 min	(Feng et al., 2019)
$BiFeO_3/CuBi_2O_4$/$BaTiO_3$	NFX	500 W xenon lamp	93.5 %, 60 min	(Zhang et al., 2020)
$BaTiO_3/\gamma$-Bi_2O_3	TC	250 W mercury lamp irradiation	98 %, 90 min	(Zheng et al., 2022)
$La(OH)_3$@$BaTiO_3$	TC	350 W Xe lamp	100 %, 120 min	(B. Wang et al., 2019)
$BaTiO_3/La_2Ti_2O_7$	CIP	Ultrasonic (40 kHz, 210 W) + 300 W Xe lamp	50.2 %, 90 min	(Y. Li et al., 2021)

factors include nature of the semiconductor, amount of the catalyst, solution pH, reaction time, light intensity, dissolved reactive oxygen species and temperature. For examples, some organic pollutants showed maximum adsorption removal and piezo-photodegradation at lower (acidic media) or higher pH (basic media) due their complex structure. Therefore, limiting their applications in real wastewater treatment because it means prior to degradation processes, the pH of the real wastewater samples needs to be adjusted. Another critical factor is the surface area of the piezo-photocatalyst, since the piezo-photodegradation efficiency increases with an increase in surface area of the catalyst. It is very important to select piezo-photocatalyst with very high surface area because of more active sites, which assist in the enhancement of piezo-photodegradation. Furthermore, this processes requires reactive high amount of reactive oxygen species (ROS) such as hydroxyl radicals and superoxide to completely oxidize organic dyes and pharmaceutical into less harmful by-products such as carbon dioxide (CO_2) and water (H_2O). Therefore, lower levels of reactive oxygen species would result in incomplete oxidation of organic pollutants.

6.3. Pathogenic bacteria

Piezocatalytic, photocatalytic and piezo-photocatalytic disinfection has attracted more attention in elimination of pathogenic bacteria. These processes usually use reactive oxygen species (ROS) such as hydroxyl radicals, superoxide, hydrogen peroxide and h^+, e^- generated when piezo-photocatalyst is exposed under light irradiation or mechanical vibration to kill bacteria (J. He et al., 2021). Generally, the idea of photocatalytic disinfection is to first remove each bacterium's cell wall, removing its protection, and then to damage its cytoplasmic membrane, causing the cellular material inside the newly torn cell envelope to degrade (Fig. 26). Ferroelectric based catalysts such as barium titanate ($BaTiO_3$) have been used as piezocatalyst/photocatalysts for bacterial disinfection due to its exceptional optical and piezoelectric/ferroelectric properties. For example, Zhao *et al.* fabricated a novel p-n type Cu_2MgSnS_4/$BaTiO_3$ (CMTS@$BaTiO_3$) heterojunction for the degradation of organic dyes and bacterial disinfection (Ali et al., 2021). In terms of bacterial disinfection, CMTS@$BaTiO_3$ obtained 72–76 % and 84–90 % inhabitation for *E.coli* and *S.aureus*, respectively, which was three times greater than pure CMTS and $BaTiO_3$. Furthermore, CMTS@$BaTiO_3$ heterojunction was tested for inactivation of *E.coli* and *S.aureus* in the presence of wastewater containing dyes (MG and MB). When compared to as-grown bacteria, inactivated levels of bacterial percentages employing CMTS@$BaTiO_3$ composites were around 94.22–101.24 % with MB and MG, respectively, against *E.coli* and 97.59 to 87.96 % for *S.aureus*. In comparison to CMTS@$BaTiO_3$, Kumar *et al.* demonstrated piezocatalytic, photocatalytic and piezo-photocatalytic disinfection of *E.coli* using unpoled and poled $BaTiO_3$ ceramic under UV light and ultrasonic vibration (Kumar et al., 2019a). During the piezocatalytic process (under ultrasonic vibration), unpoled $BaTiO_3$ showed a 56 % of bacterial disinfection within 30 min. Under light exposure and ultrasonic vibration, piezo-photocatalysis improved the bacterial degradation rate and the piezo-photocatalytic degradation of *E.coli* increased from 56 to 70 % within the same reaction time. When the poled $BaTiO_3$ ceramic were employed for piezocatalytic degradation (under ultrasonic vibration), it was found that about 97 % of bacteria were killed. Under the piezo-photocatalysis process (ultrasonic vibration and light exposure), poled $BaTiO_3$ ceramic showed some catalytic enhancement towards catalytic degradation of bacteria (99.99 % recorded within 20 min). From these results, it can be concluded that poled $BaTiO_3$ ceramic have better photocatalytic activity than unpoled $BaTiO_3$ ceramic and coupling piezocatalysis with photocatalysis further enhanced the catalytic degradation activity of $BaTiO_3$.

Kumar *et al.* investigated the photocatalytic and antibacterial activity of poled $BaTiO_3$ prepared via a solid state method (Kumar et al., 2019b). From the FESEM analysis, it was found that $BaTiO_3$ consisted of large dense grains with clear grain boundaries (Fig. 27(a)). The calculated average grain size of $BaTiO_3$ sample ranged from 40 to 60 μm (Fig. 27(b)). Both unpoled and poled $BaTiO_3$ were shown to respond under UV irradiation. The poled $BaTiO_3$ exhibited the highest photocurrent response of about 0.006 μA, which was > 100 times greater than that of unpoled $BaTiO_3$. Thus, indicating that

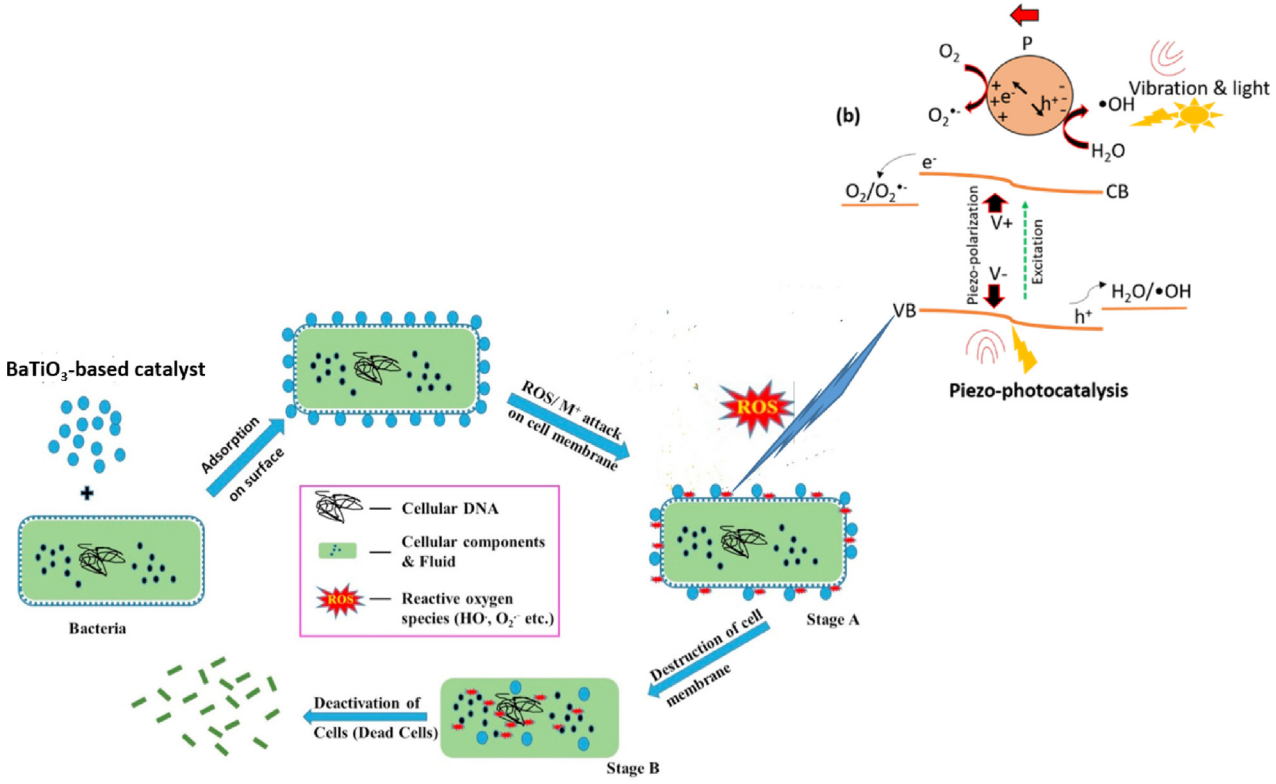

Fig. 26 Possible photocatalytic bacterial disinfection mechanism (Laxma Reddy et al., 2017).

poled $BaTiO_3$ had a higher photocatalytic activity (Fig. 27**(c-d)**). This was due to its remnant polarization which inhibited recombination of photogenerated charges. However, under dark conditions both samples (poled and unpoled $BaTiO_3$) showed no response to UV irradiation.

The colony forming unit (CFU) method was employed to study the effect of poled $BaTiO_3$ samples on absolute bacterial mortality. As shown in Fig. 27(e), the results display that there was no substantial antibacterial activity with unpoled $BaTiO_3$ and negative side of poled samples in the dark. However, the positive side of poled $BaTiO_3$ exhibited strong antibacterial activity with about 90 % bacterial destruction after 60 min when UV light was irradiated (Fig. 27(f)). In the absence of a catalyst ($BaTiO_3$ poled or unpoled), the UV light alone showed antibacterial activity since it can prevent bacterial growth by destroying their structural DNA. Kushwana and co-workers reported (Kushwaha et al., 2015) Li-Doped $Bi_{0.5}$-$Na_{0.4}5$ $K_{0.5}TiO_3$–$BaTiO_3$ (BNKLBT) for antibacterial activity against *E.coli* and *A.flavus* using standard disc diffusion method. This method involves bacterial growth using Luria–Bertani (LB) broth–agar in a petridish disc. Three different concentrations (10, 50 and 100 μg) of BNKLBT were tested against bacteria and compared with commercial antibiotics (kanamycin (k_{30})). Based on their results, the zone of inhibition increased as BNKLBT concentration increased on the disc. The reason for this trend was not explained in this work. In another report, $BaTiO_3$ nanoparticles were tested for antibacterial efficacy against *S.aureus and P. aeruginosa* by Shah *et al.*(Shah et al., 2018). The diffusion method was employed to investigate the antimicrobial activity of $BaTiO_3$ nanoparticles. The optimal concentration of 100 μg/ml ($BaTiO_3$) achieved bacterial inhibition of 85 ± 3.5 % and 80 ± 3 % against *S.aureus* and *P.aeruginosa* biofilms, respectively.

Shuai *et al.* prepared PVDF/*x*Ag-pBT composites via laser sintering method for bacterial disinfection (Shuai et al., 2020a). According to their studis, PVDF/*x*Ag-pBT composites generated piezoelectric potential/voltage. Furthmore, it was found that with an increase in Ag concentration in the PVDF/pBT composites, the piezoelectrical current and voltage firstly rose then dropped. Babu *et al.* and Parl *et al.* observed comparable enhancement after adding conductive fillers to polymer-ceramic composites (Babu and de With, 2014) (Park et al., 2012). Their assumptions on the output voltage and current improvement were based on the conductivity enhancement. The antibacterial activity of the prepared scaffolds (PVDF/4Ag-pBT and PVDF/pBT) were evaluated using zone of inhibition method. Fig. 28**(a-b)** shows the bacterial inhibition zones of the scaffolds. PVDF/4Ag-pBT was shown to be more successful in inhibiting the growth of *E.coli* as compared to PVDF/pBT scaffold. Further test including Turbidimetric test were conducted to verify antibacterial activity of the scaffolds. The transparent vials including and excluding *E.-coli* suspensions were labelled as control and blank group, respectively. The turbidity was the same for vials containing PVDF/4Ag-pBT and control. Surprisingly, the vial containing *E.coli* solution incubated with PVDF/4Ag-pBT was clear as a blank group, thus indicating that the scaffold inhibited bacterial growth of *E.coli* (Fig. 28(c)). The SEM images also confirmed that PVDF/4Ag-pBT scaffold raptured and destroyed the whole rod-shape structure of *E.coli*, whereas PVDF/pBT scaffold had minimal impact on the smooth rod-shape of *E.-*

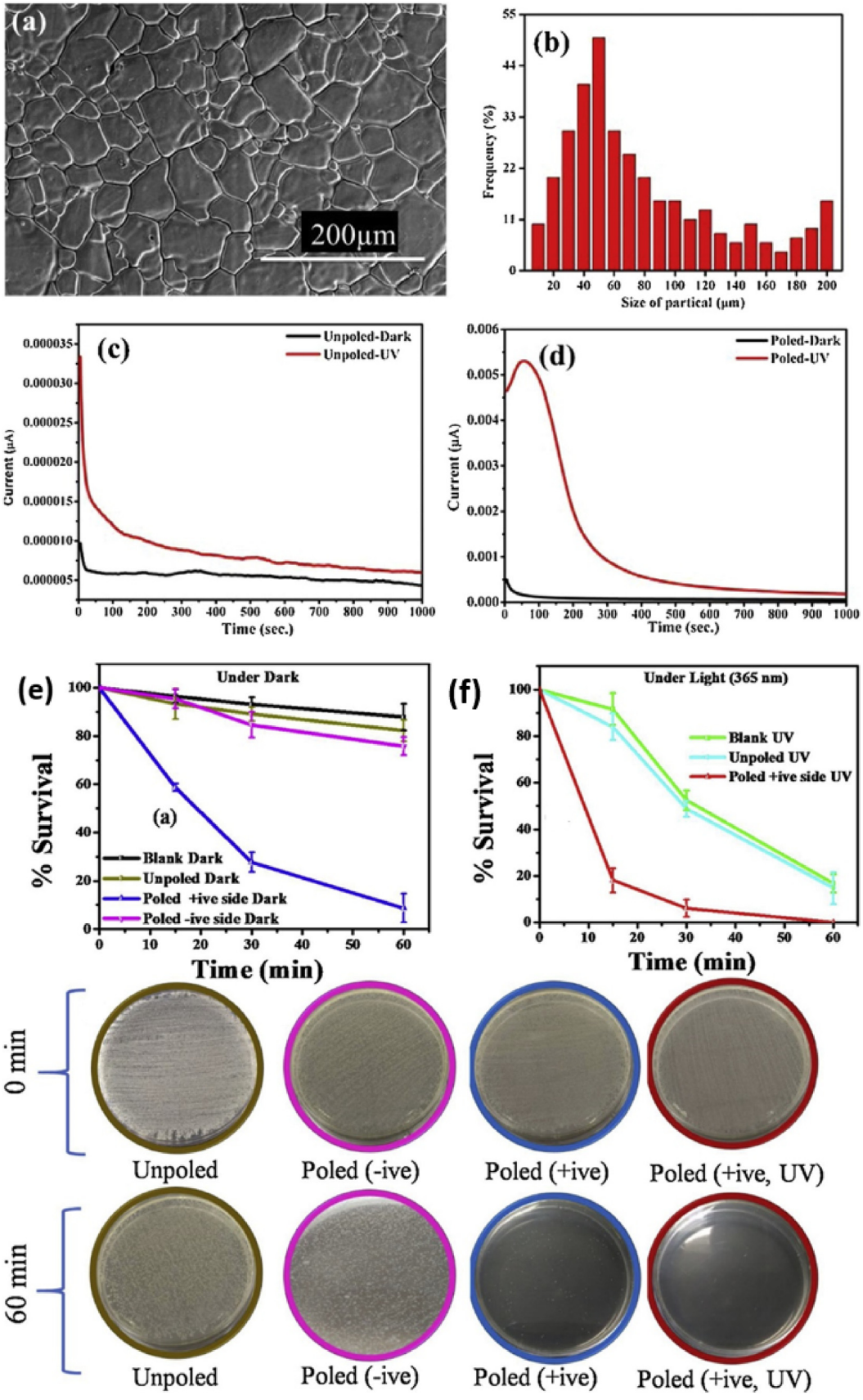

Fig. 27 (a-b) SEM images and particle size of $BaTiO_3$, (c-d) photocurrent response under dark and UV light, catalytic degradation of bacteria under (e) dark and (f) UV light (Kumar et al., 2019b).

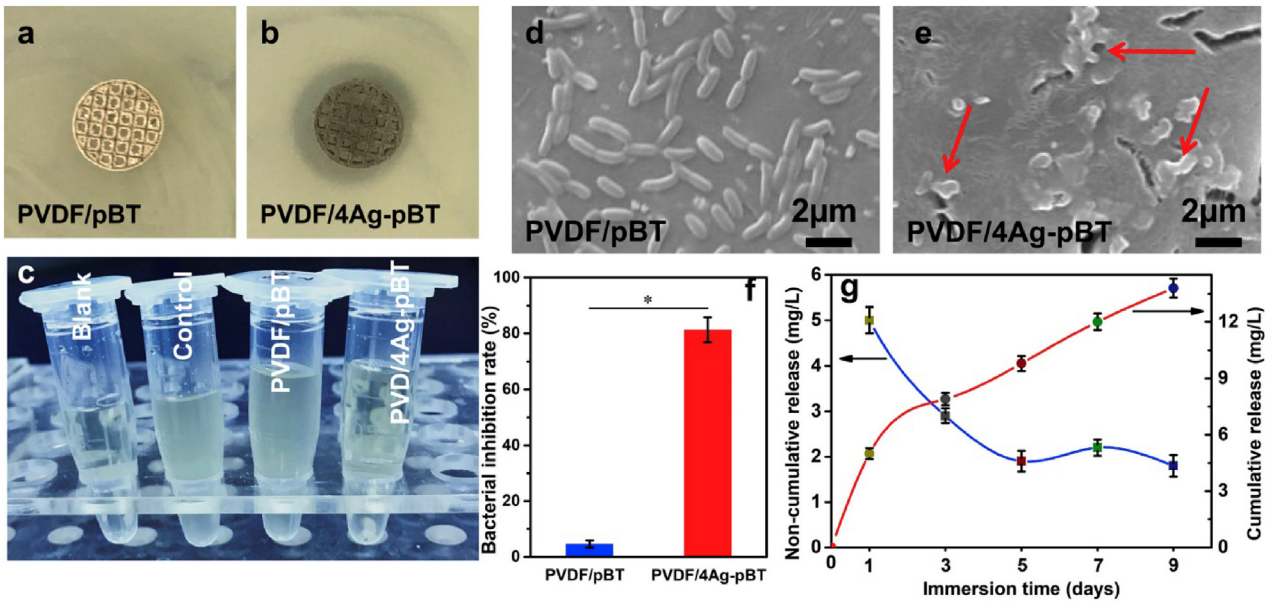

Fig. 28 (a-b) Photographs of zone of inhibition, (c) turbidity test, (d-e) SEM images of bacteria, (f) bacterial zone of inhibition rate and (g) cumulative or non-cumulative of silver ion concentration released by PVDF/4Ag-pBT (Shuai et al., 2020a).

coli (Fig. 28**(d-e)**). Fig. 28**(f-g)** displays bacterial inhibition rate of scaffolds and cumulative or non-cumulative of silver ion concentration released by PVDF/4Ag-pBT. The PVDF/4Ag-pBT scaffold inhibited bacteria at a rate of over 81 %, while the PVDF/pBT scaffold had no antibacterial activity.

Overall, $BaTiO_3$-based catalyst have been shown to be appropriate for applications involving the combination of photocatalysis, piezocatalysis and other catalysis processes. An overview of the previous studies addressing the use of $BaTiO_3$-based catalyst for water disinfection is summarized in Table 6. The use of piezo-photocatalyst based materials for bacterial disinfection is still in its infancy. The process of piezo-photocatalysis has been widely applied including hydrogen production (H_2), degradation of organic pollutants in wastewater, carbon dioxide (CO_2) conversion and hydrogen peroxide (H_2O_2) production. In piezo-photocatalytic disinfection, it is challenging to develop a general mechanism for bacteria inactivation because of a wide range of pathogens and their cell complexity. Therefore, deeper understanding of the mechanisms the piezo-photocatalytic process is still required since suggested mechanisms highly rely on the generated reactive oxygen species during redox reactions. It is still debatable whether polarized charge carriers participate in the redox catalytic process. According to certain studies, photogenerated electrons and holes play a crucial part in redox processes, and the polarization potential of piezoelectric materials merely helps to separate photogenerated charge carriers (Fu et al., 2022).

7. Conclusions, limitations and future perspectives

Barium titanate ($BaTiO_3$) offers a wide range of applications in the energy and environmental fields. In comparison to certain applications like water hydrogen production, its usage in the piezo-photocalaytic wastewater treatment and bacterial disinfection is limited and recent. This review article has presented a complete summary of current developments in the use of barium titanate-based catalysts in photocatalytic, piezocatalytic and piezo-photocatalytic decomposition of organics and bacterial disinfection in water and wastewater. The selection of $BaTiO_3$ as a suitable piezo-photocatalyst was due to its outstanding dielectric/ferroelectric/piezoelectric characteristics, low

Table 6 Some previous studies on bacterial disinfection using $BaTiO_3$-based materials.

Catalyst	Bacteria	Reaction conditions	% Removal & reaction time	Refs
$Cu_2MgSnS_4/BaTiO_3$	*E. coli and S. aureus*	Ultrasonic (40 kHz)	>90 %, 3 hr	(Ali et al., 2021)
$BaTiO_3$	*E.coli*	Vibration (8 Hz) + light irradiation (375 nm)	99.99 %, 20 min	(Kumar et al., 2019a)
	E.coli	UV light (365 nm)	90 %, 60 min	(Kumar et al., 2019b)
	P.aeruginosa & S.aureus	NA	85 ± 3.5 % & 80 ± 3 %	(Shah et al., 2018)
PVDF/*x*Ag-pBT	*E.coli*	Hammer	81 %	(Shuai et al., 2020b)
TiO_2 @$BaTiO_3$–V(P)	*S. aureus*	NA	100 %, 24 hr	(Wu et al., 2021)
Ag/t-$BaTiO_3$	*E.coli*	Ultrasonic Cleaner (40 kHz, 110 W)	>95 %, 30 min	(J. Feng et al., 2018)

toxicity, low cost, environmental friendliness, existence in broad range of sizes and morphologies, multiple crystal structures and good stability. These characteristics are undoubtedly being used in the piezo-photocatalytic elimination of a variety of organic contaminants. Since, $BaTiO_3$ as a photocatalyst suffers from poor conductivity and rapid recombination of photogenerated charge carriers. In this review, we have covered several strategies to circumvent these restrictions including morphology control, doping, metal loading, and heterojunction construction with appropriate semiconductors. Another way of improving electrons and holes separation is through coupling photocatalysis with other catalysis processes such as piezocatalysis and electrocatalysis. These strategies have achieved excellent results while conserving energy. The effectiveness of $BaTiO_3$-based catalyst for piezo-photocatalytic degradation of organic pollutants depends mainly on several factors such as pH, reaction time, amount of catalyst, ultrasonic and light power. The fundamental benefit of heterogeneous photocatalysis is its capacity to use solar energy in the form of solar photons, which gives the degradation process a large boost in environmental value. Particularly for large-scale aqueous-phase applications, solar light-assisted photodegradation of wastewater contaminants can make it an economically viable method.

Even though several reports have shown some strategic ways to improve photocatalytic activity of barium titanate, however some few other limitations and challenges needs to be highlighted for its success in wastewater treatment.

1. There is limited research on the structure of the barium titanate after being exposed to ultrasonic vibration and light irradiation. It is very important to investigate the stability of the barium titanate structure using TEM, SEM and XRD before and after wastewater treatment.
2. Even though doping barium titanate with plasmonic metals have shown significant improvement in photocatalytic activity, the practical applicability of plasmonic $BaTiO_3$ piezo-photocatalyst is limited due to the high cost and photo-corrosion associated with noble metal nanoparticles.
3. Since the size and morphology of the doped noble metals can affect the photocatalytic activity of the $BaTiO_3$, there are no reports in the literature on the size and morphology of the noble metals nanoparticles doped on the surface of $BaTiO_3$ piezo-photocatalyst. To establish the ideal condition of noble metal nanoparticles needed for photocatalytic enhancement, it is therefore necessary to assess the surface plasmon resonance (SPR) impact from different sizes and shapes.
4. From our analysis, there's limited understanding of piezo-photocatalytic mechanism for $BaTiO_3$-heterojunction piezo-photocatalyst. Therefore, for future studies it is very important to study reaction mechanisms for piezo-photocatalytic degradation of organic pollutants in detail.
5. Furthermore, many reports in literature have given limited information regarding how synthetic methods and structural properties of $BaTiO_3$ piezo-photocatalyst affects the efficiency of the process. As a result, future research should pay close attention to how these factors impact piezo-photocatalyst effectiveness.
6. The amount of organic pollutant degradation is determined by the photocatalysts' mineralization capacity. However, the majority of earlier studies on BaTiO3-based materials did not identify the total organic carbon (TOC) in the mineralization process, which should be taken into account for an accurate assessment of the whole degradation of organic contaminants.

Overall, the use of $BaTiO_3$-based piezo-photocatalysts for real-world remediation of pharmaceutical, organic dyes and microbes from wastewater has a bright future. Therefore, it is highly recommended that advanced oxidation processes such as photocatalysis and piezocatalysis should be used for wastewater treatment in the future instead of traditional techniques.

Acknowledgements

This work was supported by GES 4.0 (Global Excellence Structure 4.0), the Centre for Nanomaterials Science Research (CNSR) University of Johannesburg), National Research Foundation of South Africa (SRUG200326510622), National Research Foundation of South Africa (NRFTTK117999) and the Faculty of Science University of Johannesburg (UJ), South Africa for financial support.

References

Abdi, J., Vossoughi, M., Mahmoodi, N.M., Alemzadeh, I., 2017. Synthesis of metal-organic framework hybrid nanocomposites based on GO and CNT with high adsorption capacity for dye removal. Chem. Eng. J. 326, 1145–1158. https://doi.org/10.1016/j.cej.2017.06.054.

Acosta, M., Novak, N., Rojas, V., Patel, S., Vaish, R., Koruza, J., Rossetti, G.A., Rödel, J., 2017. BaTiO3-based piezoelectrics: Fundamentals, current status, and perspectives. Appl. Phys. Rev. 4. https://doi.org/10.1063/1.4990046.

Aguilar, A.C., Montalvo, C., Ceron, J.G., Moctezuma, E., 2011. Photocatalytic degradation of acetaminophen. Int. J. Environ. Res. 5, 1071–1078 https://doi.org/10.22059/ijer.2011.465.

Aksel, E., Jones, J.L., 2010. Advances in lead-free piezoelectric materials for sensors and actuators. Sensors 10, 1935–1954. https://doi.org/10.3390/s100301935.

Alex, K.V., Prabhakaran, A., Jayakrishnan, A.R., Kamakshi, K., Silva, J.P.B., Sekhar, K.C., 2019. Charge Coupling Enhanced Photocatalytic Activity of $BaTiO_3/MoO_3$ Heterostructures. ACS Appl. Mater. Interfaces 11, 40114–40124. https://doi.org/10.1021/acsami.9b14919.

Ali, A., Zhao, J., Yao, R., Ahmed, S., Wang, L., Guo, B., Rao, W.F., Yang, Y., 2021. Stimulated piezotronical decontamination using Cu2MgSnS4 modified BaTiO3. Mater. Today Energy 21. https://doi.org/10.1016/j.mtener.2021.100717.

Amaechi, I.C., Hadj Youssef, A., Rawach, D., Claverie, J.P., Sun, S., Ruediger, A., 2019a. Ferroelectric Fe-Cr Codoped BaTiO3 Nanoparticles for the Photocatalytic Oxidation of Azo Dyes. ACS Appl. Nano Mater. 2, 2890–2901. https://doi.org/10.1021/acsanm.9b00336.

Amaechi, I.C., Kolhatkar, G., Youssef, A.H., Rawach, D., Sun, S., Ruediger, A., 2019b. B-site modified photoferroic Cr3+-doped barium titanate nanoparticles: microwave-assisted hydrothermal synthesis, photocatalytic and electrochemical properties. RSC Adv. 9, 20806–20817. https://doi.org/10.1039/c9ra03439k.

Amaechi, I.C., Hadj Youssef, A., Kolhatkar, G., Rawach, D., Gomez-Yañez, C., Claverie, J.P., Sun, S., Ruediger, A., 2021. Ultrafast microwave-assisted hydrothermal synthesis and photocatalytic behaviour of ferroelectric Fe3+-doped BaTiO3 nanoparticles under simulated sunlight. Catal. Today 360, 90–98. https://doi.org/10.1016/j.cattod.2019.07.021.

Aminirastabi, H., Xue, H., Mitić, V.V., Lazović, G., Ji, G., Peng, D., 2020. Novel fractal analysis of nanograin growth in BaTiO3 thin film. Mater. Chem. Phys. 239. https://doi.org/10.1016/j.matchemphys.2019.122261.

An, J., Chen, H., Wei, S., Gu, J., 2015. Antibiotic contamination in animal manure, soil, and sewage sludge in Shenyang, northeast China. Environ. Earth Sci. 74, 5077–5086. https://doi.org/10.1007/s12665-015-4528-y.

Asadzadeh, M., Tajabadi, F., Dastan, D., Sangpour, P., Shi, Z., Taghavinia, N., 2021. Facile deposition of porous fluorine doped tin oxide by Dr. Blade method for capacitive applications. Ceram. Int. 47, 5487–5494. https://doi.org/10.1016/j.ceramint.2020.10.131.

Ashiri, R., Nemati, A., Sasani Ghamsari, M., 2014. Crack-free nanostructured BaTiO3 thin films prepared by sol-gel dip-coating technique. Ceram. Int. 40, 8613–8619. https://doi.org/10.1016/j.ceramint.2014.01.078.

Ashiri, R., Moghtada, A., Shahrouzianfar, A., 2015. Processing and Characterization of Carbonate-Free BaTiO3 Nanoscale Particles Obtained by a Rapid Ultrasound-Assisted Wet Chemical Approach. Metall. Mater. Trans. B Process Metall. Mater. Process. Sci. 46, 1912–1923. https://doi.org/10.1007/s11663-015-0377-z.

Augurio, A., Alvarez-Fernandez, A., Panchal, V., Pittenger, B., De Wolf, P., Guldin, S., Briscoe, J., 2022. Controlled Porosity in Ferroelectric BaTiO3Photoanodes. ACS Appl. Mater. Interfaces 14, 13147–13157. https://doi.org/10.1021/acsami.1c17419.

Babu, I., de With, G., 2014. Enhanced electromechanical properties of piezoelectric thin flexible films. Compos. Sci. Technol. 104, 74–80. https://doi.org/10.1016/j.compscitech.2014.08.022.

Basaleh, A.S., Mohamed, R.M., n.d. Synthesis and characterization of Cu-BaTiO 3 nanocomposite for atrazine remediation under visible-light radiation from wastewater. Integr. Med. Res. 9, 9550–9558. https://doi.org/10.1016/j.jmrt.2020.06.081.

Basaleh, A.S., Mohamed, R.M., 2020. Synthesis and characterization of Cu-BaTiO3 nanocomposite for atrazine remediation under visible-light radiation from wastewater. J. Mater. Res. Technol. 9, 9550–9558. https://doi.org/10.1016/j.jmrt.2020.06.081.

Beauger, A., Mutin, J.C., Niepce, J.C., 1983. Synthesis reaction of metatitanate BaTiO3 - Part 1 Effect of the gaseous atmosphere upon the thermal evolution of the system BaCO3-TiO2. J. Mater. Sci. 18, 3041–3046. https://doi.org/10.1007/BF00700786.

Bilgin Simsek, E., 2017. Solvothermal synthesized boron doped TiO2 catalysts: Photocatalytic degradation of endocrine disrupting compounds and pharmaceuticals under visible light irradiation. Appl. Catal. B Environ. 200, 309–322. https://doi.org/10.1016/j.apcatb.2016.07.016.

Bouzidi, S., Ben Hassen, A., Dhahri, J., Khirouni, K., 2019. Structural and dielectric properties of BaTi0.5 (Co0.33 Mo0.17) O3 perovskite ceramic. J. Alloys Compd. 781, 936–944. https://doi.org/10.1016/j.jallcom.2018.11.026.

Brdi, R., Mann, A.-, Ii, C., 1950. (ScH%VARZENBACH'S 77, 1947–1948.

Cabeza, Y., Candela, L., Ronen, D., Teijon, G., 2012. Monitoring the occurrence of emerging contaminants in treated wastewater and groundwater between 2008 and 2010. The Baix Llobregat (Barcelona, Spain). J. Hazard. Mater. 239–240, 32–39. https://doi.org/10.1016/j.jhazmat.2012.07.032.

Cao, H., Qiu, X., Liang, Y., Zhang, L., Zhao, M., Zhu, Q., 2006. Sol-Gel Template Synthesis and Photoluminescence of n- and p-Type Semiconductor Oxide Nanowires. ChemPhysChem 7, 497–501. https://doi.org/10.1002/cphc.200500452.

Cavas, T., 2011. In vivo genotoxicity evaluation of atrazine and atrazine-based herbicide on fish Carassius auratus using the micronucleus test and the comet assay. Food Chem. Toxicol. 49, 1431–1435. https://doi.org/10.1016/j.fct.2011.03.038.

Cernea, M., 2004. Methods for preparation of BaTiO3 thin films. J. Optoelectron. Adv. Mater. 6, 1349–1356.

Chao, C., Zhou, Y., Han, T., Yang, Y., Wei, J., Li, H., He, W., 2020. Ferroelectric polarization-enhanced photocatalytic properties and photo-induced charge carrier behavior of Au/BaTiO3. J. Alloys Compd. 825,. https://doi.org/10.1016/j.jallcom.2020.154060 154060.

Chen, D., Cheng, Y., Zhou, N., Chen, P., Wang, Y., Li, K., Huo, S., Cheng, P., Peng, P., Zhang, R., Wang, L., Liu, H., Liu, Y., Ruan, R., 2020. Photocatalytic degradation of organic pollutants using TiO2-based photocatalysts: A review. J. Clean. Prod. 268,. https://doi.org/10.1016/j.jclepro.2020.121725 121725.

Chen, P., Zhang, Y., Zhao, F., Gao, H., Chen, X., An, Z., 2016. Facile microwave synthesis and photocatalytic activity of monodispersed BaTiO3 nanocuboids. Mater. Charact. 114, 243–253. https://doi.org/10.1016/j.matchar.2016.03.003.

Cui, Y., Briscoe, J., Dunn, S., 2013. Effect of ferroelectricity on solar-light-driven photocatalytic activity of BaTiO3 - Influence on the carrier separation and stern layer formation. Chem. Mater. 25, 4215–4223. https://doi.org/10.1021/cm402092f.

Cui, Y., Goldup, S.M., Dunn, S., 2015. Photodegradation of Rhodamine B over Ag modified ferroelectric BaTiO3 under simulated solar light: Pathways and mechanism. RSC Adv. 5, 30372–30379. https://doi.org/10.1039/c5ra00798d.

Cui, Y., Briscoe, J., Wang, Y., Tarakina, N.V., Dunn, S., 2017. Enhanced Photocatalytic Activity of Heterostructured Ferroelectric BaTiO3/α-Fe2O3 and the Significance of Interface Morphology Control. ACS Appl. Mater. Interfaces 9, 24518–24526. https://doi.org/10.1021/acsami.7b03523.

Cui, Y., Sun, H., Shen, G., Jing, P., Pu, Y., 2020. Effect of Dual-Cocatalyst Surface Modification on Photodegradation Activity, Pathway, and Mechanisms with Highly Efficient Ag/BaTiO3/MnO x. Langmuir 36, 498–509. https://doi.org/10.1021/acs.langmuir.9b02714.

Dang, F., Kato, K., Imai, H., Wada, S., Haneda, H., Kuwabara, M., 2011. Growth of BaTiO3 nanoparticles in ethanol-water mixture solvent under an ultrasound-assisted synthesis. Chem. Eng. J. 170, 333–337. https://doi.org/10.1016/j.cej.2011.03.076.

Dang, H.T.M., Trinh, D.V., Nguyen, N.K., Le, T.T.T., Nguyen, D. D., Tran, H.V., Phan, M.-H., Huynh, C.D., 2018. Enhanced Photocatalytic Activity for Degradation of Organic Dyes Using Magnetite CoFe 2 O 4 /BaTiO 3 Composite. J. Nanosci. Nanotechnol. 18, 7850–7857. https://doi.org/10.1166/jnn.2018.15542.

Demircivi, P., Gulen, B., Simsek, E.B., Berek, D., 2020. Enhanced photocatalytic degradation of tetracycline using hydrothermally synthesized carbon fiber decorated BaTiO3. Mater. Chem. Phys. 241,. https://doi.org/10.1016/j.matchemphys.2019.122236 122236.

Demircivi, P., Simsek, E.B., 2019. Visible-light-enhanced photoactivity of perovskite-type W-doped BaTiO3 photocatalyst for photodegradation of tetracycline. J. Alloys Compd. 774, 795–802. https://doi.org/10.1016/j.jallcom.2018.09.354.

Du, L., Liu, W., 2012. Occurrence, fate, and ecotoxicity of antibiotics in agro-ecosystems. A review. Agron. Sustain. Dev. 32, 309–327. https://doi.org/10.1007/s13593-011-0062-9.

Du, X., Zhou, M., 2021. Strategies to enhance catalytic performance of metal–organic frameworks in sulfate radical-based advanced oxidation processes for organic pollutants removal. Chem. Eng. J. 403,. https://doi.org/10.1016/j.cej.2020.126346 126346.

El-Sayed, O., Mousa, W.M., Zeinert, A., Lahmar, A., El Marssi, M., Battisha, I.K., 2020. Calcination temperature effect on dielectric, structural and morphology properties of BaTiO3 nano-structure prepared by modified sol - Gel technique. Adv. Nat. Sci. Nanosci. Nanotechnol. 11. https://doi.org/10.1088/2043-6254/ab798d.

Fan, H., Li, H., Liu, B., Lu, Y., Xie, T., Wang, D., 2012. Photoinduced charge transfer properties and photocatalytic activity in Bi 2O 3/BaTiO 3 composite photocatalyst. ACS Appl. Mater. Interfaces 4, 4853–4857. https://doi.org/10.1021/am301199v.

Feng, Y., Li, Hao, Ling, L., Yan, S., Pan, D., Ge, H., Li, Hexing, 2018. Enhanced Photocatalytic Degradation Performance by Fluid-induced Piezoelectric Field. https://doi.org/10.1021/acs.est.8b00946.

Feng, J., Fu, Y., Liu, X., Tian, S., Lan, S., Xiong, Y., 2018a. Significant Improvement and Mechanism of Ultrasonic Inactivation to Escherichia coli with Piezoelectric Effect of Hydrothermally Synthesized t-BaTiO3. ACS Sustain. Chem. Eng. 6, 6032–6041. https://doi.org/10.1021/acssuschemeng.7b04666.

Feng, J., Sun, J., Liu, X., Zhu, J., Xiong, Y., Tian, S., 2019. Enhancement and mechanism of nano-BaTiO3 piezocatalytic degradation of tricyclazole by co-loading Pt and RuO2. Environ. Sci. Nano 6, 2241–2252. https://doi.org/10.1039/c9en00367c.

Feng, J., Sun, J., Liu, X., Zhu, J., Tian, S., Wu, R., Xiong, Y., 2020. Coupling effect of piezomaterial and DSA catalyst for degradation

of metronidazole: Finding of induction electrocatalysis from remnant piezoelectric filed. J. Catal. 381, 530–539. https://doi.org/10.1016/j.jcat.2019.11.037.

Fernández, C., Larrechi, M.S., Callao, M.P., 2010. An analytical overview of processes for removing organic dyes from wastewater effluents. TrAC - Trends Anal. Chem. 29, 1202–1211. https://doi.org/10.1016/j.trac.2010.07.011.

Fu, B., Li, J., Jiang, H., He, X., Ma, Y., Wang, J., Hu, C., 2022. Modulation of electric dipoles inside electrospun BaTiO3@TiO2 core-shell nanofibers for enhanced piezo-photocatalytic degradation of organic pollutants. Nano Energy 93. https://doi.org/10.1016/j.nanoen.2021.106841.

Fu, Q., Liu, Y., Mo, J., Lu, Y., Cai, C., Zhao, Z., Wang, S., Nie, S., 2021. Improved Capture and Removal Efficiency of Gaseous Acetaldehyde by a Self-Powered Photocatalytic System with an External Electric Field. ACS Nano 15, 10577–10586. https://doi.org/10.1021/acsnano.1c03230.

Gao, S., Xing, H., Zhang, J., Liu, Y., Du, H., Zhu, Z., Wang, J., Li, X., Zhang, S., Yao, Y., Ren, L., 2021. Oxalic acid functionalization of BaTiO3 nanobelts for promoting their piezo-degradation organic contaminants. J. Mater. 7, 1275–1283. https://doi.org/10.1016/j.jmat.2021.03.002.

Geetha, P., Sarita, P., Rao, D.K., 2016. Synthesis, Structure, Properties and Applications of Barium Titanate Nanoparticles. Int. J. Adv. Technol. Eng. Sci. 4, 178–187.

Gupta, V.K., Ali, I., Saleh, T.A., Nayak, A., Agarwal, S., 2012. Chemical treatment technologies for waste-water recycling - An overview. RSC Adv. 2, 6380–6388. https://doi.org/10.1039/c2ra20340e.

Gupta, V.K., Kumar, R., Nayak, A., Saleh, T.A., Barakat, M.A., 2013. Adsorptive removal of dyes from aqueous solution onto carbon nanotubes: A review. Adv. Colloid Interface Sci. 193–194, 24–34. https://doi.org/10.1016/j.cis.2013.03.003.

Gupta, V.K., Suhas, 2009. Application of low-cost adsorbents for dye removal - A review. J. Environ. Manage. 90, 2313–2342. https://doi.org/10.1016/j.jenvman.2008.11.017.

Habib, A., Haubner, R., Stelzer, N., 2008. Effect of temperature, time and particle size of Ti precursor on hydrothermal synthesis of barium titanate. Mater. Sci. Eng. B Solid-State Mater. Adv. Technol. 152, 60–65. https://doi.org/10.1016/j.mseb.2008.06.018.

Hasbullah, N.N., Chen, S.K., Tan, K.B., Talib, Z.A., Liew, J.Y.C., Lee, O.J., 2019. Photoluminescence activity of BaTiO 3 nanocubes via facile hydrothermal synthesis. J. Mater. Sci. Mater. Electron. 30, 5149–5157. https://doi.org/10.1007/s10854-019-00813-3.

Hassan, B.A.R., Yusoff, Z.B.M., Othman, M.A.H., Bin, S., 2012. information is available at the end of the Chapter, A., Http://dx.doi.org/10.5772/55358, We are IntechOpen , the world ' s leading publisher of Open Access books Built by scientists , for scientists TOP 1 %. Intech 13.

He, C., Jing, P., Wang, P., Ji, J., Ouyang, T., Cui, Y., Pu, Y., 2021a. A novel hierarchical BaTiO3/AgI heterojunction with boosting spatial charge kinetics for photocatalytic degradation of organic pollutant. Ceram. Int. 47, 33426–33434. https://doi.org/10.1016/j.ceramint.2021.08.249.

He, J., Kumar, A., Khan, M., Lo, I.M.C., 2021b. Critical review of photocatalytic disinfection of bacteria: from noble metals- and carbon nanomaterials-TiO2 composites to challenges of water characteristics and strategic solutions. Sci. Total Environ. 758,. https://doi.org/10.1016/j.scitotenv.2020.143953 143953.

He, X., Lee, H.J., Ryu, S.S., Choi, Y.K., Ju, H., 2014. Effects of the processing parameters in the synthesis of BaTiO3 nanoparticle by using the co-precipitation method. J. Korean Phys. Soc. 65, 404–407. https://doi.org/10.3938/jkps.65.404.

He, Z., Yu, P., Wang, H., Gao, J., Zhao, Y., Zhang, H., Zhao, Y., Miao, Z., 2021c. Surface plasmon resonance-induced Ag-BaTiO3 composites for catalytic performance. J. Am. Ceram. Soc. 104, 4389–4397. https://doi.org/10.1111/jace.17804.

Holkar, C.R., Jadhav, A.J., Pinjari, D.V., Mahamuni, N.M., Pandit, A.B., 2016. A critical review on textile wastewater treatments: Possible approaches. J. Environ. Manage. 182, 351–366. https://doi.org/10.1016/j.jenvman.2016.07.090.

Hong, K., Xu, H., Konishi, H., Li, X., 2010. Direct Water Splitting Through Vibrating Piezoelectric Microfibers in Water 997–1002. https://doi.org/10.1021/jz100027t.

Hong, K.S., Xu, H., Konishi, H., Li, X., 2012. Piezoelectrochemical effect: A new mechanism for azo dye decolorization in aqueous solution through vibrating piezoelectric microfibers. J. Phys. Chem. C 116, 13045–13051. https://doi.org/10.1021/jp211455z.

Huang, A., Yan, M., Lin, J., Xu, L., Gong, H.e., Gong, H., 2021. A review of processes for removing antibiotics from breeding wastewater. Int. J. Environ. Res. Public Health 18. https://doi.org/10.3390/ijerph18094909.

Itoh, K., Zeng, L.Z., Nakamura, E., Mishima, N., 1985. Crystal Structure of BaTiO3in the Cubic Phase. Ferroelectrics 63, 29–37. https://doi.org/10.1080/00150198508221381.

Ji, X., Zhu, Y., Lian, X., Fan, B., Liu, X., Xiao, P., Zhang, Y., 2022. Hydroxylation mechanism of phase regulation of nanocrystal BaTiO3 synthesized by a hydrothermal method. Ceram. Int. 48, 2281–2288. https://doi.org/10.1016/j.ceramint.2021.10.006.

Jiao, H., Zhao, K., Ma, L., Tang, Y., 2017. A simple one-step hydrothermal synthesis and photocatalysis of bowl-like BaTiO3 nanoparticles. Inorg. Nano-Metal Chem. 47, 647–654. https://doi.org/10.1080/15533174.2016.1212227.

Kanhere, P., Shenai, P., Chakraborty, S., Ahuja, R., Zheng, J., Chen, Z., 2014. Mono- and co-doped NaTaO3 for visible light photocatalysis. Phys. Chem. Chem. Phys. 16, 16085–16094. https://doi.org/10.1039/c4cp01000k.

Kappadan, S., Thomas, S., Kalarikkal, N., 2020a. BaTiO3/ZnO heterostructured photocatalyst with improved efficiency in dye degradation. Mater. Chem. Phys. 255,. https://doi.org/10.1016/j.matchemphys.2020.123583 123583.

Kappadan, S., Thomas, S., Kalarikkal, N., 2021. Enhanced photocatalytic performance of BaTiO3/g-C3N4 heterojunction for the degradation of organic pollutants. Chem. Phys. Lett. 771,. https://doi.org/10.1016/j.cplett.2021.138513 138513.

Karunakaran, C., Vinayagamoorthy, P., Jayabharathi, J., 2014. Optical, electrical, and photocatalytic properties of polyethylene glycol-assisted sol-gel synthesized BaTiO3@ZnO core-shell nanoparticles. Powder Technol. 254, 480–487. https://doi.org/10.1016/j.powtec.2014.01.061.

Katheresan, V., Kansedo, J., Lau, S.Y., 2018. Efficiency of various recent wastewater dye removal methods: A review. J. Environ. Chem. Eng. 6, 4676–4697. https://doi.org/10.1016/j.jece.2018.06.060.

Kaur, J., Singhal, S., 2014. Facile synthesis of ZnO and transition metal doped ZnO nanoparticles for the photocatalytic degradation of Methyl Orange. Ceram. Int. 40, 7417–7424. https://doi.org/10.1016/j.ceramint.2013.12.088.

Kavian, R., Saidi, A., 2009. Sol-gel derived BaTiO3 nanopowders. J. Alloys Compd. 468, 528–532. https://doi.org/10.1016/j.jallcom.2008.01.045.

Khairy, M., Zakaria, W., 2014. Effect of metal-doping of TiO2 nanoparticles on their photocatalytic activities toward removal of organic dyes. Egypt. J. Pet. 23, 419–426. https://doi.org/10.1016/j.ejpe.2014.09.010.

Khan, M.A.M., Kumar, S., Ahamed, M., Ahmed, J., Kumar, A., Shar, M.A., 2021a. BaTiO3@rGO nanocomposite: enhanced photocatalytic activity as well as improved electrode performance. J. Mater. Sci. Mater. Electron. 32, 12911–12921. https://doi.org/10.1007/s10854-020-04514-0.

Khan, M.A.M., Kumar, S., Ahmed, J., Ahamed, M., Kumar, A., 2021b. Influence of silver doping on the structure, optical and photocatalytic properties of Ag-doped BaTiO3 ceramics. Mater. Chem. Phys. 259,. https://doi.org/10.1016/j.matchemphys.2020.124058 124058.

Koe, W.S., Lee, J.W., Chong, W.C., Pang, Y.L., Sim, L.C., 2020. An overview of photocatalytic degradation: photocatalysts, mechanisms, and development of photocatalytic membrane. Environ. Sci. Pollut. Res. 27, 2522–2565. https://doi.org/10.1007/s11356-019-07193-5.

Kumar, S., Sharma, M., Kumar, A., Powar, S., Vaish, R., 2019a. Rapid bacterial disinfection using low frequency piezocatalysis effect. J. Ind. Eng. Chem. 77, 355–364. https://doi.org/10.1016/j.jiec.2019.04.058.

Kumar, S., Sharma, M., Powar, S., Kabachkov, E.N., Vaish, R., 2019b. Impact of remnant surface polarization on photocatalytic and antibacterial performance of BaTiO 3. J. Eur. Ceram. Soc. 39, 2915–2922. https://doi.org/10.1016/j.jeurceramsoc.2019.03.029.

Kurniawan, T.A., Yanyan, L., Ouyang, T., Albadarin, A.B., Walker, G., 2018. BaTiO3/TiO2 composite-assisted photocatalytic degradation for removal of acetaminophen from synthetic wastewater under UV–vis irradiation. Mater. Sci. Semicond. Process. 73, 42–50. https://doi.org/10.1016/j.mssp.2017.06.048.

Kushwaha, H.S., Halder, A., Jain, D., Vaish, R., 2015. Visible Light-Induced Photocatalytic and Antibacterial Activity of Li-Doped Bi0.5Na0.45K0.5TiO3–BaTiO3 Ferroelectric Ceramics. J. Electron. Mater. 44, 4334–4342. https://doi.org/10.1007/s11664-015-4007-y.

Laxma Reddy, P.V., Kavitha, B., Kumar Reddy, P.A., Kim, K.H., 2017. TiO2-based photocatalytic disinfection of microbes in aqueous media: A review. Environ. Res. 154, 296–303. https://doi.org/10.1016/j.envres.2017.01.018.

Li, M., Gu, L., Li, T., Hao, S., Tan, F., Chen, D., Zhu, D., Xu, Y., Sun, C., Yang, Z., 2020. Tio2-seeded hydrothermal growth of spherical batio3 nanocrystals for capacitor energy-storage application. Crystals 10. https://doi.org/10.3390/cryst10030202.

Li, X., Kang, B., Dong, F., Zhang, Z., Luo, X., Han, L., Huang, J., Feng, Z., Chen, Z., Xu, J., Peng, B., Wang, Z.L., 2021a. Enhanced photocatalytic degradation and H2/H2O2 production performance of S-pCN/WO2.72 S-scheme heterojunction with appropriate surface oxygen vacancies. Nano Energy 81,. https://doi.org/10.1016/j.nanoen.2020.105671 105671.

Li, Q., Li, R., Zong, L., He, J., Wang, X., Yang, J., 2013a. Photoelectrochemical and photocatalytic properties of Ag-loaded BaTiO 3/TiO2 heterostructure nanotube arrays. Int. J. Hydrogen Energy 38, 12977–12983. https://doi.org/10.1016/j.ijhydene.2013.04.073.

Li, R., Li, Q., Zong, L., Wang, X., Yang, J., 2013b. BaTiO3/TiO2 heterostructure nanotube arrays for improved photoelectrochemical and photocatalytic activity. Electrochim. Acta 91, 30–35. https://doi.org/10.1016/j.electacta.2012.12.073.

Li, Y., Li, R., Zhai, Y., Huang, Y., Lee, S., Cao, J., 2021b. Improved photocatalytic activity of BaTiO3/La2Ti2O7 heterojunction composites via piezoelectric-enhanced charge transfer. Appl. Surf. Sci. 570,. https://doi.org/10.1016/j.apsusc.2021.151146 151146.

Li, H., Sang, Y., Chang, S., Huang, X., Zhang, Y., Yang, R., Jiang, H., Liu, H., Wang, Z.L., 2015. Enhanced Ferroelectric-Nanocrystal-Based Hybrid Photocatalysis by Ultrasonic-Wave-Generated Piezophototronic Effect. Nano Lett. 15, 2372–2379. https://doi.org/10.1021/nl504630j.

Li, S., Zhao, Z., Yu, D., Zhao, J.Z., Su, Y., Liu, Y., Lin, Y., Liu, W., Xu, H., Zhang, Z., 2019. Few-layer transition metal dichalcogenides (MoS2, WS2, and WSe2) for water splitting and degradation of organic pollutants: Understanding the piezocatalytic effect. Nano Energy 66. https://doi.org/10.1016/j.nanoen.2019.104083.

Liang, Z., Yan, C., Rtimi, S., Bandara, J., 2018. Piezoelectric materials for catalytic / photocatalytic removal of pollutants : Recent advances and outlook Applied Catalysis B : Environmental Piezoelectric materials for catalytic / photocatalytic removal of pollutants : Recent advances and outlook. Appl. Catal. B Environ. 241, 256–269. https://doi.org/10.1016/j.apcatb.2018.09.028.

Liang, Z., Yan, C.F., Rtimi, S., Bandara, J., 2019. Piezoelectric materials for catalytic/photocatalytic removal of pollutants: Recent advances and outlook. Appl. Catal. B Environ. 241, 256–269. https://doi.org/10.1016/j.apcatb.2018.09.028.

Lilge, T.S., Ramires das Neves Stigger, A., Fernandes, C.D., Gularte, L.T., Raubach, C.W., da Silva Cava, S., Gomes Jardim, P.L., Giroldo Valerio, M.E., Moreira, M.L., 2020. Increase of Voc using heterojunctions of BaTiO3 without sensitization. Ceram. Int. 46, 4907–4913. https://doi.org/10.1016/j.ceramint.2019.10.227.

Lin, E., Wu, J., Qin, N., Yuan, B., Bao, D., 2018. Silver modified barium titanate as a highly efficient piezocatalyst. Catal. Sci. Technol. 8, 4788–4796. https://doi.org/10.1039/c8cy01127c.

Lin, E., Qin, N., Wu, J., Yuan, B., Kang, Z., Bao, D., 2020. BaTiO3 Nanosheets and Caps Grown on TiO2 Nanorod Arrays as Thin-Film Catalysts for Piezocatalytic Applications. ACS Appl. Mater. Interfaces 12, 14005–14015. https://doi.org/10.1021/acsami.0c00962.

Lin, E., Kang, Z., Wu, J., Huang, R., Qin, N., Bao, D., 2021. BaTiO3 nanocubes/cuboids with selectively deposited Ag nanoparticles: Efficient piezocatalytic degradation and mechanism. Appl. Catal. B Environ. 285,. https://doi.org/10.1016/j.apcatb.2020.119823 119823.

Lin, X., Xing, J., Wang, W., Shan, Z., Xu, F., Huang, F., 2007. Photocatalytic activities of heterojunction semiconductors Bi 2O3/BaTiO3: A strategy for the design of efficient combined photocatalysts. J. Phys. Chem. C 111, 18288–18293. https://doi.org/10.1021/jp073955d.

Liu, D., Jin, C., Shan, F., He, J., Wang, F., 2020a. Synthesizing BaTiO3 Nanostructures to Explore Morphological Influence, Kinetics, and Mechanism of Piezocatalytic Dye Degradation. ACS Appl. Mater. Interfaces 12, 17443–17451. https://doi.org/10.1021/acsami.9b23351.

Liu, X., Lv, S., Fan, B., Xing, A., Jia, B., 2019. Ferroelectric polarization-enhanced photocatalysis in BaTiO3-TiO2 core-shell heterostructures. Nanomaterials 9. https://doi.org/10.3390/nano9081116.

Liu, Y., Mo, J., Fu, Q., Lu, Y., Zhang, N., Wang, S., Nie, S., 2020c. Enhancement of Triboelectric Charge Density by Chemical Functionalization. Adv. Funct. Mater. 30, 1–33. https://doi.org/10.1002/adfm.202004714.

Liu, X., Shen, X., Sa, B., Zhang, Y., Li, X., Xue, H., 2021. Piezotronic-enhanced photocatalytic performance of heterostructured BaTiO3/SrTiO3 nanofibers. Nano Energy 89, 1–9. https://doi.org/10.1016/j.nanoen.2021.106391.

Liu, J., Sun, Y., Li, Z., 2012. Ag loaded flower-like BaTiO 3 nanotube arrays: Fabrication and enhanced photocatalytic property. CrystEngComm 14, 1473–1478. https://doi.org/10.1039/c1ce05949a.

Liu, X., Xiao, L., Zhang, Y., Sun, H., 2020b. Significantly enhanced piezo-photocatalytic capability in BaTiO3 nanowires for degrading organic dye. J. Mater. 6, 256–262. https://doi.org/10.1016/j.jmat.2020.03.004.

Liu, Q., Zhai, D., Xiao, Z., Tang, C., Sun, Q., Bowen, C.R., Luo, H., Zhang, D., 2022. Piezo-photoelectronic coupling effect of BaTiO3@TiO2 nanowires for highly concentrated dye degradation. Nano Energy 92. https://doi.org/10.1016/j.nanoen.2021.106702.

Lu, L., Liang, N., Sun, H., Zhang, Q., Hao, X., 2022. Highly efficient sono-piezo-photo synergistic catalysis in bismuth layered ferroelectrics via finely distinguishing sonochemical and electromechanochemical processes. J. Mater. 8, 47–58. https://doi.org/10.1016/j.jmat.2021.05.007.

Mahlaule, L.M., Mbita, Z., Mathipa, M.M., Tetana, Z.N., Hintsho-Mbita, N.C., 2019. Biological therapeutics of AgO nanoparticles against pathogenic bacteria and A549 lung cancer cells Biological therapeutics of AgO nanoparticles against pathogenic bacteria and A549 lung cancer cells. Mater. Res. Express 6,. https://doi.org/10.1088/2053-1591/ab36e3 105402.

Masekela, D., Hintsho-Mbita, N.C., Mabuba, N., 2020. Diethylamine functionalised Moringa oleifera leaves for the removal of

chromium(VI) and bacteria from wastewater. Int. J. Environ. Anal. Chem. 00, 1–21. https://doi.org/10.1080/03067319.2020.1762873.

Masekela, D., Hintsho-mbita, N.C., Mabuba, N., 2022a. Application of a piezo-photocatalytic thin film (FTO / BaTiO 3 / SnO 2) for enhanced degradation of organic pollutants and disinfection of wastewater. Ceram. Int. https://doi.org/10.1016/j.ceramint.2022.10.251.

Masekela, D., Yusuf, T.L., Hintsho-Mbita, N.C., Mabuba, N., 2022b. Low Cost, Recyclable and Magnetic Moringa Oleifera Leaves for Chromium(VI) Removal From Water. Front. Water 4, 1–13. https://doi.org/10.3389/frwa.2022.722269.

Mengying, S., Zhang, Y., Xie, M., Adamaki, V., Khanbareh, H., Bowen, C.R., 2017. As featured. In. https://doi.org/10.1039/c7cs00387k.

Mi, L., Zhang, Q., Wang, H., Wu, Z., Guo, Y., Li, Y., Xiong, X., Liu, K., Fu, W., Ma, Y., Wang, B.Z., Qi, X.W., 2020. Synthesis of BaTiO3 nanoparticles by sol-gel assisted solid phase method and its formation mechanism and photocatalytic activity. Ceram. Int. 46, 10619–10633. https://doi.org/10.1016/j.ceramint.2020.01.066.

Mittal, M., Sardar, S., Jana, A., 2021. Nanofabrication techniques for semiconductor chemical sensors, Handbook of Nanomaterials for Sensing Applications. Elsevier Inc. https://doi.org/10.1016/b978-0-12-820783-3.00023-3.

Mo, W.Y., Chen, Z., Leung, H.M., Leung, A.O.W., 2017. Application of veterinary antibiotics in China's aquaculture industry and their potential human health risks. Environ. Sci. Pollut. Res. 24, 8978–8989. https://doi.org/10.1007/s11356-015-5607-z.

Moghtada, A., Ashiri, R., 2016. Enhancing the formation of tetragonal phase in perovskite nanocrystals using an ultrasound assisted wet chemical method. Ultrason. Sonochem. 33, 141–149. https://doi.org/10.1016/j.ultsonch.2016.05.002.

Mondal, D., Roy, S., Bardhan, S., Roy, J., Kanungo, I., Basu, R., Das, S., 2022. Recent advances in piezocatalytic polymer nanocomposites for wastewater remediation. Dalt. Trans. 51, 451–462. https://doi.org/10.1039/d1dt02653d.

Mushtaq, F., Chen, X., Hoop, M., Torlakcik, H., Pellicer, E., Sort, J., Gattinoni, C., Nelson, B.J., Pané, S., 2018. Piezoelectrically Enhanced Photocatalysis with BiFeO3 Nanostructures for Efficient Water Remediation. iScience 4, 236–246. https://doi.org/10.1016/j.isci.2018.06.003.

Nageri, M., Kumar, V., 2018. Manganese-doped BaTiO3 nanotube arrays for enhanced visible light photocatalytic applications. Mater. Chem. Phys. 213, 400–405. https://doi.org/10.1016/j.matchemphys.2018.04.003.

Nageri, M., Shalet, A.B., Kumar, V., 2017. SnO2-loaded BaTiO3 nanotube arrays: fabrication and visible-light photocatalytic application. J. Mater. Sci. Mater. Electron. 28, 9770–9776. https://doi.org/10.1007/s10854-017-6729-5.

Nguyen, V.K., Nguyen Thi, V.N., Tran, H.H., Tran Thi, T.P., Truong, T.T., Vo, V., 2021. A facile synthesis of g-C3N4/BaTiO3 photocatalyst with enhanced activity for degradation of methylene blue under visible light. Bull. Mater. Sci. 44. https://doi.org/10.1007/s12034-020-02277-2.

Nishioka, S., Maeda, K., 2015. Hydrothermal synthesis of rhodium-doped barium titanate nanocrystals for enhanced photocatalytic hydrogen evolution under visible light. RSC Adv. 5, 100123–100128. https://doi.org/10.1039/c5ra20044j.

Nithya, P.M., Devi, L.G., 2019. Effect of surface Ag metallization on the photocatalytic properties of BaTiO 3: Surface plasmon effect and variation in the Schottky barrier height. Surfaces and Interfaces 15, 205–215. https://doi.org/10.1016/j.surfin.2019.03.005.

Niu, B., Xu, Z., 2019. Innovating e-waste recycling: From waste multi-layer ceramic capacitors to Nb–Pb codoped and ag-Pd-Sn-Ni loaded BaTiO 3 nano-photocatalyst through one-step ball milling process. Sustain. Mater. Technol. 21, e00101.

Ojo, B.O., Arotiba, O.A., Mabuba, N., 2022. Sonoelectrochemical degradation of ciprofloxacin in water on a Ti/BaTiO3 electrode. J. Environ. Chem. Eng. 10,. https://doi.org/10.1016/j.jece.2022.107224 107224.

Oliveira, M.C., Ribeiro, R.A.P., Longo, E., Bomio, M.R.D., Motta, F.V., de Lazaro, S.R., 2020. Temperature dependence on phase evolution in the BaTiO3 polytypes studied using ab initio calculations. Int. J. Quantum Chem. 120, 1–10. https://doi.org/10.1002/qua.26054.

Orhan, E., Varela, J.A., Zenatti, A., Gurgel, M.F.C., Pontes, F.M., Leite, E.R., Longo, E., Pizani, P.S., Beltràn, A., Andrès, J., 2005. Room-temperature photoluminescence of BaTiO 3: Joint experimental and theoretical study. Phys. Rev. B - Condens. Matter Mater. Phys. 71, 1–7. https://doi.org/10.1103/PhysRevB.71.085113.

Orimolade, B.O., Arotiba, O.A., 2020. Bismuth vanadate in photoelectrocatalytic water treatment systems for the degradation of organics: A review on recent trends. J. Electroanal. Chem. 878,. https://doi.org/10.1016/j.jelechem.2020.114724 114724.

Orimolade, B.O., Zwane, B.N., Koiki, B.A., Tshwenya, L., Peleyeju, G.M., Mabuba, N., Zhou, M., Arotiba, O.A., 2020. Solar photoelectrocatalytic degradation of ciprofloxacin at a FTO/BiVO4/MnO2 anode: Kinetics, intermediate products and degradation pathway studies. J. Environ. Chem. Eng. 8,. https://doi.org/10.1016/j.jece.2019.103607 103607.

Orimolade, B.O., Idris, A.O., Feleni, U., Mamba, B., 2021a. Recent advances in degradation of pharmaceuticals using Bi2WO6 mediated photocatalysis – A comprehensive review. Environ. Pollut. 289. https://doi.org/10.1016/j.envpol.2021.117891.

Orimolade, B.O., Idris, A.O., Feleni, U., Mamba, B., 2021b. Recent advances in degradation of pharmaceuticals using Bi2WO6 mediated photocatalysis – A comprehensive review. Environ. Pollut. 289,. https://doi.org/10.1016/j.envpol.2021.117891 117891.

P.M, N., Devi, L.G., 2020. Heavy atom perturbation by the incorporation of iodine ion into BaTiO3 lattice: Reduction of fluorescence and enhancement of rate of interfacial charge transfer process under the visible light irradiation. Surfaces and Interfaces 18, 100411. https://doi.org/10.1016/j.surfin.2019.100411.

Panda, P.K., Sahoo, B., 2015. P[1] P. K. Panda and B. Sahoo, "PZT to lead free piezo ceramics: A review," Ferroelectrics, vol. 474, no. 1, pp. 128–143, 2015.ZT to lead free piezo ceramics: A review. Ferroelectrics 474, 128–143. https://doi.org/10.1080/00150193.2015.997146.

Pandey, P.K., Kass, P.H., Soupir, M.L., Biswas, S., Singh, V.P., 2014. Contamination of water resources by pathogenic bacteria. AMB Express 4, 1–16. https://doi.org/10.1186/s13568-014-0051-x.

Pardeshi, S.K., Patil, A.B., 2008. A simple route for photocatalytic degradation of phenol in aqueous zinc oxide suspension using solar energy. Sol. Energy 82, 700–705. https://doi.org/10.1016/j.solener.2008.02.007.

Park, K.I., Lee, M., Liu, Y., Moon, S., Hwang, G.T., Zhu, G., Kim, J.E., Kim, S.O., Kim, D.K., Wang, Z.L., Lee, K.J., 2012. Flexible nanocomposite generator made of BaTiO 3 nanoparticles and graphitic carbons. Adv. Mater. 24, 2999–3004. https://doi.org/10.1002/adma.201200105.

Peleyeju, M.G., Arotiba, O.A., 2018. Recent trend in visible-light photoelectrocatalytic systems for degradation of organic contaminants in water/wastewater. Environ. Sci. Water Res. Technol. 4, 1389–1411. https://doi.org/10.1039/c8ew00276b.

Peleyeju, M.G., Viljoen, E.L., 2021. WO3-based catalysts for photocatalytic and photoelectrocatalytic removal of organic pollutants from water – A review. J. Water Process Eng. 40,. https://doi.org/10.1016/j.jwpe.2021.101930 101930.

Pfaff, G., 1992. Sol-gel synthesis of barium titanate powders of various compositions. J. Mater. Chem. 2, 591–594. https://doi.org/10.1039/JM9920200591.

Piskunov, S., Heifets, E., Eglitis, R.I., Borstel, G., 2004. Bulk properties and electronic structure of SrTiO3, BaTiO 3, PbTiO3 perovskites: An ab initio HF/DFT study. Comput. Mater. Sci. 29, 165–178. https://doi.org/10.1016/j.commatsci.2003.08.036.

Pithan, C., Hennings, D., Waser, R., 2005. Progress in the synthesis of nanocrystalline BaTiO3 powders for MLCC. Int. J. Appl. Ceram. Technol. 2, 1–14. https://doi.org/10.1111/j.1744-7402.2005.02008.x.

Prasadarao, A.V., Suresh, M., Komarneni, S., 2001. PH dependent coprecipitated oxalate precursors - A thermal study of lead titanate. J. Mater. Sci. 36, 767–770. https://doi.org/10.1023/A:1004809613444.

Qi, K., Cheng, B., Yu, J., Ho, W., 2017. Review on the improvement of the photocatalytic and antibacterial activities of ZnO. J. Alloys Compd. 727, 792–820. https://doi.org/10.1016/j.jallcom.2017.08.142.

Qi, J., Li, Y., Zhang, X., Wang, J., Zhang, Q., Xue, Y., Cheng, J., Li, M., Han, X., Ma, Z., Fang, D., 2020. Solid-state synthesis semiconducting BaTiO3 nanoparticles at low temperature. Mater. Chem. Phys. 242,. https://doi.org/10.1016/j.-matchemphys.2019.122496 122496.

Rai, H.S., Bhattacharyya, M.S., Singh, J., Bansal, T.K., Vats, P., Banerjee, U.C., 2005. Removal of dyes from the effluent of textile and dyestuff manufacturing industry: A review of emerging techniques with reference to biological treatment. Crit. Rev. Environ. Sci. Technol. 35, 219–238. https://doi.org/10.1080/10643380590917932.

Rao, B.G., Mukherjee, D., Reddy, B.M., 2017. Novel approaches for preparation of nanoparticles, Nanostructures for Novel Therapy: Synthesis, Characterization and Applications. Elsevier Inc. https://doi.org/10.1016/B978-0-323-46142-9.00001-3.

Rastogi, M., Bowen, C., Kushwaha, H.S., Vaish, R., 2016a. First principles insights into improved catalytic performance of BaTiO3-graphene nanocomposites in conjugation with experimental investigations. Mater. Sci. Semicond. Process. 51, 33–41. https://doi.org/10.1016/j.mssp.2016.04.008.

Rastogi, M., Kushwaha, H.S., Vaish, R., 2016b. Highly efficient visible light mediated azo dye degradation through barium titanate decorated reduced graphene oxide sheets. Electron. Mater. Lett. 12, 281–289. https://doi.org/10.1007/s13391-015-5274-8.

Ray, S.K., Cho, J., Hur, J., 2021. A critical review on strategies for improving efficiency of BaTiO3-based photocatalysts for wastewater treatment. J. Environ. Manage. 290,. https://doi.org/10.1016/j.jenvman.2021.112679 112679.

Ren, P., Fan, H., Wang, X., 2012. Electrospun nanofibers of ZnO/BaTiO 3 heterostructures with enhanced photocatalytic activity. Catal. Commun. 25, 32–35. https://doi.org/10.1016/j.catcom.2012.04.003.

Ren, P., Fan, H., Wang, X., 2013. Solid-state synthesis of Bi2O3/BaTiO3 heterostructure: Preparation and photocatalytic degradation of methyl orange. Appl. Phys. A Mater. Sci. Process. 111, 1139–1145. https://doi.org/10.1007/s00339-012-7331-6.

Rotaru, R., Peptu, C., Samoila, P., Harabagiu, V., 2017. Preparation of ferroelectric barium titanate through an energy effective solid state ultrasound assisted method. J. Am. Ceram. Soc. 100, 4511–4518. https://doi.org/10.1111/jace.15003.

Saucier, C., Karthickeyan, P., Ranjithkumar, V., Lima, E.C., dos Reis, G.S., de Brum, I.A.S., 2017. Efficient removal of amoxicillin and paracetamol from aqueous solutions using magnetic activated carbon. Environ. Sci. Pollut. Res. 24, 5918–5932. https://doi.org/10.1007/s11356-016-8304-7.

Schneller, T., Waser, R., Kosec, M., Payne, D., 2013. Theodor Schneller · Rainer Waser Marija Kosec · David Payne.

Selvarajan, S., Malathy, P., Suganthi, A., Rajarajan, M., 2017. Fabrication of mesoporous BaTiO3/SnO2 nanorods with highly enhanced photocatalytic degradation of organic pollutants. J. Ind. Eng. Chem. 53, 201–212. https://doi.org/10.1016/j.jiec.2017.04.026.

Senthilkumar, P., Jency, D.A., Kavinkumar, T., Dhayanithi, D., Dhanuskodi, S., Umadevi, M., Manivannan, S., Giridharan, N.V., Thiagarajan, V., Sriramkumar, M., Jothivenkatachalam, K., 2019. Built-in Electric Field Assisted Photocatalytic Dye Degradation and Photoelectrochemical Water Splitting of Ferroelectric Ce Doped BaTiO3 Nanoassemblies. ACS Sustain. Chem. Eng. 7, 12032–12043. https://doi.org/10.1021/acssuschemeng.9b00679.

Shah, A.A., Khan, A., Dwivedi, S., Musarrat, J., Azam, A., 2018. Antibacterial and Antibiofilm Activity of Barium Titanate Nanoparticles. Mater. Lett. 229, 130–133. https://doi.org/10.1016/j.matlet.2018.06.107.

Sharma, D., Upadhyay, S., Satsangi, V.R., Shrivastav, R., Waghmare, U.V., Dass, S., 2016. Nanostructured BaTiO3/Cu2O heterojunction with improved photoelectrochemical activity for H2 evolution: Experimental and first-principles analysis. Appl. Catal. B Environ. 189, 75–85. https://doi.org/10.1016/j.apcatb.2016.02.037.

Sharma, M., Vaish, R., Ibrahim, S.M., 2020. Effect of poling condition on piezocatalysis activity of BaTiO 3 -cement composites. Mater. Lett. 280,. https://doi.org/10.1016/j.matlet.2020.128583 128583.

Shuai, C., Liu, G., Yang, Y., Qi, F., Peng, S., Yang, W., He, C., Wang, G., Qian, G., 2020a. A strawberry-like Ag-decorated barium titanate enhances piezoelectric and antibacterial activities of polymer scaffold. Nano Energy 74,. https://doi.org/10.1016/j.nanoen.2020.104825 104825.

Sirés, I., Brillas, E., 2012a. Remediation of water pollution caused by pharmaceutical residues based on electrochemical separation and degradation technologies: A review. Environ. Int. 40, 212–229. https://doi.org/10.1016/j.envint.2011.07.012.

Sirés, I., Brillas, E., 2012b. Remediation of water pollution caused by pharmaceutical residues based on electrochemical separation and degradation technologies : A review. Environ. Int. 40, 212–229. https://doi.org/10.1016/j.envint.2011.07.012.

Sirés, I., Brillas, E., Oturan, M.A., Rodrigo, M.A., Panizza, M., 2014. Electrochemical advanced oxidation processes: Today and tomorrow. A review. Environ. Sci. Pollut. Res. 21, 8336–8367. https://doi.org/10.1007/s11356-014-2783-1.

Sun, W., Li, C., Li, J., Liu, W., 2006. Microwave-hydrothermal synthesis of tetragonal BaTiO3 under various conditions. Mater. Chem. Phys. 97, 481–487. https://doi.org/10.1016/j.matchemphys.2005.08.051.

Sun, Y., Li, X., Vijayakumar, A., Liu, H., Wang, C., Zhang, S., Fu, Z., Lu, Y., Cheng, Z., 2021. Hydrogen Generation and Degradation of Organic Dyes by New Piezocatalytic 0.7BiFeO3-0.3BaTiO3Nanoparticles with Proper Band Alignment. ACS Appl. Mater. Interfaces 13, 11050–11057. https://doi.org/10.1021/acsami.1c01407.

Surmenev, R.A., Chernozem, R.V., Skirtach, A.G., Bekareva, A.S., Leonova, L.A., Mathur, S., Ivanov, Y.F., Surmeneva, M.A., 2021. Hydrothermal synthesis of barium titanate nano/microrods and particle agglomerates using a sodium titanate precursor. Ceram. Int. 47, 8904–8914. https://doi.org/10.1016/j.ceramint.2020.12.011.

Suzuki, K., Kijima, K., 2006. Preparation and dielectric properties of polycrystalline films with dense nano-structured BaTiO3 by chemical vapor deposition using inductively coupled plasma. Vacuum 80, 519–529. https://doi.org/10.1016/j.vacuum.2005.08.025.

Tan, K.B., Vakili, M., Horri, B.A., Poh, P.E., Abdullah, A.Z., Salamatinia, B., 2015. Adsorption of dyes by nanomaterials: Recent developments and adsorption mechanisms. Sep. Purif. Technol. 150, 229–242. https://doi.org/10.1016/j.seppur.2015.07.009.

Torres, R.A., Pétrier, C., Combet, E., Carrier, M., Pulgarin, C., 2008. Ultrasonic cavitation applied to the treatment of bisphenol A. Effect of sonochemical parameters and analysis of BPA by-products. Ultrason. Sonochem. 15, 605–611. https://doi.org/10.1016/j.ultsonch.2007.07.003.

Utara, S., Hunpratub, S., 2018. Ultrasonic assisted synthesis of BaTiO3 nanoparticles at 25 °C and atmospheric pressure. Ultrason. Sonochem. 41, 441–448. https://doi.org/10.1016/j.ultsonch.2017.10.008.

Wang, W., Cao, L., Liu, W., Su, G., Zhang, W., 2013. Low-temperature synthesis of BaTiO3 powders by the sol-gel-hydrother-

mal method. Ceram. Int. 39, 7127–7134. https://doi.org/10.1016/j.ceramint.2013.02.055.

Wang, L., Haugen, N.O., Wu, Z., Shu, X., Jia, Y., Ma, J., Yu, S., Li, H., Chai, Q., 2019b. Ferroelectric BaTiO3@ZnO heterostructure nanofibers with enhanced pyroelectrically-driven-catalysis. Ceram. Int. 45, 90–95. https://doi.org/10.1016/j.ceramint.2018.09.137.

Wang, J., Hou, T., Cao, F., Li, M., Lv, L., 2020a. Harvesting the Vibration Energy with BaTiO3@Graphene for the Piezocatalytic Degradation of Methylene Blue. J. Environ. Sci. Eng. Technol. 8, 84–91 https://doi.org/10.12974/2311-8741.2020.08.8.

Wang, R., Lu, K.Q., Tang, Z.R., Xu, Y.J., 2017. Recent progress in carbon quantum dots: synthesis, properties and applications in photocatalysis. J. Mater. Chem. A 5, 3717–3734. https://doi.org/10.1039/c6ta08660h.

Wang, Y., Sun, X., Xian, T., Liu, G., Yang, H., 2021. Photocatalytic purification of simulated dye wastewater in different pH environments by using BaTiO3/Bi2WO6 heterojunction photocatalysts. Opt. Mater. (Amst). 113,. https://doi.org/10.1016/j.optmat.2021.110853 110853.

Wang, J., Wang, S., 2016. Removal of pharmaceuticals and personal care products (PPCPs) from wastewater: A review. J. Environ. Manage. 182, 620–640. https://doi.org/10.1016/j.jenvman.2016.07.049.

Wang, B., Wei, K., Chen, F., Wang, Y., He, G., Li, W., Liu, J., He, Q., 2019a. Effects of active species on degrading A-ring of tetracycline in the Z-scheme heterostructured core-shell La(OH)3@BaTiO3 composition. J. Alloys Compd. 804, 100–110. https://doi.org/10.1016/j.jallcom.2019.06.356.

Wang, Y., Yang, H., Sun, X., Zhang, H., Xian, T., 2020b. Preparation and photocatalytic application of ternary n-BaTiO3/Ag/p-AgBr heterostructured photocatalysts for dye degradation. Mater. Res. Bull. 124,. https://doi.org/10.1016/j.materresbull.2019.110754 110754.

Wang, R.X., Zhu, Q., Wang, W.S., Fan, C.M., Xu, A.W., 2015. BaTiO3-graphene nanocomposites: Synthesis and visible light photocatalytic activity. New J. Chem. 39, 4407–4413. https://doi.org/10.1039/c4nj02272f.

Wei, K., Wang, B., Hu, J., Chen, F., Hao, Q., He, G., Wang, Y., Li, W., Liu, J., He, Q., 2019. Photocatalytic properties of a new Z-scheme system BaTiO3/In2S3 with a core-shell structure. RSC Adv. 9, 11377–11384. https://doi.org/10.1039/c8ra10592h.

Wei, X., Xu, G., Ren, Z., Wang, Y., Shen, G., Han, G., 2008. Size-controlled synthesis of BaTiO3 nanocrystals via a hydrothermal route. Mater. Lett. 62, 3666–3669. https://doi.org/10.1016/j.matlet.2008.04.022.

Wen, W., Hai, J., Yao, J., Gu, Y., Kobayashi, H., n.d. Supporting Information Univariate Lattice Parameter Modulation of Single-Crystal-like Anatase TiO 2 Hierarchical Nanowire Arrays to Improve.

Wu, M., Ding, T., Wang, Y., Zhao, W., Xian, H., Tian, Y., Zhang, T., Li, X., 2020b. Rational construction of plasmon Au assisted ferroelectric-BaTiO3/Au/g-C3N4 Z-scheme system for efficient photocatalysis. Catal. Today 355, 311–318. https://doi.org/10.1016/j.cattod.2019.04.061.

Wu, J., Qin, N., Bao, D., 2018a. Effective enhancement of piezocatalytic activity of BaTiO3 nanowires under ultrasonic vibration. Nano Energy 45, 44–51. https://doi.org/10.1016/j.nanoen.2017.12.034.

Wu, J., Wang, W., Tian, Y., Song, C., Qiu, H., Xue, H., 2020a. Piezotronic effect boosted photocatalytic performance of heterostructured BaTiO3/TiO2 nanofibers for degradation of organic pollutants. Nano Energy 77,. https://doi.org/10.1016/j.nanoen.2020.105122 105122.

Wu, C., Wei, X., Zhao, K., Jiang, J., Jiao, M., Cheng, J., Tang, Z., Guo, Z., Tang, Y., 2021. Novel dam-like effect based on piezoelectric energy conversion for drug sustained release of drug-loaded TiO2 @ BaTiO3 coaxial nanotube coating. Ceram. Int. 47, 17550–17559. https://doi.org/10.1016/j.ceramint.2021.03.073.

Xia, C., Shi, E., Zhong, W., Guo, J., 1996. Hydrothermal synthesis of BaTiO 3 nano / microcrystals 166, 961–966.

Xian, T., Yang, H., Di, L.J., Dai, J.F., 2015. Enhanced photocatalytic activity of BaTiO3@g-C3N4 for the degradation of methyl orange under simulated sunlight irradiation. J. Alloys Compd. 622, 1098–1104. https://doi.org/10.1016/j.jallcom.2014.11.051.

Xiang, H., Shao, Y., Gao, N., Lu, X., An, N., Tan, C., Zheng, Z., 2018. Degradation of diuron by chlorination and UV/chlorine process: Degradation kinetics and the formation of disinfection by-products. Sep. Purif. Technol. 202, 365–372. https://doi.org/10.1016/j.seppur.2018.03.073.

Xiao, S., Song, Y., Tian, Z., 2015. Enhanced mineralization of antibiotic berberine by the photoelectrochemical process in presence of chlorides and its optimization by response surface methodology. Environ. Earth Sci. 4947–4955. https://doi.org/10.1007/s12665-015-4209-x.

Xiong, X., Tian, R., Lin, X., Chu, D., Li, S., 2015. Formation and photocatalytic activity of BaTiO3 nanocubes via hydrothermal process. J. Nanomater. 2015, 12–15. https://doi.org/10.1155/2015/692182.

Xu, X., Cao, D., Yang, H., He, M., 2018. Application of piezoelectric transducer in energy harvesting in pavement. Int. J. Pavement Res. Technol. 11, 388–395. https://doi.org/10.1016/j.ijprt.2017.09.011.

Xu, S., Liu, Z., Zhang, M., Guo, L., 2019. Piezotronics enhanced photocatalytic activities of Ag-BaTiO3 plasmonic photocatalysts. J. Alloys Compd. 801, 483–488. https://doi.org/10.1016/j.jallcom.2019.06.115.

Yu, C., Tan, M., Li, Y., Liu, C., Yin, R., Meng, H., Su, Y., Qiao, L., Bai, Y., 2021. Ultrahigh piezocatalytic capability in eco-friendly BaTiO3 nanosheets promoted by 2D morphology engineering. J. Colloid Interface Sci. 596, 288–296. https://doi.org/10.1016/j.jcis.2021.03.040.

Yu, C., Tan, M., Tao, C., Hou, Y., Liu, C., Meng, H., Su, Y., Qiao, L., Bai, Y., 2022. Remarkably enhanced piezo-photocatalytic performance in BaTiO3/CuO heterostructures for organic pollutant degradation. J. Adv. Ceram. 11, 414–426. https://doi.org/10.1007/s40145-021-0544-4.

Zhan, H., Yang, X., Wang, C., Chen, J., Wen, Y., Liang, C., Greer, H.F., Wu, M., Zhou, W., 2012. Multiple nucleation and crystal growth of barium titanate. Cryst. Growth Des. 12, 1247–1253. https://doi.org/10.1021/cg201259u.

Zhang, J., Chen, X., Bai, Y., Li, C., Gao, Y., Li, R., Li, C., 2019b. Boosting photocatalytic water splitting by tuning built-in electric field at phase junction. J. Mater. Chem. A 7, 10264–10272. https://doi.org/10.1039/c8ta08199a.

Zhang, Y., Huang, X., Yeom, J., 2019c. A Floatable Piezo - Photocatalytic Platform Based on Semi - Embedded ZnO Nanowire Array for High - Performance Water Decontamination. Nano-Micro Lett. 11, 1–14. https://doi.org/10.1007/s40820-019-0241-9.

Zhang, L., Jaroniec, M., 2018. Toward designing semiconductor-semiconductor heterojunctions for photocatalytic applications. Appl. Surf. Sci. 430, 2–17. https://doi.org/10.1016/j.apsusc.2017.07.192.

Zhang, Y., Sun, H., Yang, C., Su, H., Liu, X., 2019d. Modulating Photovoltaic Conversion Efficiency of BiFeO3-Based Ferroelectric Films by the Introduction of Electron Transport Layers. ACS Appl. Energy Mater. 2, 5540–5546. https://doi.org/10.1021/acsaem.9b00722.

Zhang, Y., Shen, G., Sheng, C., Zhang, F., Fan, W., 2021b. The effect of piezo-photocatalysis on enhancing the charge carrier separation in BaTiO3/KNbO3 heterostructure photocatalyst. Appl. Surf. Sci. 562,. https://doi.org/10.1016/j.apsusc.2021.150164 150164.

Zhang, Y., Hawboldt, K., Zhang, L., Lu, J., Chang, L., Dwyer, A., 2022. Carbonaceous nanomaterial-TiO2 heterojunctions for visible-light-driven photocatalytic degradation of aqueous organic

pollutants. Appl. Catal. A Gen. 630,. https://doi.org/10.1016/j.apcata.2021.118460 118460.

Zhang, X., Wu, F., Wu, X.W., Chen, P., Deng, N., 2008. Photodegradation of acetaminophen in TiO2 suspended solution. J. Hazard. Mater. 157, 300–307. https://doi.org/10.1016/j.jhazmat.2007.12.098.

Zhang, X., Wang, X., Chai, J., Xue, S., Wang, R., Jiang, L., Wang, J., Zhang, Z., Dionysiou, D.D., 2020. Applied Catalysis B : Environmental Construction of novel symmetric double Z-scheme BiFeO 3 / CuBi 2 O 4 / BaTiO 3 photocatalyst with enhanced solar-light-driven photocatalytic performance for degradation of nor fl oxacin. Appl. Catal. B Environ. 272,. https://doi.org/10.1016/j.apcatb.2020.119017 119017.

Zhang, X., Yue, J., Zhao, Y., Yan, Z., Zhu, G., Liu, L., Xu, H., Yu, A., 2021a. Synthesis of tetragonal BaTiO3 nano-particle via a novel tartaric acid co-precipitation process. Ceram. Int. 47, 7263–7267. https://doi.org/10.1016/j.ceramint.2020.11.006.

Zhang, A., Zhang, Z., Chen, J., Sheng, W., Sun, L., Xiang, J., 2015. Effect of calcination temperature on the activity and structure of MnOx/TiO2 adsorbent for Hg0 removal. Fuel Process. Technol. 135, 25–33. https://doi.org/10.1016/j.fuproc.2014.10.007.

Zhang, S.W., Zhang, B.P., Li, S., Li, X.Y., Huang, Z.C., 2016. SPR enhanced photocatalytic properties of Au-dispersed amorphous BaTiO3 nanocomposite thin films. J. Alloys Compd. 654, 112–119. https://doi.org/10.1016/j.jallcom.2015.09.053.

Zhang, G.C., Zhong, J., Xu, M., Yang, Y., Li, Y., Fang, Z., Tang, S., Yuan, D., Wen, B., Gu, J., 2019a. Ternary BiVO4/NiS/Au nanocomposites with efficient charge separations for enhanced visible light photocatalytic performance. Chem. Eng. J. 375. https://doi.org/10.1016/j.cej.2019.122093.

Zhao, Y., Zhang, X., Liu, J., Wang, C., Li, J., Jin, H., 2018. Graphene oxide modified nano-sized BaTiO3 as photocatalyst. Ceram. Int. 44, 15929–15934. https://doi.org/10.1016/j.ceramint.2018.06.013.

Zhao, W., Zhang, Q., Wang, H., Rong, J., E, L., Dai, Y., 2020. Enhanced catalytic performance of Ag2O/BaTiO3 heterostructure microspheres by the piezo/pyro-phototronic synergistic effect. Nano Energy 73, 104783. https://doi.org/10.1016/j.nanoen.2020.104783.

Zheng, S., Ding, B., Qian, X., Yang, Y., Mao, L., Zheng, S., Zhang, J., 2022. High efficiency degradation of tetracycline and rhodamine B using Z-type BaTiO3/γ-Bi2O3 heterojunction. Sep. Purif. Technol. 278,. https://doi.org/10.1016/j.seppur.2021.119666 119666.

Zheng, Y., Jia, Y., Li, H., Wu, Z., Dong, X., 2020. Enhanced piezo-electro-chemical coupling of BaTiO3/g-C3N4 nanocomposite for vibration-catalysis. J. Mater. Sci. 55, 14787–14797. https://doi.org/10.1007/s10853-020-05001-x.

Zhou, L., Dai, S., Xu, S., She, Y., Li, Y., Leveneur, S., Qin, Y., 2021. Piezoelectric effect synergistically enhances the performance of Ti32-oxo-cluster/BaTiO3/CuS p-n heterojunction photocatalytic degradation of pollutants. Appl. Catal. B Environ. 291,. https://doi.org/10.1016/j.apcatb.2021.120019 120019.

Zhou, X., Wu, S., Li, C., Yan, F., Bai, H., Shen, B., Zeng, H., Zhai, J., 2019. Piezophototronic effect in enhancing charge carrier separation and transfer in ZnO/BaTiO3 heterostructures for high-efficiency catalytic oxidation. Nano Energy 66,. https://doi.org/10.1016/j.nanoen.2019.104127 104127.

Zou, W., Gao, B., Ok, Y.S., Dong, L., 2019. Integrated adsorption and photocatalytic degradation of volatile organic compounds (VOCs) using carbon-based nanocomposites: A critical review. Chemosphere 218, 845–859. https://doi.org/10.1016/j.chemosphere.2018.11.175.